THE GENETIC BASIS OF TYPE 2 DIABETES: THE ROLE OF *SEL1L* IN GLUCOSE AND ENERGY HOMEOSTASIS

A Dissertation

Presented to the Faculty of the Graduate School

of Cornell University

in Partial Fulfillment of the Requirements for the Degree of

Doctor of Philosophy

by

Rajni Singh

January 2013

THE GENETIC BASIS OF TYPE 2 DIABETES: THE ROLE OF *SEL1L* IN GLUCOSE AND ENERGY HOMEOSTASIS

Rajni Singh, Ph.D.

Cornell University 2013

Type 2 diabetes is a growing epidemic that has been accompanied by a similarly drastic increase in obesity. Its occurrence is associated with β-cell dysfunction, decreased β-cell mass, and insulin and leptin resistance. An increasing body of evidence suggests that endoplasmic reticulum (ER) stress may play an important role in the development of diabetes. The accumulation of terminally misfolded proteins in the ER results in ER stress if the folding capacity and degradation within the ER is insufficient. In this condition of disequilibrium, the unfolded protein response (UPR) is activated to restore ER homeostasis. The mouse and human *suppressor-enhancer-lin12-1-like* (*Sel1L*) gene encodes a structurally complex protein with high expression in the adult pancreas and central nervous system. Evidence from *in vitro* studies and lower organisms implicates SEL1L as a crucial factor in endoplasmic reticulum-associated degradation (ERAD) of unfolded or misfolded proteins, a pathway of the UPR. However, the physiological role of SEL1L in the whole organism remains elusive. The Long lab has generated the first mouse model featuring the global deletion of *Sel1L*. Mice homozygous for this hypomorphic allele are early embryonic lethal. Our embryological and *in vitro* data indicated that the absence of *Sel1L* led to changes in organelle morphology, the initiation of apoptotic pathways,

decreased cell viability, and defective cellular degradation. Due to the embryonic lethality of the homozygous *Sel1L* mutant mice, the viable heterozygote (*Sel1L*$^{+/-}$) mice were used to understand the contribution of ERAD to the development of obesity-induced diabetes. We found that mice heterozygous for *Sel1L* are predisposed to high-fat diet-induced hyperglycermia, glucose intolerance, reduced β-cell mass, and impaired insulin secretion in comparison to wild-type mice. Finally, to further investigate the tissue-specific roles of SEL1L, we generated mice with the conditional deletion of *Se1lL* in β-cells and hypothalamic neurons. Mice with *RIP-Cre*-mediated deletion of *Sel1L* (mutant) showed elevated blood glucose levels in comparison to control mice by 2 weeks of age. Additionally, mutant mice exhibit progressive glucose intolerance and severely defective glucose-stimulated insulin secretion. In adulthood, mutant mice develop hyperphagic obesity and peripheral leptin and insulin resistance. Altogether, these deviances in glucose and energy homeostasis at the level of the β-cell and hypothalamic neuron, respectively, are attributed to ER stress in the absence of SEL1L. These data collectively provide compelling evidence for the causal role of ER stress in the manifestation of Type 2 diabetes.

BIOGRAPHICAL SKETCH

Rajni Singh was born on July 27, 1985 to Anil Kumar Singh and Nutan Singh in Trenton, NJ. She spent the majority of her youth in Hopewell, NJ, where her father built a beautiful home. Attending the reputable public schools in this district allowed Rajni to be academically challenged. During her freshman year of high school, Rajni failed her first exam in biology. She was determined to never let that happen again. In her efforts to prove to herself that she will not be defeated by science, she became fascinated by it. She loved carrying out the various dissections, writing weekly lab reports, teaching her fellow students during group projects, and learning about life! Every year she would take science courses as her electives, such as ecology, astronomy, anatomy, and physiology. Being in this area of NJ proved to be ideal for her intellectual curiosity, as she was able to attend programs and conferences at Bristol-Myers Squibb, the Princeton Plasma Physics Lab, and various NJ universities. When it came time to commence her higher education, Cook College at Rutgers University was a natural choice. While obtaining her undergraduate degree in Animal Science, she was able to enjoy the intimacy of a small school setting along with all the resources of the large university setting. She was very involved in community affairs and interacted frequently with the faculty, staff and other students at her college. As her coursework became more advanced, she grew more invested in research as well. The diversity of research opportunities she had in addition to her father's struggle with diabetes led her to pursue graduate school as the logical next progression in developing her research interests.

Rajni was fortunate to attend one of the finest institutes in the country, Cornell University, to pursue her Ph.D. in Molecular and Integrative Physiology. Here, she was able to not only perform research on understanding the development of Type 2 diabetes (under the mentorship of Dr. Qiaoming Long), but also participate in a range of teaching and service activities. She had particularly rewarding experiences being a part of the Future Faculty Teaching Certificate Program and the Big Brothers Big Sisters Program of Tompkins County. Her diverse experiences altogether have reinforced her love for science, teaching, and an academic setting. She is looking forward to starting a postdoctoral position at the National Institute of Diabetes and Digestive and Kidney Diseases under the supervision of Dr. Sushil Rane after defending her dissertation.

Thank you, Mom and Dad

ACKNOWLEGEMENTS

I frequently find myself talking to strangers about my research. Individuals who I meet on a plane ride, the checkout line at the grocery store, or small business owners of various shops I stop in. When I tell them that I do research related to understanding Type 2 diabetes, the number of people who are personally affected by this disease truly astonishes me. I often hear "I have Type 2 diabetes" or "My wife was just diagnosed with diabetes." They will tell me about how they have struggled with managing their diabetes or share success stories about transforming their lifestyles. But what resonates with me most from these conversations and random encounters is their expression of sincere interest and appreciation for what I do.

I am fortunate to be truly fascinated and inspired by the research that I do. This dissertation is the culmination of a process that has been extraordinarily challenging, but equally rewarding. Through all the failed experiments and a few successful ones, I can genuinely say that I love this research. Passion alone, however, has not gotten me this far. I am also fortunate to have had many people who have supported my growth and progress as a scientist.

My principle investigator, Dr. Qiaoming Long, took me on as a rotation student in my first year as a physiology graduate student. I was intrigued by his sincere enthusiasm for his research program and the exciting new prospective projects in his lab at the time. Had it not been for his innovative projects and mentorship, I would have a blank thesis and a mundane job. I thank him for challenging me and nurturing my growth as an independent thinker and researcher.

Throughout my years at Cornell, I have had an extraordinarily invested special committee. Dr. Robin Davisson, Dr. Xingen Lei, and Dr. Geoffrey Sharp, in addition to Dr. Long, have always had my best interests in mind and kept me on the right track towards where I am today. I am truly honored and humbled to have had them on my committee. I can only hope that one day I, too, can achieve the same level of accomplishment and success that they have in academia.

I'd also like to acknowledge members of the Long lab for their technical support and insightful input into my projects, including Adam Francisco, Wei-hua Chang, Chris Krumm, Shuai Li, Vivian Liu and several visiting scholars. I am especially thankful for my dedicated undergraduate student, Abby Morrison, for her patience and hard work. As my lab is located in the Department of Animal Science, I have grown fond of Morrison Hall and its research community. I have enjoyed the diversity of research that the department fosters, and have appreciated the expertise of many of the faculty, staff and other graduate students whom I have consulted about my experiments and data. I am also thankful for the generous funding the department has provided for me as a graduate student. The assistantships gave me the opportunity to improve my teaching capabilities and interact with a diverse undergraduate student population. Dr. Ron Butler, Dr. Pat Johnson, and Dr. John Parks have been particularly supportive faculty members in my research and teaching endeavors.

Several collaborators have made my dissertation research possible. Xi Yan and Xinhui Wang of Dr. Lei's lab have been instrumental in teaching me islet perfusions and isolations. Additionally, Dr. Colin Young of Dr. Davisson's lab has been an essential part our brain-specific research by performing necessary surgeries and providing valuable insight into the project.

Many people have played supporting roles in easing my responsibilities as a graduate student. With regard to my research, I recognize the staff within the Cornell Center for Animal Resources and Education. In addition to providing appropriate training for lab animal experimentation, they also consistently monitored our mouse colony for any issues that would disrupt our research. I am especially grateful for the company of the animal technicians during early-morning experiments in the facility. With regard to fulfilling all other requirements for graduation, the Office of Graduate Education at the College of Veterinary Medicine has been a crucial resource. In particular, I'd like to thank our Graduate Education manager, Janna Lamey, for her dedication and personalized assistance to students in the BBS program. I also appreciate the administrative staff members in the Department of Animal Science who have helped with placing orders, photocopying, scheduling rooms and equipment and answering random questions I have had throughout the years.

The Center for Teaching Excellence has transformed my understanding of teaching and learning in higher education. Their seminars, symposiums, and courses have enabled me to develop a unique and discipline-specific teaching philosophy. I thank Dr. Richard Kiely and Dr. David Way for initiating the comprehensive and compelling teaching certificate program that I participated in.

I have forged many meaningful friendships in my lifetime. My friends are my extended family. Through the difficulties I have struggled with and through any success I have achieved, they are constants in my life. I feel truly blessed that these are people who have consistently listened when I needed to vent, assisted me when I needed help, advocated for me, challenged me to be open-minded,

remained positive in trying times, and never let me feel alone. They have been the distractions that I needed when I was so absorbed in my work. I have shared innumerable joyous memories and occasions with my friends and can rely on them to make me smile and laugh when I need it most. My oldest friends, Aggy Feulner, Sarah Kelley, and Julie Spencer, remind me that true friendships stand the test of time despite how much we have changed. I also must recognize my closest friends from college, most of whom I met on my very first day in the B-wing of Nicholas Hall. "B-wing" and it's honorary members include, Fred and Tara Lozy, Jerry Benjamin, Jon-Kerwin Lagasca, Jon Cruz, Colin and Kelly Vuong, Sara Strauss, Sarah Welch, Miranda Chan, Nakeefa Bernard, Punam Patel, Eddie Amoyan, Mookie Thakore, Vineet Dhiman, Michael Esmail, and Josh Cuzzone. In a sense, I feel like we have all grown up together because college was a new beginning for all of us. And equally important are the friends that I have made as a graduate student here at Cornell. They include Anna Zenno, Jeffrey Peacock, Kevin George, Yin He, Alex Beatty, Krystal Lum, Patrick and Kristin Murphy, Karl Rueggeberg, Joannalynn Delacruz, Ayesa Kaur, Natalie Henkkaus, Song Lee, Damien Garbett, Ken Kawamoto, Xiao Wang, Joe and Jessica Clauss, Nicole Kelver, Katie Seeley, Pete Clauss, and my amazing and loving boyfriend, Srich. Despite the often dreary and cold Ithaca weather, they have always been my sunshine.

I must also extend my gratitude to our generous family friends, especially the Feulner family. During my father's illness, they went above and beyond to assist him and my mother in their greatest time of need. Knowing that we can always depend on them, our neighbors, and other close family friends has given me peace of mind while living in Ithaca and allowed me to focus on my research.

My family is the most important priority in my life. I have always looked up to my younger brother, Rohit, and older sister, Rohini. Despite how different the three of us are, I'm amazed at their brilliance and expertise in the areas they chose to pursue. I thank my extended family in India and Minnesota for being supportive of my academic endeavors from a young age. I cannot forget to acknowledge the contribution of our dog, Chipper, who always brought a smile to my face in stressful times.

But the most influential people in my life have been my extraordinary parents. They came to this country several decades ago from India and made many sacrifices so that their children could have the best education and opportunities available. My mother is the most selfless and assiduous person that I know. She has endured great tragedy and loss in her life but this has only made her more resilient. I know that she lives every day with the hope that my siblings and I will have a secure and happy future.

My father was trained as an engineer at a top institution in India. Growing up, he would always have three or four side projects going on in our home and thought it was appropriate to use these projects as a teaching experience for his children. I distinctly remember his incessant questions while working. "How does this car part work?" or "What's the first step in building a bookshelf?" Even if we weren't actively working on a project, he would *still* ask questions. "How does this microwave heat food?" I would become so irritated and apathetic. All I wanted to do was play outside or watch TV. Now, as I complete my Ph.D. in physiology, I realize that he was subconsciously invoking my inner curiosity. After all, physiology is just the study of how stuff works. Today these sorts of questions drive my fascination and my research.

I have dedicated this dissertation to my incredible mother and father, for a lifetime of unconditional love and support. Although my father passed away in October of 2011, he will always inspire me. This dissertation was written in loving memory of his wisdom and encouragement.

TABLE OF CONTENTS

LIST OF FIGURES

LIST OF ABBREVIATIONS

4-PBA	4-phenylbutyric acid
AGRP	Agouti-Related Peptide
ARC	Arcuate Nucleus
ATF6α	Activating Transcription Factor 6
ATG7	Autophagy-Related Protein 7
BAK	Bcl-2 homologous Antagonist/Killer
BAX	Bcl-2–Associated X protein
BCL2	B-cell Lymphoma-2
BIM	Bcl-2-like Protein 11
BDNF	Brain-derived Neurotrophic Factor
BiP	Binding Immunoglobin Protein (Also known as GRP78)
BMI	Body Mass Index
BSA	Bovine Serum Albumin
CART	Cocaine- and Amphetamine-Regulated Transcript
CHOP	CCAAT/enhancer Binding Protein
CREBH	cyclic-AMP-Responsive- Element-Binding Protein H
CRH	Corticotropin-Releasing Hormone
DAPI	4',6-diamidino-2-phenylindole
DER	Derlin Family
DIO	Diet-induced Obesity
DMSO	Dimethyl Sulfoxide
DN	Dominant-Negative
Dox	Doxycycline
EDEM	ER Degradation-Enhancing α-mannosidase-Like Protein
eIF2α	Eukaryotic Initiation Factor 2
ELISA	Enzyme-Linked Immunosorbent Assay
ER	Endoplasmic Reticulum
ERAD	ER- Associated Degradation
FFA	Free Fatty Acids
FNII	Fibronectin II domain
FTO	Fat Mass and Obesity-Associated Gene
GFP	Green Fluorescent Protein
GRP78	78 kDa Glucose-Regulated Protein (Also known as BiP)
GSIS	Glucose-Stimulated Insulin Secretion
GTT	Glucose Tolerance Test
GWAS	Genome-Wide Association Studies
HBSS	Hank's Buffered Saline Salt Solution
HERP	Homocysteine-Induced Endoplasmic Reticulum Protein
HFD	High-Fat Diet
hIAPP	human Islet Amyloid Polypeptide
HNF	Hepatocyte Nuclear Factor

HRD1	HMG-CoA Reductase Degradation Protein 1
ICV	Intracerebroventricular
IKKβ	Inhibitor of Nuclear Factor Kappa-B Kinase
INS-1	Rat Insulinoma Cell Line-1
IRE1α	Inositol-Requiring Enzyme 1
IRS2	Insulin Receptor Substrate
ITT	Insulin Tolerance Test
JNK	C-Jun N-Terminal Kinase
KCNJ11	Potassium Inwardly-rectifying channel, Subfamily J, Member 11
MC4R	Melanocortin-Receptor
MEF	Mouse Embryonic Fibroblast
MIN6	Mouse Insulinoma Cell Line-6
MIP	Mouse Insulin Promoter
MODY	Maturity Onset Diabetes of the Young
mTOR	mammalian Target of Rapamycin (mTOR)
NC	Normal Chow
NFκB	Nuclear Factor Kappa-light-chain-enhancer of activated B cells
NHK	Null Hong Kong alpha1-antitrypsin
NPY	Neuropeptide Y
NRXN3	Neurexin 3
Ob-Rb	Obese (Leptin) Receptor (long form)
OS9	Amplified in Osteosarcoma 9
PBS	Phosphate-Buffered Saline
PDI	Protein Disulfide Isomerase
PDX1	Pancreatic and Duodenal Homeobox 1
PERK	Protein kinase RNA-like Endoplasmic Reticulum Kinase
PFA	Paraformaldehyde
PPARG	Peroxisome Proliferator-Activated Receptor-γ
POMC	Pro-opiomelanocortin
PVN	Paraventricular Nucleus
RIP	Rat Insulin II Promoter
RPN	Non-ATPase base subunit of the 19S Regulatory Particle
RT-PCR	Real-time Reverse-Transcription Polymerase Chain Reaction
SEC61	ER membrane protein translocator (aka translocon)
SEL1L	Suppressor-Enhancer of Lin-12-1-Like protein
SOCS3	Suppressor of Cytokine Signaling 3
SREBP	Sterol Regulatory Element-Binding Proteins
STAT3	Signal Transducer and Activator of Transcription 3
T2D	Type 2 Diabetes
TLR	Toll-Like Receptors
TM	Tunicamycin
TNFα	Tumor Necrosis Factor
TPR	Tetratricopeptide Repeats

TRH	Thyrotropin-Releasing Hormone
TSC1	Tuberous Sclerosis Protein 1
TUDCA	Tauroursodeoxycholic Acid
TUNEL	Terminal deoxynucleotidyl transferase dUTP Nick End Labeling
UBC6e	Ubiquitin-Conjugating Enzyme 6e
UBE1	Ubiquitin-activating Enzyme
UCH-L1	Ubiquitin Carboxyl-terminal Hydrolase L1
UGGT	UGT-glucose: glycoprotein glucosyltransferase
UPR	Unfolded Protein Response
VIMP	VCP-Interacting Membrane Protein
VMH	Ventromedial Hypothalamus
WFS1	Wolframin 1
XBP1	X-box Binding Protein 1
XBP1s	X-box Binding Protein 1, spliced
XTP3-B	ER Lectin 1
α-MSH	Melanocyte-Stimulating Hormone
β-geo	β-galactosidase-neomycin cassette

CHAPTER 1: INTRODUCTION AND LITERATURE REVIEW

1.1 An Overview of Type 2 Diabetes

The World Health Organization predicts that 346 million people worldwide are currently living with diabetes. This number is expected to double by 2030, indicating that this disease is reaching global epidemic proportions (1). The multiple complications that arise from the disease can be severe and fatal, and include heart disease and stroke, high blood pressure, kidney disease, retinopathy, and neuropathy.

Diabetes mellitus, or simply diabetes, is the condition defined by elevated blood glucose levels (hyperglycemia). Therefore, this disorder originates in the pancreas, a glandular organ that has integral exocrine and endocrine functions in vertebrates. The islets of Langerhans are responsible for mediating the endocrine functions of the pancreas, and there are approximately one million of these cell clusters in the human pancreas (2). The β-cell is one of four cell types in the islets, and its most notable function is the production and secretion of insulin, an anabolic hormone, in response to elevated blood glucose. Insulin stimulates glucose uptake and promotes glycogen synthesis in tissues to maintain normal blood glucose levels. While Type 1 diabetes (T1D) is characterized by the specific destruction of β-cells and a consequent lack of insulin production, Type 2 diabetes (T2D) is associated with a reduced ability of β-cells to secrete enough insulin and a failure of peripheral tissues to respond to insulin. Although T1D and T2D are the most common forms, cases of gestational diabetes, monogenic

diabetes, and other rare forms do exist. It is estimated that T2D accounts for 90% of people with diabetes worldwide (3).

Therefore, T2D manifests from two major defects: insulin resistance and a progressive decline in β-cell function. Insulin resistance is commonly observed during our normal life cycles, in situations of pregnancy, puberty, and with aging. Healthy β-cells are able to adapt to this resistance through changes in functional responsiveness of the cell and also in total β-cell mass (4). Through adjusting these two parameters, many insulin-resistant individuals do not ultimately develop hyperglycemia. When there is an inherent inability of the β-cells to initiate this adaptive response (*i.e.* the secretory capacity deteriorates), normal glucose tolerance cannot be maintained. The result is glucose intolerance and increased fasting glucose levels, leading to T2D. Aside from defects in insulin secretion and action, loss of β-cell mass and an insulin deficiency also contribute to the pathogenesis of T2D. Postmortem studies have shown T2 diabetic patients have reduced β-cell mass (up to 63%) and increased β-cell apoptosis rates (5). Apoptosis is likely to play a critical role in the reduction of β-cell mass seen in T2D, but the specific mechanisms by which this programmed cell death occurs has yet to be determined.

Research on the pathophysiology of T2D has evolved from focusing on the endocrine pancreas to placing more emphasis on a network of organs affected by this metabolic state. These organs include adipose tissue, the brain, the liver, and skeletal muscle. This complex integration of factors contributing to the progression of T2D is summarized in Figure 1.1:

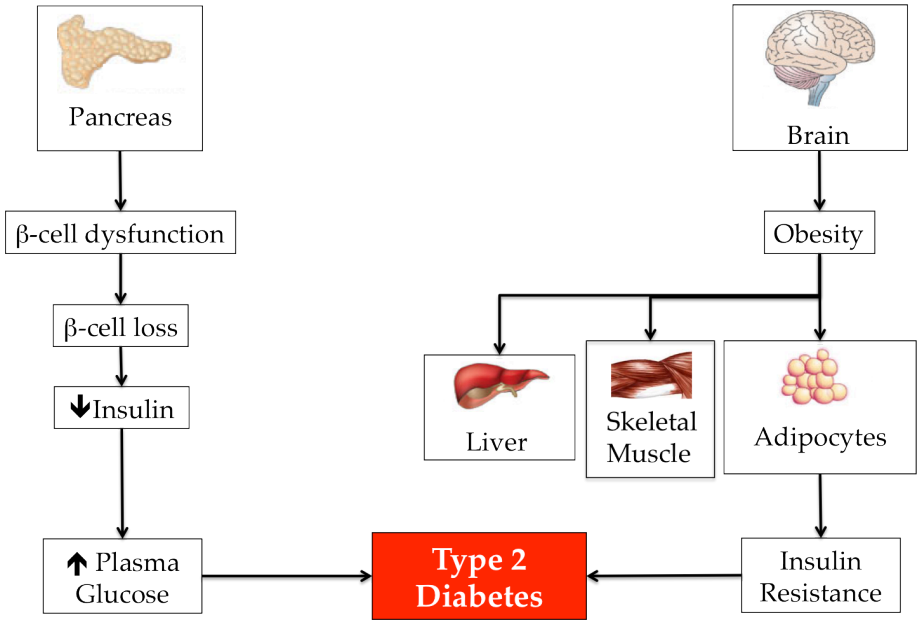

Figure 1.1: The Pathogenesis of Type 2 Diabetes (T2D). The manifestation of T2D involves several key organs, including the pancreas, brain, adipose tissue, liver and skeletal muscle. In the pancreas, β-cell dysfunction and β-cell loss cause a decrease in circulating insulin, resulting in elevated plasma glucose levels. In the brain, leptin-sensitive hypothalamic neurons are no longer responsive to the anorexigenic effects of leptin, causing an increase in food intake and a decrease in energy expenditure. Over time, this results in an expansion of adipose tissue and obesity, which is associated with insulin resistance. The failure of peripheral tissues, such as liver and skeletal muscle, to respond to insulin also exacerbates glucose intolerance in T2D.

This change in paradigm can be attributed to the correlation between T2D and metabolic syndrome. The metabolic syndrome is an insulin-resistant state that is defined by obesity, elevated triglycerides, decreased high-density lipoprotein cholesterol, hypertension, and impaired fasting glucose (6). Together, these factors confer an increased risk for both cardiovascular disease and T2D (6). About 80% of patients with T2D are considered overweight or obese (having a body mass index, or BMI, over 25) (3). In obese individuals, the increased deposition of adipose tissue leads to elevated levels of its secretory products, including non-esterified fatty acids, glycerol, pro-inflammatory cytokines and

hormones. These products have been shown to contribute to the development of insulin resistance in not only adipose tissue, but also in the liver and skeletal muscle (7).

Adipose tissue also produces leptin, a hormone that has potent effects on energy balance and is therefore a key component in the pathogenesis of T2D (8). These effects are mainly mediated specifically by leptin binding its receptors in the arcuate nucleus (ARC) of the hypothalamus, although leptin receptors exist on other neuronal populations (9). There, it influences two sets of neurons that act as sensors of whole-body energy status, and initiates signals to maintain energy stores at a constant level. Neurons that co-express agouti-related peptide (AGRP) and neuropeptide Y (NPY) are inhibited by leptin and insulin, while neurons that co-express pre-opiomelanocortin (POMC) and cocaine- and amphetamine-regulated transcript (CART) are stimulated by leptin and insulin (10-12). Both neurons synapse onto second-order neurons in other regions of the hypothalamus to exert their effects. These regions include the paraventricular nucleus (PVN), ventromedial hypothalamus (VMH), and lateral hypothalamus. Ultimately, leptin stimulation decreases food intake and weight gain, while leptin inhibition has the opposite outcomes. Many of the anorexigenic effects of leptin are mediated by POMC processing in the ARC (13). POMC undergoes significant posttranslational modifications to give rise to a range of biologically active peptides, including α-melanocyte stimulating hormone (α-MSH). α-MSH is an agonist of the melanocortin-4 receptor (MC4R), which is prevalently expressed in the PVN, while AGRP is an antagonist of this receptor (14). The downstream targets of MC4R signaling include brain-derived neurotrophic

factor (BDNF), corticotropin-releasing hormone (CRH), thyrotropin-releasing hormone (TRH), melanin-concentrating hormone (MCH), and orexins (15).

Mice lacking the leptin gene, known as *ob*/*ob* mice, are profoundly obese due to hyperphagia. The *ob*/*ob* mouse is a powerful and common animal model for T2D. Mutations in the human leptin gene have been identified as a cause of obesity, but occur infrequently (16). About 5% of severe human obesity is due to a mutation of the *MC4R* gene (17). Mutations in the *POMC* gene, which therefore prevents the production of α-MSH, produce severe human obesity as well (18). *MC4R* and *POMC* mutations result in a syndrome of hyperphagic obesity in humans, indicating that the central melanocortin pathway is mainly involved in the control of food intake. This provides some insight into the genetic basis of central leptin resistance. Obese individuals commonly exhibit leptin resistance, with high circulating levels of leptin due to increased adiposity, yet no anorexigenic response to the leptin in the brain (19). The result is the failure to produce a feeling of satiety after eating, leading to increased food intake and exacerbated adiposity.

The precise mechanisms linking increased adiposity to insulin resistance are unknown, but proinflammatory cytokines such as tumor necrosis factor alpha (TNFα) and interleukins-1 and -6 have been shown to disrupt insulin action in adipocytes, myocytes, and hepatocytes (7). Insulin resistance involving both the liver and muscle is a distinctive feature of T2 diabetic individuals. The resulting glucose intolerance is further exacerbated by an increase in hepatic glucose production. This accelerated rate of hepatic glucose output is a major determinant of the elevated fasting plasma glucose concentration in T2D (20).

Altogether, hyperglycemia due to β-cell dysfunction and peripheral insulin resistance defines T2D. However, due to its complexity, the pathogenesis of this disease is still poorly understood. There is compelling genetic, biochemical and clinical evidence for genetic as well as environmental factors that contribute to its development. The genetic basis includes genes that confer susceptibility to impaired β-cell secretion, decreased β-cell viability, and insulin and leptin resistance (both peripheral and central). The environmental basis includes poor nutrition and decreased physical activity. Despite this extensive research, T2D is defined as a multifactorial disease with unknown origins.

Accumulating evidence points to an intracellular stress localized at the endoplasmic reticulum (ER) as a major contributor to the manifestation of T2D. This is justified by the physiological challenge presented to the organs involved in T2D, all of which have a high capacity for secretory protein synthesis. The unfolded protein response (UPR) is the adaptive response of the mammalian cell to maintain homeostasis within the ER and prevent this intracellular stress. Therefore, failure of the UPR could potentially explain the transition from physiology to pathology in the context of T2D.

1.2 The Unfolded Protein Response

The ER is a highly versatile organelle with a central role in lipid and protein biosynthesis (21). The lumen provides a specialized environment that facilitates the post-translational modifications and folding of secreted proteins. These post-translational modifications include lipidation, hydroxylation, and oligomerization, but the most common modifications amongst the secreted

proteins are N-linked glycosylation and disulfide oxidation (22). Proteins that have attained their native conformation are cleared for exit from the ER and continue through the secretory pathway. Improperly folded proteins, however, are either retained to complete additional folding cycles or are targeted for degradation in a process referred to as "quality control" (23). This will be discussed in further detail later.

When there is disequilibrium between ER protein load and the folding capacity of the machinery, ER stress is the result. Some physiological causes of ER stress include hypoxia, exposure to environmental and experimental toxins, excess nutrients, and genetic mutations that impede proper folding of proteins (24). ER stress elicits the UPR, which alleviates ER stress, restores ER homeostasis, and prevents cell death.

There are three central signaling pathways in the UPR, depicted in Figure 1.2, and each is regulated by an individual transmembrane ER stress "sensor."

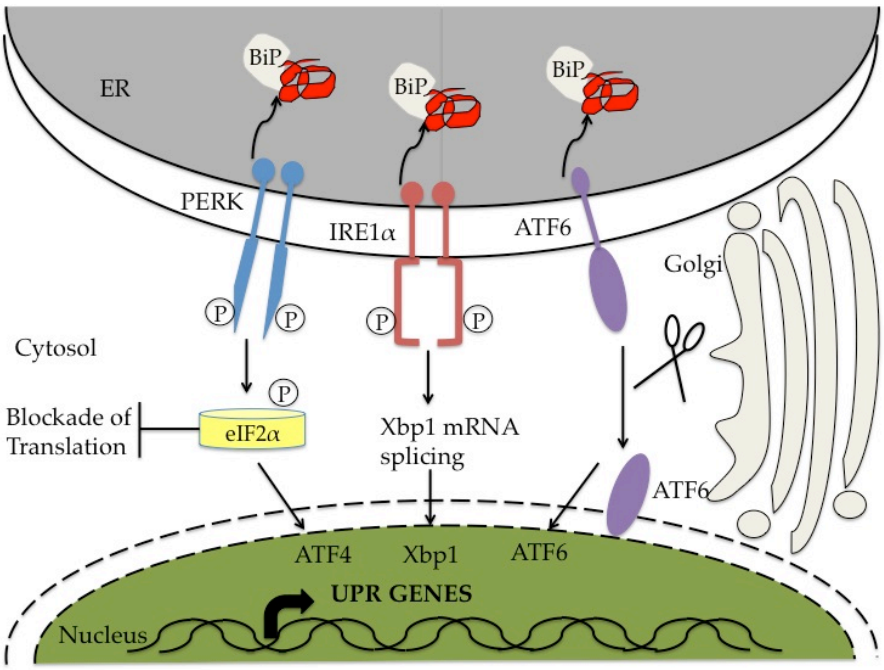

Figure 1.2: The Unfolded Protein Response (UPR). The UPR is the cell's adaptive response to ER stress. With an increase in misfolded proteins in the ER lumen, the chaperone BiP dissociates from three ER transmembrane sensors of ER stress: PERK, IRE1α, and ATF6. This dissociation activates three signaling pathways, each producing a distinct transcription factor that translocates to the nucleus to induce the transcription of various UPR genes. Altogether, the upregulation of UPR genes will ameliorate ER stress. Adapted from Figure 1 of (25).

These sensors are IRE1α, PERK, and ATF6α. Each pathway has an ultimate downstream effecter that goes on to mediate the induction of ER stress response element genes (ERSEs) (26). The molecular chaperone GRP78, also known as BiP, remains associated with the luminal domains of IRE1α and PERK in their inactive state. Upon ER stress, unfolded proteins in the ER lumen necessitate GRP78 dissociation, resulting in oligomerization and autophosphorylation of IRE1α and PERK (27). ATF6α is also regulated by GRP78, and GRP78 dissociation from the sensor causes ATF6 to be transported to the Golgi apparatus and become activated (28). Briefly, IRE1α splices XBP1 mRNA

(XBP1s). The spliced XBP1 mRNA encodes a basic leucine zipper transcription factor that upregulates UPR target genes (29). Activated PERK directly phosphorylates the Ser51 residue of α-subunit of eukaryotic initiation factor 2 (eIF2α). This in turn inhibits protein translation by reducing the formation of ribosomal initiation complexes and recognition of AUG initiation codons (30). It simultaneously increases the translation of the transcription factor ATF4, which goes on to bind ERSEs. ATF6α transits to the Golgi where it is protealytically cleaved. The cleaved ATF6 transcription factor translocates to the nucleus to mediate UPR effects (31).

Ultimately, there are four distinct processes that result from the induction of UPR genes (Figure 1.3): an increase in the folding capacity of the cell through transcriptional activation of ER chaperones, reduction of the biosynthetic load by translational attenuation, degradation of misfolded proteins by ER-associated degradation (ERAD), and apoptosis (22).

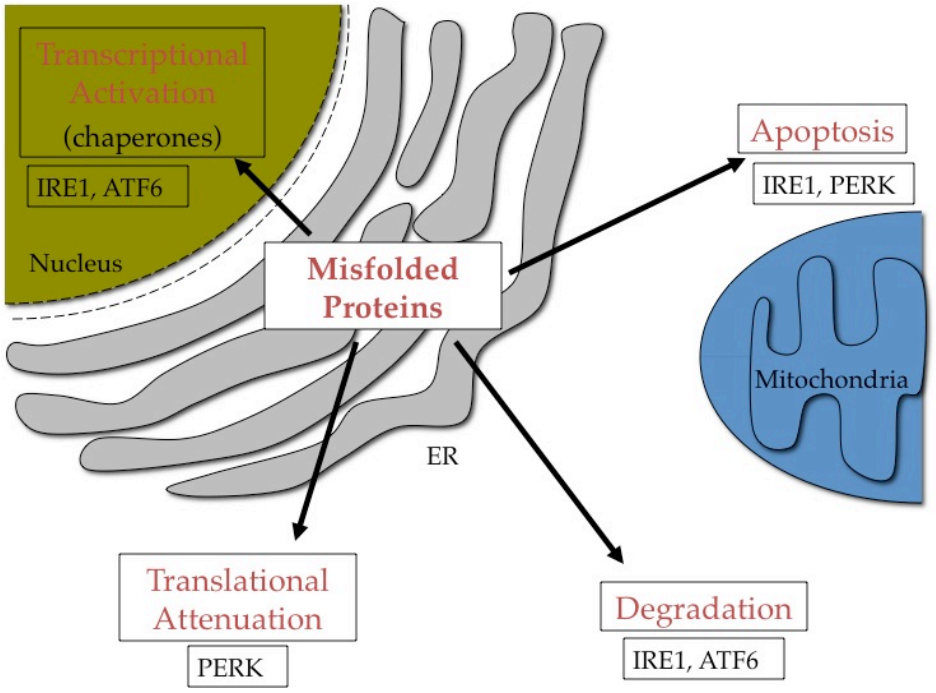

Figure 1.3: Outcomes of the Unfolded Protein Response. The adaptive outcomes of the UPR include transcriptional activation of chaperones (mediated by IRE1 and ATF6), translational attenuation (mediated by PERK), and ER-associated degradation (ERAD, mediated by IRE1 and ATF6). If these outcomes fail to restore ER homeostasis, apoptotic pathways are activated.

Apoptosis is initiated in cells as the last resort when the UPR cannot successfully adapt to the stress. Apoptosis is a tightly regulated and controlled process that involves specific biochemical and morphological changes, including cell membrane blebbing, formation of apoptotic bodies, chromatin condensation, and DNA fragmentation (32). Two central pathways are known to mediate apoptosis: the extrinsic pathway, which uses cell surface death receptors, and the intrinsic pathway, which utilizes the mitochondria and endoplasmic reticulum (part of the UPR). The UPR signals that are involved in facilitating the intrinsic pathway originate from IRE1α and PERK dimerization during ER stress. Collectively, C/EBP homologous protein transcription factor (CHOP), c-Jun NH_2-terminal

kinase (JNK), and caspases have been implicated in ER stress-related cell death (26). Downstream activation of CHOP and JNK mediates cell death through regulation of the B-cell lymphoma-2 (BCL2) family of proteins. Under normal conditions, the pro-apoptotic Bax and Bak are kept inactive by interaction with BCL2 both on the mitochondrial and ER membranes (33). Bim, another member of the BCL2 family, is inhibited by binding to cytoskeletal dynein. Both JNK and CHOP eliminate the anti-apoptotic effect of BCL2; CHOP blocks expression of BCL2, whereas JNK phosphorylates it. JNK also phosphorylates Bim, which leads to its release from the cytoskeleton and to its activation (34). Together, these changes allow activation of Bax and Bak, transmission of the signal from the ER to the mitochondria, alternations in mitochondrial membrane potential, and execution of death. Caspases are activated possibly on the ER membrane itself, as well as in the apoptosome (a protein complex formed once apoptosis is initiated), after transmission of the death signal to mitochondria and the release of cytochrome *c* (35).

1.3 ER Stress in Tissues Associated with T2D

The UPR is activated in many of the tissues and cell types that are central to the pathogenesis of diabetes and obesity. *In vivo* and *in vitro* evidence from models that recapitulate T2D confirms the presence of ER stress in the liver, adipose tissue, hypothalamus and β-cells, as summarized below.

1.3.1 *Liver and Adipose Tissue*

The liver is one of the most productive secretory organs in the body. Its secretory products include bile acids, lipoproteins, and all major plasma proteins including albumin, fibrinogen, and blood clotting factors. Therefore, the UPR has an important role in maintaining ER homeostasis for proper liver function. This is evidenced by the fact that physiological ER stress is observed in the liver of rodents that are re-fed after fasting; but this diminishes within a few hours (36). Chronic hepatic ER stress, however, is seen in both obese mice and humans (37). In addition to insulin resistance, obesity is also associated with hepatic steatosis (the accumulation of lipids within the hepatocyte). An increasing body of evidence supports the link between steatosis and ER stress in the liver, thus pointing to an important role for the UPR in lipid metabolism. Steatosis in *ob*/*ob* mice has been associated with an accumulation of the transcription factors SREBP1c and SREBP2, which promote lipogenesis and cholesterol biosynthesis (38). ER stress causes this accumulation by excessive proteolytic cleavage and activation of the transcription factors. This was further confirmed by the hepatic adenoviral delivery of GRP78, which decreases SREBP1c activation, triglyceride and cholesterol contents, and improves insulin signaling in the liver (38). Hepatic ER stress also reduces the secretion of apolipoprotein B100 (apoB100), which is required for very-low-density lipoprotein (VLDL) assembly and potentially protects against steatosis (39).

Transcription factors such as XBP1 and CREBH (a hepatocyte-specific form of CREB) have been identified as key regulators of gluconeogenic enzymes in the liver. XBP1s can interact directly with FOXO1, which plays an important role in gluconeogenesis and glycogenolysis in the insulin pathway. FOXO1 can

be targeted to the proteasome by XBP1s, thereby inhibiting gluconeogenesis and consequently hepatic glucose output (40). The CREBH transcription factor, which is cleaved by the same process as ATF6 in conditions of ER stress, can also activate the transcription of gluconeogenic genes (41). RNAi-mediated knockdown of CREBH in diabetic mice can improve fasting hyperglycemia due to decreased glucose production in the liver (42).

Obesity also leads to chronic ER stress in adipose tissue. In both dietary (high-fat diet, or HFD) and genetic (leptin-deficient) mouse models of obesity, the adipose tissues show elevated expression of several ER stress markers in comparison to their lean counterparts (37). This elevation in biochemical markers has also been seen in the fat depots of obese, insulin-resistant individuals versus non-obese counterparts (43). Obesity is particularly associated with IRE1α and PERK activation, JNK1 activation, and upregulation of XBP1s and chaperone expression in adipose tissue. The increased expression of IRE1- and ATF6-dependent chaperones in adipocytes *in vivo* is mimicked *in vitro* by adipocyte exposure to lipopolysaccharide, saturated free fatty acids (FFAs), or high glucose (44). The heightened inflammatory response observed in adipose tissue of obese individuals is also associated with ER stress. FFA-induced ER stress in adipocytes is proinflammatory via PERK-dependent activation of IKKβ, an important regulator of the expression of inflammatory genes (45).

1.3.2 *Hypothalamus*

The hypothalamus is critical in the development of T2D because it is the site of central leptin and insulin resistance (46). The failure of hypothalamic neurons to respond to these anorexigenic hormones appears to involve a

combination of ER stress and inflammation. HFD-fed mice as well as *ob*/*ob* mice show increased ER stress in their hypothalami in comparison to lean controls (47). ER stress in the hypothalamus causes leptin resistance in lean mice, as assessed by a decrease in downstream markers of leptin signaling such as STAT3 phophorylation and neuropeptide expression. In accordance with this, chemical chaperones such a 4-phenylbutyric acid (4-PBA) and tauroursodeoxycholic acid (TUDCA), are able to decrease ER stress and improve leptin signaling *in vitro* and *in vivo* (47).

A HFD in rodents can also induce inflammatory protein expression in the hypothalamus (48). Administration of long-chain saturated fatty acids through an intracerebroventricular (ICV) route reveals that toll-like receptor (TLR) signaling is the main event that causes increased cytokine expression and ER stress in the brain. TLRs play a critical role in the innate immune response and participate in the first line of defense against pathogens (49). Ablation of TLR4 through genetic and pharmacological approaches leads to protection from HFD-induced ER stress, cytokine expression, body mass gain, and leptin resistance. Accordingly, overnutrition caused by a HFD has also been shown to activate NFκB, or nuclear factor kappa-light-chain-enhancer of activated B cells (50). NFκB is a downstream transcription factor in TLR signaling, and is immediately regulated by IκB kinase (IKK). The activation of the IKK/NFκB pathway by HFD-feeding was blocked with TUDCA infusion into the third ventricle (ICV) of mice. This finding suggests that overnutrition-induced NFκB activation in the hypothalamus is, at least partly, mediated by ER stress. Furthermore, IKK/NFκB activation contributes to central leptin and insulin resistance. The proposed

mechanism for this association is that NFκB promotes the expression of *Socs3*, an inhibitor of leptin and insulin signaling.

This evidence points to developing new strategies to reduce inflammation and ER stress in the hypothalamus of obese subjects, for the purpose of overcoming central leptin and insulin resistance. Exercise has been shown to increase the expression of interleukin-6 (IL-6) in obese rodents, a cytokine that has the potential to be anti-inflammatory (51). This natural anti-inflammatory response can reduce IKK/NFκB activation and ER stress, thus improving leptin and insulin sensitivity in the hypothalamus.

The effects of ER stress in the hypothalamus are not limited to immediate leptin and insulin signaling. Several obesity-linked variants of MC4R are retained in the ER of immortalized neurons, causing an increase in the expression of ER chaperones, increased ER-associated degradation, and decreased expression of the receptor at the plasma membrane (52). Here, ER stress is caused by a misfolded protein (MC4R variant) and affecting its trafficking and ultimately its localization. Treatment with 4-PBA restores the receptor to the cell surface and is also able to rescue the function of one variant.

1.3.3 *β-cells*

Although there is impaired insulin sensitivity in obese individuals, diabetes ensues only when insulin resistance coexists with insulin deficiency. In order to execute its normal function of insulin secretion in response to nutrient signals, namely glucose stimulation, the β-cell necessitates exquisite regulation of insulin production and release. Therefore, any increase in insulin secretion

results in a corresponding increase in proinsulin biosynthesis to maintain readily available pools of insulin within secretory vesicles (53). Insulin is translated as a preproinsulin molecule, which translocates into the ER lumen and undergoes signal peptide cleavage to yield proinsulin. Proinsulin is subjected to a folding process that involves disulfide bond formation (54). Once the proinsulin molecule has achieved its native alignment and conformation, it is delivered to the Golgi apparatus and subsequently packaged into secretory vesicles. Here, proinsulin is cleaved by a series of endopeptidases to give rise to mature insulin (55). Two likely conditions would result in disequilibrium of ER protein load and processing capacity, leading to β-cell ER stress. First, the state of insulin resistance presents a situation of biosynthetic overload to the β-cell due to the adaptive response mentioned previously. Second, genetic mutations in the insulin gene could also generate an ER imbalance. If the ER homeostasis is disrupted, insulin will not be effectively released, and β-cell dysfunction arises.

In humans, seven mutations in the insulin gene, which disrupt proper disulfide bond formation and proinsulin folding in the ER, have been shown to cause neonatal diabetes (56). The *Akita* mouse model recapitulates this diabetic state, as these mice are heterozygous for a mutation in the insulin-2 gene (57). The *Akita* mouse is characterized by hyperglycemia, decreased insulin secretion, and progressive apoptosis of β-cells over time. Electron microscopy of islets from these mice reveals distention of the ER lumen, indicating the misfolded proinsulin is retained in the ER and is likely causing the metabolic phenotype (58). Not surprisingly, several mutations in UPR genes are associated with young-onset diabetes, including *WFS1* (an ER transmembrane protein) in

Wolfram syndrome and *EIF2AK3* (encoding PERK) in Wollcott-Rallison syndrome (59, 60).

Global and tissue-specific knockouts of *PERK* in mice have shown that PERK is of particular relevance for the fetal and early neonatal development of β-cell mass and function (61). This pathway is also important in the translational control of insulin. Mice homozygous for a Ser51Ala substitution in *eIF2α*, precluding its phosphorylation by PERK or other kinases, die of hypoglycemia within hours after birth because of defective gluconeogenesis. The pancreata from these mice exhibit β-cell defects and insulin depletion at late embryonic and neonatal stages (62). Conditional expression of homozygous Ser51Ala mutant eIF2α in β-cells causes a severe diabetic phenotype due to unregulated proinsulin translation. The β-cells also have defective intracellular trafficking of ER cargo proteins and increased oxidative damage, leading to massive β-cell apoptosis (63). IRE1 activation promotes insulin mRNA degradation in β-cells exposed to chronic high glucose levels, providing immediate translational relief to the ER (64). Over time, however, this suppression of insulin biosynthesis leads to β-cell dysfunction(65). Similarly, ATF6 activation inhibits insulin promoter activity by downregulating key transcription factors that affect insulin gene expression (66).

There are multiple sources of ER stress in human T2D. The β-cell secretes another product in addition to insulin, islet amyloid polypeptide (IAPP). Also known as amylin, IAPP is also expressed in β-cells, and is trafficked through the insulin secretory pathway and co-secreted with insulin (67). The 37-amino acid residue peptide in humans (hIAPP) has the propensity to form amyloid, or

abnormal extracellular deposits of protein, in the islets (68). In T2D, insulin resistance disproportionately increases hIAPP compared with insulin expression. Postmortem analysis revealed that more than 90% of T2D patients have hIAPP amyloid in their islets, and the presence of amyloid was associated with β-cell death (69). The cytotoxicity of hIAPP is the result of structures that act intracellularly to induce β-cell apoptosis, and ER stress is speculated to mediate this apoptosis (70).

As previously elaborated on, obesity and a diet high in fat are major risk factors for the development of diabetes. Two leading causes of obesity are over-consumption and the intake of high-fat and refined sugary foods. Palmitate (a saturated fatty acid) induces β-cell ER stress due to rapid degradation of carboxypeptidase E and alteration of β-cell calcium influxes. These changes ultimately disrupt the folding and maturation of proinsulin (71). The mammalian target of rapamycin (mTOR) operates as an important transducer of ER stress in β-cells by modulating the synthesis of IRE1α and JNK activity (72). A recent discovery implicates that palmitate treatment of clonal β-cells hampers ER to Golgi protein trafficking via production of ceramides, leading to ER stress (73). These experiments also result in significant cell death. Specifically, glucolipotoxicity refers to the glucose- and free fatty acid (FFA)- induced apoptosis. High levels of saturated fatty acids were also reported to increase apoptosis in rat and human islets (74). Glucose seems to be an important amplifier of lipotoxicity, but the mechanisms by which fatty acids and glucose induce ER stress and apoptosis are not entirely understood.

Experimental HFDs are given to mice to mimic the "Western" diet that will induce obesity and the complications that are associated with it, specifically insulin resistance and T2D. Currently, several mouse models for ER stress-related genes have been developed, and administration of the HFD has led to a diabetic phenotype in many cases. For example, mice that are heterozygous for *Xbp1*, *Eif2α*, *Sec61*, and *Pdx1* (a transcription factor that is responsible for endocrine differentiation and insulin gene expression) exhibit impaired glucose homeostasis in addition to other characteristics of diabetes while on the diet, and these characteristics were shown to be ER stress-dependent (47, 62, 75, 76).

Taken together, an extensive body of previous work demonstrates a critical role for UPR signaling in obesity and diabetes by mechanisms that are not fully elucidated. One outcome of the UPR that has garnered increasing attention is the ER-associated degradation (ERAD) pathway. Several of the UPR targets are genes encoding proteins that facilitate ERAD, which in principle provides the most rapid and direct means to clear the ER of potentially toxic proteins. In addition to its stress-induced role in the UPR, the ERAD pathway is also used to regulate the levels of specific enzymes, lipid carriers, and secreted proteins (77). For these reasons, ERAD plays an essential role in maintaining normal cellular physiology and preventing disease.

1.4 ERAD and Protein Quality Control

ERAD works in coordination with the quality control process to eliminate aberrant proteins and prevent intracellular toxicity of misfolded proteins (77).

The key steps of ERAD are substrate recognition and protein targeting to translocation machinery, retrotranslocation, ubiquitylation, and proteasomal targeting and degradation (78). Each step is highly complex and involves several components that operate in parallel during ER stress. The current understanding of ERAD is primarily based on genetic and biochemical analyses in yeast, a model organism that demonstrates the conservation and evolutionary importance of this process. This section will discuss the mammalian homologues of the yeast ERAD-related genes, although evidence for their roles is inconclusive.

The folding machinery involved in quality control plays an important role in the recognition of substrates that ultimately go on to be degraded. Most nascent proteins that enter the ER lumen are co-translationally modified with an N-linked oligosaccharide, $GlcNAc_2$-Man_9-Glc_3 (of which $GlcNAc_2$ is N–acetylglucosamine, Man is mannose, and Glc is glucose). Glucosidases in the ER remove two terminal glucose residues and the resulting monoglucosylated N-acetylglucosamine binds to lectin-like factors, which contain sugar-binding domains (79). Calnexin and calreticulan constitute the lectin machinery of the ER and are responsible for promoting proper folding of glycoproteins. Following release from the calnexin-calreticulan folding cycle, the final glucose is removed and the resulting glycoprotein contains a $GlcNAc_2$-Man_9 moiety. The addition of an oligosaccharide unit to a protein contributes to backbone stability, and attaining the native conformation prevents exposure of hydrophobic patches. If exposed, as in an unfolded state, these patches can lead to aggregation (80). In this case, the misfolded protein is recognized by UDP-glucose:glycoprotein glucosyltransferase (UGGT), which adds a glucose to the glycan (81). This

prompts its re-entry into the calnexin-calreticulan cycle until the protein's final conformation is achieved.

Similarly, disulfide bond formation promotes protein stability and facilitates assembly into multimeric complexes. Protein disulfide isomerases (PDIs) catalyze the formation of disulfide linkages while also maintaining an oxidizing environment within the ER (82). In addition to the calnexin-calreticulan cycle and PDI, the 70 kDa heat shock protein- family of chaperones play a major role in proper protein folding (83). This family of chaperones includes GRP78 (or BiP), which has an established role in initiating the UPR. Its molecular structure enables GRP78 to bind client misfolded proteins with high affinity to prevent aggregation (84). Together, GRP78, lectin-like factors, and disulfide isomerases work in coordination with other distinct families of proteins to identify terminally misfolded proteins (both glycosylated and non-glycosylated) and target them to the retrotranslocon at the ER membrane (85, 86).

The targeting step of ERAD is closely associated with substrate recognition. The factors involved at this step are typically lectin-like proteins with domains capable of binding mannose-containing derivatives. For example, EDEM contains a α-mannosidase-like domain, while OS9 and XTP3-B contain a mannose-6-phosphate receptor-like domain(87-89). It is believed that these three proteins function in delivering substrates to the retrotranslocation channel.

The retrotranslocation step extrudes the misfolded proteins from the ER lumen and ultimately deposits them into the cytoplasm. Candidates for this channel include the SEC61 complex and the derlin family of proteins (DER1, DER2, DER3) (90, 91) . As an intermediate step, the retrotranslocation machinery

interacts with both targeting and ubiquitylation machinery. Ubiquitylation is the process of targeting a misfolded protein for proteasomal degradation and requires an E1 ubiquitin-activating enzyme (*e.g.* UBE1), an E2 ubiquitin-conjugating enzyme (*e.g.* UBC6e), and an E3 ubiquitin ligase (*e.g.* HRD1-SEL1L complex) (92-94) . The AAA^+ ATPase, p97, provides energy for further extracting the ubiquitylated protein into the cytoplasm. While the retrotranslocation and ubiquitylation components are ER membrane-localized, p97 is associated with the membrane via its interaction with VIMP (91, 95). It can also associate with the 19S cap of the 26S proteasome, which provides a convenient segue for direct degradation of substrates. Ubiquitin receptors (RPN10, RPN13, RPN5) in the cap facilitate the initial interaction with the substrate, which is ultimately moved into the 20S catalytic core for fragmentation into smaller peptide units (96, 97).

Impairment of ERAD has been shown to contribute to several diseases. Huntington's disease, Parkinson's disease, Alzheimer's disease, cystic fibrosis, and pulmonary emphysema are all associated with an accumulation of misfolded proteins and defective ERAD (98-101). These findings reinforce the potential importance of ERAD in maintaining ER and cellular homeostasis. However, it must also be acknowledged that ERAD works in coordination with another protein quality control process, known as autophagy(102). Autophagy is the engulfment of misfolded proteins or protein aggregates within double-membrane vesicles that subsequently fuse to a lysosome, containing the proper enzymes for degrading the contents (103). Further experimentation is needed to determine the circumstances under which autophagy or ERAD dominate in removing misfolded proteins. In addition to these traditional degradation pathways, a novel mechanism of protein translocation has also been discovered.

In the condition of acute ER stress, certain secreted and membrane proteins are directly rerouted into the cytosol for proteasome-mediated degradation (104). This process, termed preemptive quality control, is signal sequence-dependent and reduces the burden of misfolded proteins entering the ER lumen.

Given the causal connection between protein misfolding and human disease, it is important to understand the role of ERAD in mammalian physiology. Although evidence points to the activation of the UPR in target tissues affected by obesity and diabetes, the importance of the ERAD mechanism in the pathophysiology of metabolic disease has not been extensively investigated. SEL1L is an ER membrane protein with a complex structure that enables it to confer many versatile functions. The cellular functions of SEL1L have been explored in a wide range of species, from *C. elegans* to *A. thaliana* to human cell lines.

1.5 SEL1L Protein Structure

SEL1L, or *Suppressor-Enhancer-Lin-12-1-Like*, is the mammalian ortholog of the *Sel-1* gene in *C. elegans*. It was originally identified in a genetic screen as a negative regulator of Notch (*Lin-12*) signaling, a pathway that specifies cell fate and directs differentiation (105). The human *SEL1L* gene is located on chromosome 14q24.3-q31 and consists of 21 exons, ultimately encoding a 794-amino acid full-length protein. This region of chromosome 14 includes only five other protein-coding genes, and *SEL1L* is at the boundary of a so-called "gene desert area" (106). The evolutionary origin and functional significance of these large areas devoid of genes is mostly unknown. Some evidence suggests that gene deserts resist chromosomal rearrangements and contain multiple distant

regulatory elements physically linked to their flanking genes, allowing the integrity of SEL1L's structure and function to be maintained (107). The evolutionary importance of *SEL1L* is demonstrated in its high cross-species conservation. Its primary sequence is conserved in bacteria and yeast, but advanced structural complexity of gene during evolution suggests a divergence in its function (108).

At the protein level, the human SEL1L shares 99% amino acid identity with chimpanzee, 97% with dog, and 93% with mouse. Although similarity to *A. thaliana* and *S. cerevisiae* is lower, the protein structure still shares strict amino acid identity at the C-terminal region in these species. The protein structure of SEL1L contains several unique domains that most likely contribute to its potentially diverse functions *in vivo* (demonstrated in Figure 1.4).

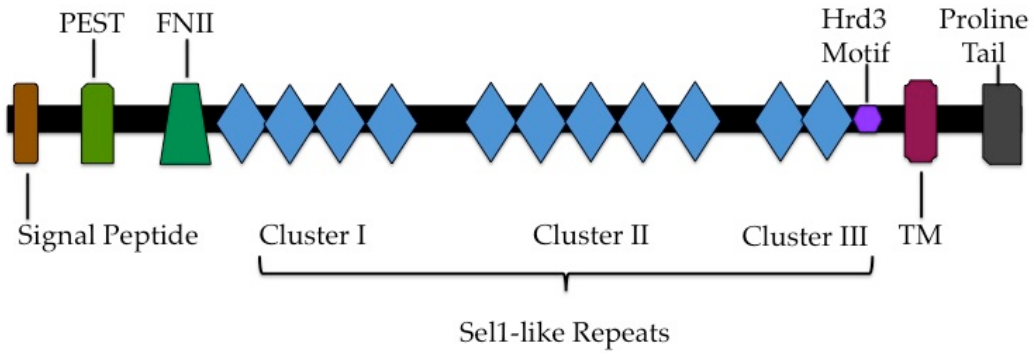

Figure 1.4: SEL1L Protein Structure. The SEL1L protein in multimodular, with protein-protein interactions reinforced by the fibronectin type II domain (FNII), the Sel1-like repeats, and the proline tail. The Sel1-like repeat clusters and the Hrd3 motif are conserved in lower organisms.

The N-terminal end of SEL1L contains a fibronectin type II domain (FNII). Aside from fibronectin, this collagen-binding domain is also found in a range of proteins, including blood coagulation factor XII, bovine seminal plasma proteins, and mannose-6-phosphate receptor (109, 110). This domain also enables binding

to heparin, DNA and actin. It is not conserved in SEL1L invertebrate orthologs and only appears in the chordate lineage, indicating that this domain likely confers a new function for the full-length protein in higher organisms (106). Another distinct feature of the SEL1L structure is a set of three tandem clusters of SEL-1-like repeats. These repeats are a subtype of tetratricopeptide repeats (TPR), which contain two antiparallel alpha-helices. TPR motifs in a series generate a right-handed helical structure with an amphipathic channel that might accommodate the complementary region of a target protein (111). These units can mediate protein-protein interactions and have proven to play essential roles in protein folding, protein transport and cell cycle regulation. The Sel1-like repeats are highly conserved in SEL1L's taxonomic evolution. Adjacent to the last repeat cluster, towards the C-terminal end of the protein, is the Hrd3-like motif. This motif was originally found in the yeast Hrd3p protein, which acts at the ER membrane as an E3 ubiquitin ligase (as described previously). It is the most highly conserved motif in the SEL1L protein sequence. At the C-terminal end is a proline-rich motif, which also serves the function of making protein-protein interactions more favorable. This motif can facilitate intermolecular interactions such as signal transduction, cell-to-cell communication, and cytoskeletal organization (112). Other notable sequences in the SEL1L protein include a cleavable signal peptide, a PEST sequence (target for rapid degradation), an ER membrane-localization signal, and a transmembrane domain.

Existing experimental evidence points to at least five SEL1L isoforms, likely resulting from alternative splicing events in the full-length mRNA. SEL1LA corresponds to the full-length protein structure depicted in Figure 1.4,

which localizes at the ER. Two variants of SEL1LA have recently been identified and designated p38 and p28. Studies in breast cancer carcinoma cell lines indicate that these N-terminal derivatives are also responsive to ER stress, but localize at endosomal vesicles (113). Isoforms SEL1LB and –C retain most of the N-terminal region of the protein, including the FNII domain and part of the SEL-1-like repeats. Studies in human cell lines demonstrate that both of these isoforms are secreted glycoproteins, also found in secretory and degradative compartments and areas of cell-to-cell contact (114). SEL1LD includes only the evolutionarily conserved Hrd3 motif and the transmembrane domain, while –E is a further truncated version of SEL1LB/C (106).

1.6 SEL1L Expression and Function

SEL1L immunohistochemical staining in both human fetal and adult tissues illustrates the ubiquitous expression of SEL1L throughout the whole organism (115). However, staining appears to be most intense in protein-secreting cells of mostly endocrine tissues. These tissues include the breast, prostate, salivary gland, thyroid, and pancreas (both acinar and endocrine cells). Analysis of SEL1L expression in fetal tissues also shows strong neuroepithelial staining at an early stage of human development (6-7 weeks). At later stages of development, SEL1L expression transitions to protein-secreting structures such as the liver and pancreas (106).

As a constituent of ERAD, this role of SEL1L has been extensively studied in lower organisms and mouse and human cell lines. For example, in *C. elegans*, RNAi-mediated knockdown of sel-1 results in the upregulation of GRP78 in an xbp1-dependent manner (116). Conversely, pancreatic islets from *Akita* mice,

with constitutive expression of misfolded insulin, show an upregulation of both HRD1 and SEL1L in comparison to wild-type mice (117). Molecular and biochemical analyses in mammalian cell lines have led to the development of an advanced ERAD model, operating at the interface of the ER and cytosol (91, 118). SEL1L most likely participates in the retrotranslocation of misfolded proteins by associating with HRD1 and facilitating the movement and ubiquitylation of ERAD substrates. This function is represented in Figure 1.5:

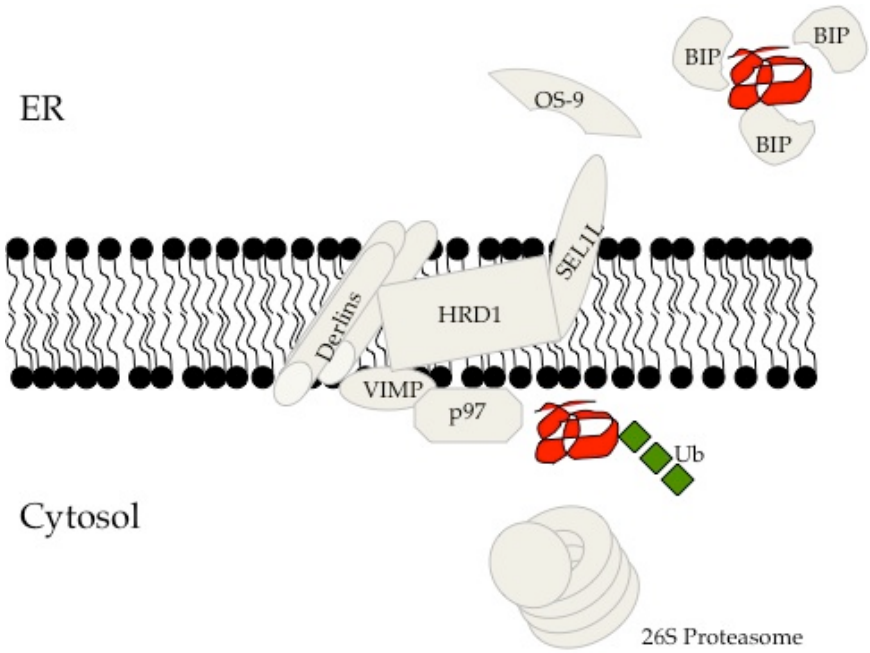

Figure 1.5: The Role of SEL1L in the Retrotranslocation of Misfolded Proteins: Molecular and biochemical analyses implicate a role for SEL1L at the translocation step of ER-associated degradation (ERAD). It nucleates the complex responsible moving misfolded proteins from the ER lumen and into the cytosol. It is associates with the E3 ubiquitin ligase, HRD1, the derlin family of proteins, and OS9.

Although evidence mostly suggests that ERAD is the primary function of SEL1L, other studies have highlighted its potential role in proliferation and

consequently in cancer. This function could be modulated by its interaction with Notch or by involvement in the TGFβ pathway (119).

1.7 SEL1L and Disease

A significant downmodulation of SEL1L expression was seen in breast cancer and pancreatic cancer, both *in vivo* and *in vitro*, suggesting that it may have tumor suppressor activity (120, 121). Histopathalogical analysis also revealed that SEL1L is a predictive marker for cell transformation, from adenoma to carcinoma, in cancers of the esophagus, breast, pancreas, prostate, lung and colon (122-126). An increase in its expression at this stage may be a mechanism by which cancerous cells enhance their survival and ability to cope with protein synthesis. With regard to neurological disorders, a polymorphism in *SEL1L* intron 3 is linked to susceptibility to Alzheimer's Disease in Italian patients, while a homozygous mutation in a highly conserved Sel1-like repeat is associated with early-onset cerebellar ataxia in Finnish hounds (127, 128). The latter association is also correlated to an elevation of ER stress markers in the cerebellum of affected dogs.

The *SEL1L* gene can also be indirectly associated with liver and pancreatic diseases due to its promoter activity. Two transcriptional regulators, hepatocyte nuclear factor-1α and -4α (HNF), are considered master regulators of hepatocyte and islet transcription and specifically bind the *SEL1L* promoter in these cell types. Mutations in these factors are seen in patients with mature-onset diabetes of the young (MODY), a monogenic and rare form of diabetes (129).

1.8 Research Goal

In summary, the molecular mechanisms of T2D are incompletely understood. Increasing evidence suggests that ER stress plays an important causative role in the development of insulin resistance and β-cell dysfunction, two essential characteristics of T2D. A better understanding of the UPR and ERAD pathways, key cellular adaptive mechanisms to ER stress, would likely lead to new strategies for the treatment of T2D and other diseases associated with misfolded proteins. Interestingly, SEL1L is highly expressed in tissues involved in the pathogenesis of T2D, namely the liver, pancreas, and brain. However, the *in vivo* function of SEL1L remains unknown. Therefore, the overarching aim of this dissertation is to determine the physiological role of SEL1L in the whole organism , with emphasis on glucose and energy balance. In order to address this, our lab has developed two mouse models. The first is a *Sel1L* global knockout generated by a targeted gene trap insertion (Figure 1.6). The second exhibits *Cre*-mediated recombination of a floxed (Flanking lox P sites) *Sel1L* allele (Figure 1.7). The characterization of these models has provided invaluable insight into the genetic basis of T2D and a possible cause of cellular dysfunction in this disease state.

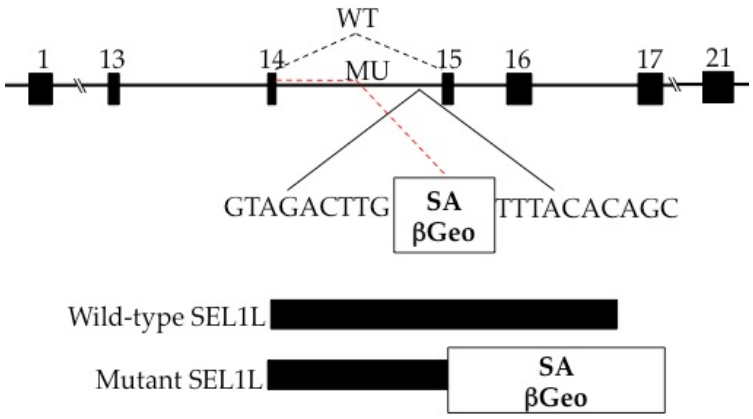

Figure 1.6: The Global *Sel1L* Knockout Mouse Model. The first mouse model for *Sel1L* was generated through the insertion of a gene trap in intron 14. The gene trap consists of a splicing acceptor (SA) attached to β-galactosidase and neomycin cassette (β-Geo). The mutant mice express a truncated version of the SEL1L protein conjugated to β-galactosidase, due to abnormal splicing.

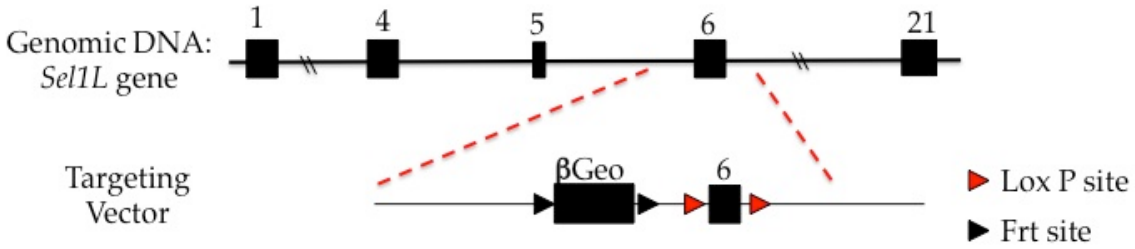

Figure 1.7: The Conditional *Sel1L* Knockout Mouse Model. These mice contain a targeting vector with lox P recombination sites flanking exon 6 of the *Sel1L* gene. The vector also contains a β-galactosidase and neomycin cassette (β-Geo) for selection, flanked with frt recombination sites. Once the target vector is integrated into the genomic DNA, the selection cassette is removed by crossing with mice overexpressing the *Flp* transgene. After, crossing with mice over-expressing the *Cre* transgene in particular tissues will disrupt *Sel1L* gene expression.

The second chapter will focus on the biological importance of *Sel1L* and its function in degradation of misfolded proteins during development. Next, I will elucidate a critical role for SEL1L in insulin secretion. In the fourth chapter, I will

explore the role of ERAD in the neuronal pathways that regulate food intake and body weight. Finally, I will propose a model for the role of ER stress in the pathogenesis of T2D and targets for a clinical approach to treat this potentially fatal and costly disease.

CHAPTER 2: THE ROLE OF *Sel1L* IN MOUSE EMBRYONIC DEVELOPMENT

2.1 Abstract

The mouse and human *Suppressor-Enhancer-Lin-12-1-Like* (*Sel1L*) gene encodes a structurally complex protein with exceptionally high expression in the adult pancreas and central nervous system. Evidence from *in vitro* studies in lower organisms implicates a role for SEL1L in ERAD, a proteosome-mediated pathway induced by the accumulation of terminally unfolded or misfolded proteins in the endoplasmic reticulum (a condition referred to as ER stress). However, its physiological role in the whole organism remains elusive. The Long lab has generated mice carrying a gene trap insertion in intron 14 of the *Sel1L* gene. Mice homozygous for the mutation ($Sel1L^{-/-}$, mutant) die during mid-gestation, with increased apoptosis in the liver and central nervous system. Furthermore, electron microscopy revealed distention and fragmentation of the ER and altered ultrastructural morphology in the $Sel1L^{-/-}$ embryonic liver. Mouse embryonic fibroblasts (MEFs) derived from embryonic day 12.5 were used to further characterize the cellular phenotypes of the *Sel1L* mutants. The proliferation of $Sel1L^{-/-}$ MEFs was significantly reduced as compared to the $Sel1L^{+/+}$ (wild-type) and $Sel1L^{+/-}$ (heterozygous) MEF counterparts. Pharmacological challenge of the MEFs with tunicamycin, an *N*-glycosylation inhibitor, revealed that $Sel1L^{-/-}$ MEFs are sensitive to ER stress, and exhibit decreased cell viability in comparison to $Sel1l^{+/+}$ MEFs. Finally, immunoblot and immunocytochemical analyses indicated $Sel1L^{-/-}$ MEFs have a compromised ability to degrade misfolded proteins. Together, these results suggest that *Sel1L* is

critically required for maintaining ER homeostasis during mouse embryonic development.

2.2 Introduction

The endoplasmic reticulum (ER) maintains an ideal environment for protein folding, maturation and transport. This is achieved by the collective function of chaperones, glycosylation enzymes, and reductases within the ER lumen. Additionally, a sophisticated quality control system exists in the ER to retrieve improperly folded proteins (130). This system ensures that misfolded proteins are retained in the ER for further folding cycles, or targeted for proteasome-mediated degradation in the cytosol. Despite these optimal conditions for protein folding, the load of protein entering the ER lumen can exceed its folding capacity. Alterations in ER homeostasis lead to an accumulation of misfolded or unfolded proteins, a condition termed "ER stress."

There are many physiological and environmental causes of ER stress, including oxidative stress, glucose deprivation, viral infection, and genetic mutations (131). To cope with this intracellular disturbance, eukaryotic cells employ a highly conserved pathway, known as the unfolded protein response (UPR), to restore homeostasis. The UPR is mediated by three ER membrane-associated proteins, PERK, IRE1α, and ATF6α, which ultimately affect changes in gene expression in response to ER stress (132). PERK phosphorylates eIF2α to attenuate protein translation and decrease the load of protein entering ER. Phosphorylated eIF2α also selectively stimulates ATF4 translation to induce transcriptional regulation of UPR genes. IRE1α cleaves XBP1 mRNA to a spliced form that acts as a transcription factor to upregulate UPR genes encoding factors

involved in ER protein folding and degradation. ATF6α traffics to Golgi for cleavage by S1P and S2P to release a nuclear form of ATF6α that works synergistically or separately with XBP1s to regulate UPR gene expression (26).

UPR signaling pathways therefore converge to give rise to several general outcomes to attenuate ER stress. They include an increase in the transcription of chaperones, a decrease in overall translation, and enhanced ERAD. ERAD is part of the cell's normal quality control surveillance system, but essentially works in coordination with other UPR processes to maintain ER homeostasis. In fact, induction of the UPR increases ERAD capacity, and ERAD efficiency requires an intact UPR (133). During ERAD, chaperones in the ER recognize terminally misfolded proteins and target them to machinery at the interface of the ER and cytosol, known as the translocon. The translocon then ubiquitylates the substrate and provides energy for its extrusion into the cytosol, where it is a target for proteasome-mediated degradation (78).

Misfolded proteins are associated with a host of diseases, including pulmonary emphysema, cystic fibrosis, Alzheimer's Disease, and diabetes (134). This affirms the essential role of both the UPR and ERAD in normal physiology. ERAD factors have been identified through genetic and biochemical approaches, many conserved from yeast to humans. Of particular interest is the Suppressor-Enhancer-Lin-12-1-Like (SEL1L) protein, an ER transmembrane protein that nucleates the ERAD translocation machinery and interacts with components such as HRD1 (E3 ubiquitin ligase) and OS9 (substrate delivery to the translocon) (91, 118) . Evidence from yeast, *Arabidopsis thaliana*, and human embryonic kidney 293 cells indicate that there is increased expression of the *Sel1L* transcript

during ER stress conditions (93, 135, 136). Furthermore, this upregulation is downstream of IRE1 and ATF6 activation.

In humans, SEL1L appears to be highly expressed in the pancreas and central nervous system (106). Its multimodular protein structure enables it to have numerous potential functions, particularly those requiring protein-protein interactions. Yet the physiological role of SEL1L is mostly unknown. To determine this, the Long lab at Cornell University has developed the first knockout model for *Sel1L* (137). This model uses a gene trap insertion, consisting of a splice acceptor fused to a β-galactosidase-neomycin (β-geo) cassette, between exons 14 and 15 of the *Sel1L* gene. Therefore, the disrupted transcription results in a truncated SEL1L protein fused with β-geo in the mutant mouse ($Sel1L^{-/-}$). Heterozygous mice ($SelL^{+/-}$) show no observable phenotypic difference in comparison to wild-type mice ($Sel1L^{+/+}$), and were used in mating to generate mutant mice. From these matings, no live $Sel1L^{-/-}$ mice were produced, suggesting the homozygous mutation is embryonically lethal in mice. Based on genotyping and morphological characterization at various embryonic stages, it was determined that nearly half of the $Sel1L^{-/-}$ mice are not alive by embryonic day 11.5 (E11.5) (137) . Thus, SEL1L is essential for mouse embryonic development.

Based on the previous evidence regarding SEL1L function, we speculate that the loss of SEL1L will disengage cellular ERAD, and therefore an entire arm of the UPR process. In order to understand the *in vivo* function of SEl1L during development, the embryological phenotype of the $Sel1L^{-/-}$ mice was characterized using cellular, biochemical, and molecular techniques.

2.3 Materials and Methods

Mice

The *Sel1L* global knockout mice were generated by a gene trap insertion (SA-β-geo-polyA) between exons 14 and 15 of chromosome 12. The gene-trapped mouse embryonic stem cell line, CA0017 (Sanger Institute Gene Trap Resource), was microinjected into C57BL/6 blastocysts. The resulting chimeric male founders were backcrossed to C57BL/6 females to generate heterozygous mice. *Sel1L*$^{+/-}$ mice were then intercrossed to generate homozygous *Sel1L*$^{-/-}$ embryos. The following primers were used for genotyping the embryos and mice: F1-*Sel1L*, 5′-TGGGACAGAGCGGGCTTGGAAT-3′; R1-*Sel1L*, 5′-CACCAGGAGTCAAAGGCATCACTG-3′; R-βGeo, 5′-ATTCAGGCTGCGCAACTGTTGGG-3′. All animal experiments were performed in accordance with the Cornell Animal Care and Use Guidelines.

TUNEL Assay

Embryos were dissected from pregnant females at E12.5 and fixed overnight in 4% PFA/PBS. The next day, they were washed several times with phosphate-buffered saline (PBS) and stored overnight in a 30% sucrose/PBS solution. The following day, they were embedded in OCT and frozen on dry ice before subsequent storage at -80°C. Staining was performed according to instructions for the Chemicon International Apoptog Peroxidase *In Situ* Apoptosis Detection Kit S7100 (Millipore Corporation). The ImmPact DAB peroxidase kit (Vector Technologies) was used as the substrate, and a

hemotoxylin counterstain (Gill's, diluted 1:10) was applied. Results were visualized using light microscopy.

Transmission Electron Microscopy

Embryos were dissected from a pregnant female at E12.5. Using a dissection microscope, the livers from each embryo were removed and fixed in Karnovsky's Fixative Mix (EMS technologies: 2% PFA, 2.5% Glutaraldehyde, 0.1 M Na-phosphate buffer) at 4° for 3 hours, then washed with the Na-phosphate buffer, 3 X 10 minutes. Post-fixation in 1% osmium tetraoxide, sectioning, and additional post-fixation in uranyl acetate were done by the Electron Microscopy and Histology Core Facility, Department of Cell and Molecular Biology, Weill Cornell Medical College for. Image capturing was performed using the JOEL 100CX-II transmission electron microscope.

Mouse Embryonic Fibroblast (MEF) Cell Lines

To establish MEF cell lines from each genotype, embryos were dissected at E12.5–E13.5 of gestation and homogenized in 1 ml of MEF media (Dulbecco's modified Eagle's medium with 10% fetal bovine serum, 1% sodium pyruvate, 1% Glutamax, and 1% Pen-Strep). The homogenate was plated in a 6-cm dish with 5 ml of media and cultured overnight. The next day, cells were passaged 1:1 to remove any large, dead debris. Cells were then split 1:3 every 2–3 days. To establish immortalized MEF cell lines, primary MEF cells of defined genotypes were maintained at 80–90% confluency in 10-cm dishes for two to three months. To generate the growth curve, MEFs were plated at a density of 2 X 10^4 cell/well

in a 6-well plate and collected for counting using a hemocytometer 2, 4, and 6 days after plating.

Crystal Violet Assay

Cell viability using the crystal violet assay was performed essentially as described (138). Briefly, MEFs from *Sel1L*$^{+/+}$ and *Sel1L*$^{-/-}$ embryos were plated at a density of 2 X 10^5 cells per genotype in a 6-cm plate. The next day, they were treated with 2 μg/ml tunicamycin (TM) for 0, 1, 2, or 4 hours. After treatment, MEFs were trypsinized and re-plated into 10-cm plates and grown for 5 days in normal MEF media. Then, the media was removed and 1 ml of crystal violet (0.2% w/v in 2% ethanol) was added to each plate. Stained MEFs were solubilized with 600 μl of 1% SDS, and absorbance of the resulting solution was measured at 570 nm. Relative cell viability was calculated as a percentage of absorbance of TM-treated cells relative to that of non-TM treated cells.

Expression Plasmids, MEF Cell Transfection, and Cycloheximide-Chase Assay

The pNHK-GFP fusion expression plasmid was a kindly provided by Dr. Nobuko Hosokawa of Kyoto University. The full-length (FL) and dominant-negative SEL1L-GFP fusion constructs were generated by PCR amplification of the corresponding *Sel1L* cDNA fragments followed by subcloning into the EcoRI and BamHI sites in pEGFP-N2 vector (Clontech). The PCR primers used to amplify the full-length and 5′ portion *Sel1L* cDNA fragments were: F2-Sel1l, 5′-GAATTCCGCCACCATGCAGGTCCGCGTCAGG-3′; R2-Sel1l, 5′-GGATCCtCTGTGGTGGCTGCTGCTC-3′; R3-Sel1l, 5′-GGATCCTAACTTGAACGCCTCTTCC-3′. The expression of fusion proteins was

verified by GFP fluorescence microscopy in transfected HEK293 cells. MEFs of defined genotypes were seeded at a density of 500,000 cells/well in 6-well dishes. The next day, MEF cells were rinsed twice with PBS, once with Opti-MEM reduced serum medium (Invitrogen), and incubated with 1 ml of Opti-MEM reduced serum medium containing 3 μg of expression plasmid encoding GFP-tagged NHK (for co-transfection, 3 μg of each expression plasmid was used) and 2 μl of polyethylenimine. After incubation for 12-16 hours, the transfection media was removed, and cells were treated with 50 μg/ml of cycloheximide in normal media for 0, 1.5, 3, 4.5 or 6 hours. MEF cell lysates were prepared by adding 100 μl of RIPA buffer to each well, then using a cell scraper for collection. BCA was used for protein quantification of each lysate. For western blotting, 20 μg of each lysate was mixed with an equal volume of 2X sample buffer (100 mm Tris, 25% glycerol, 2% SDS, 0.01% bromphenol blue, 10% 2-mercaptoethanol), boiled for 5 min and loaded into a 9% SDS-PAGE gel. Electrophoresis, blotting, and antibody probing were performed using standard procedures (139). Immunodetection was done using the Pierce ECL Western Blotting Substrate according to the manufacturer's specifications. GFP (Abcam) and tubulin (Cell Signaling) antibodies were used at 1:5,000 and 1:10,000, respectively).

2.4 Results

2.4.1 *Sel1L*$^{-/-}$ embryos show upregulation of UPR markers and increased apoptosis in the central nervous system

TUNEL staining, as an indicator of apoptosis, was performed using frozen sections of *Sel1L*$^{-/-}$ and *SelL1*$^{+/+}$ embryos isolated at embryonic day 12.5 (E12.5). At

this stage of mouse development, the expression of SEL1L is particularly high in the neural tube and dorsal root ganglia (106). As shown in Figure 2.1, significantly more TUNEL-positive cells (indicated the black arrows) were detected in the forebrain and dorsal root ganglia of the *Sel1L*$^{-/-}$ embryo than in the *Sel1L*$^{+/+}$ embryo.

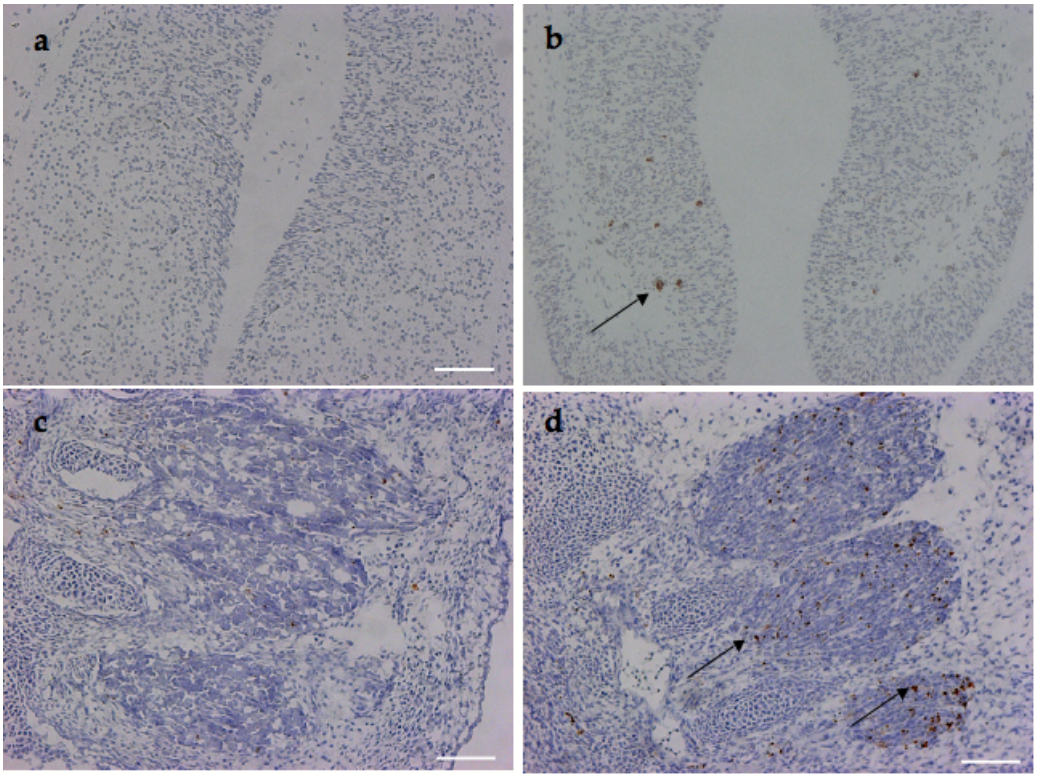

Figure 2.1: *Sel1L*$^{-/-}$ embryos show increased apoptosis in comparison to *Sel1L*$^{+/+}$ embryos. TUNEL assay for apoptosis in the forebrain (a,b) and dorsal root ganglia (c,d) of *Sel1L*$^{+/+}$ (a, c) and *Sel1L*$^{-/-}$ (b, d) E12.5 embryos (10X magnification). Seen in Figure 3 of (137).

Quantitative RT-PCR with *Sel1L* embryos also revealed an upregulation of several UPR markers in the *Sel1L*$^{-/-}$ embryo (137). These results indicate that the absence of *Sel1L* ultimately leads to apoptosis in localized regions of the brain. We speculated that the probable cause of this apoptosis in the mutant embryo is

the ER stress generated by the accumulation of misfolded proteins that are unable to be degraded due to lack of *Sel1L*.

2.4.2 The endoplasmic reticulum in the *Sel1L*$^{-/-}$ embryonic liver shows a distorted morphology

The liver is the largest internal organ in the mouse embryo, and has essential metabolic, endocrine, and exocrine functions. As a productive organ in terms of relative protein synthesis and secretion, it is highly susceptible to ER stress and the UPR. During mouse development, the mouse liver bud undergoes accelerated growth between E9.5 and E15 (140).

To determine if SEL1L-deficiency causes morphological changes in the ER of mouse embryonic cells, the liver bud was isolated from E12.5 *Sel1L*$^{-/-}$ and *Sel1L*$^{+/+}$ embryos for electron microscopic observation. The images, shown as Figure 2.2, revealed the mutant liver ultrastructure is distorted in comparison to the wild-type liver ultrastructure.

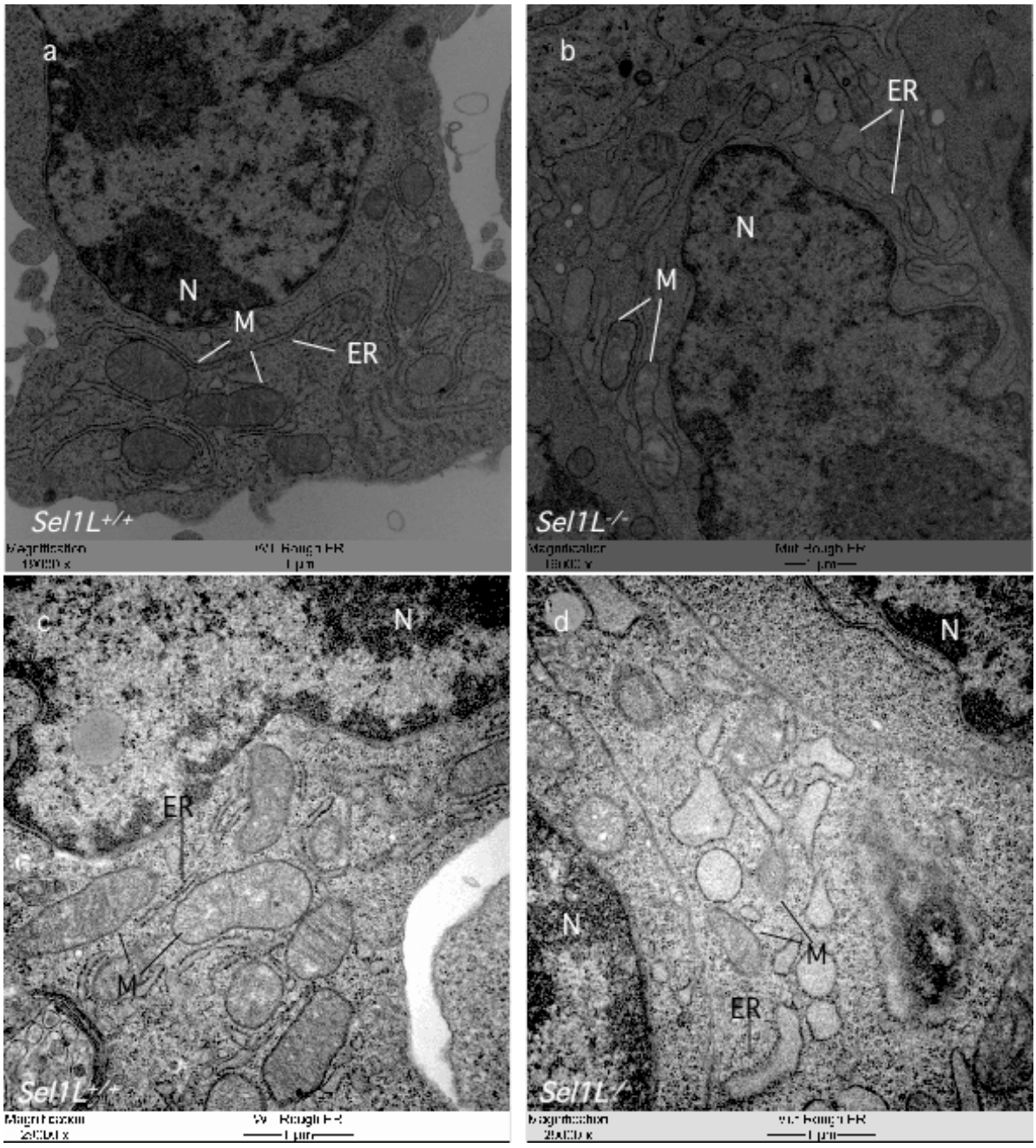

Figure 2.2: The endoplasmic reticulum in the *Sel1L*$^{-/-}$ embryonic liver shows a distorted morphological ultrastructure. Electron microscopy of *Sel1L* embryonic liver buds with, (a) *Sel1L*$^{+/+}$ embryonic liver, 19000X (b) *Sel1L*$^{-/-}$ embryonic liver, 19000X (c) *Sel1L*$^{+/+}$ embryonic liver, 29000X (d) *Sel1L*$^{-/-}$ embryonic liver, 29000X. Seen in Figure 2 of (137). N= Nucleus, ER= Endoplasmic reticulum, M= Mitochondria

The *Sel1L*$^{-/-}$ hepatocytes (2.2b and 2.2d) exhibited distention of the endoplasmic reticulum membranes and had mitochondria that are deformed and appeared less abundant than in the *Sel1L*$^{+/+}$ hepatocytes (2.2a and 2.2c). Alterations of ER morphology are another indication of the presence of ER stress. The changes in mitochondrial numbers and morphology further suggest that sustained ER stress may cause pivotal changes in the mitochondrial structure that go on to mediate proapoptotic signaling (141).

2.4.3 *Sel1L*$^{-/-}$ MEFs exhibit growth retardation and decreased cell viability

Mouse embryonic fibroblasts (MEFs), derived from E12.5 *Sel1L* embryos, allow the extrapolation of the function of *Sel1L* in growth and development in an *in vitro* model. The growth curve for the primary *Sel1L* MEFs (Figure 2.3) indicated that within two days of plating, the *Sel1L*$^{-/-}$ MEFs show significantly slower growth than both the *Sel1L*$^{+/+}$ and *Sel1L*$^{+/-}$ MEFs. The *Sel1L*$^{+/-}$ MEF growth phenotype is similar to that of the *Sel1L*$^{+/+}$ MEF phenotype, and a minor difference was observed between the two genotypes over the six-day growth period. The cause of growth retardation in *Sel1L*$^{-/-}$ MEFs is currently unknown but could be attributed to the activation of the translational attenuation pathway of the UPR. Although the interplay between ERAD and other pathways is poorly defined, endogenous ER stress due to a defective ERAD pathway can compromise the growth of the cell as protein aggregation increases.

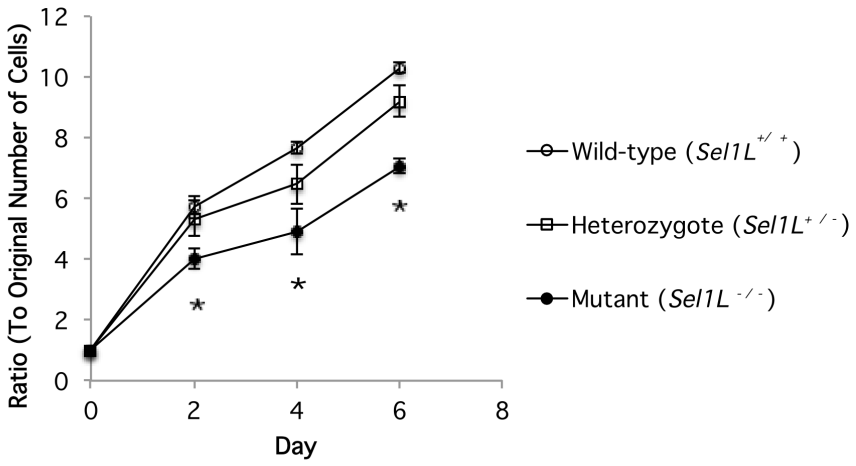

Figure 2.3: *Sel1L*$^{-/-}$ MEFs show growth retardation in comparison to their *Sel1L*$^{+/+}$ MEF counterparts. These are growth curves of *Sel1L* primary MEFs (E12.5) for each genotype. MEFs were isolated and seeded at a density of 2 X 10^4 cells per well in a 6-well plate (Day 0). *, $p<0.01$, mutant versus wild-type (n=3 independent experiments).

Immortalized MEFs were developed from the primary cell culture and used to analyze the MEF response to exogenous stress. *Sel1L*$^{-/-}$ MEFs and *Sel1L*$^{+/+}$ MEFs were treated with tunicamycin (TM, 2 μg/ml) for up to 4 hours (Figure 2.4a). Tunicamycin induces ER stress by blocking N-linked glycosylation of newly synthesized glycoproteins, thus causing an accumulation of improperly folded proteins within the lumen of the endoplasmic reticulum (138). The *Sel1L*$^{-/-}$ MEFs displayed a sharp decrease in cell viability over time in comparison to the *Sel1L*$^{+/+}$ MEFs, as quantified by a crystal violet assay. Thus, *Sel1L*$^{-/-}$ MEFs are more susceptible to exogenous ER stress than *Sel1L*$^{+/+}$ MEFs. Although the 0 hour time point for the mutant MEFs was originally less viable than its wild-type counterpart, the percent viability seen in Figure 2.4b was calculated as a ratio of the absorbance of the ER-stressed samples (1, 2, 4 hour) to the non-ER-stressed samples (0 hour).

a

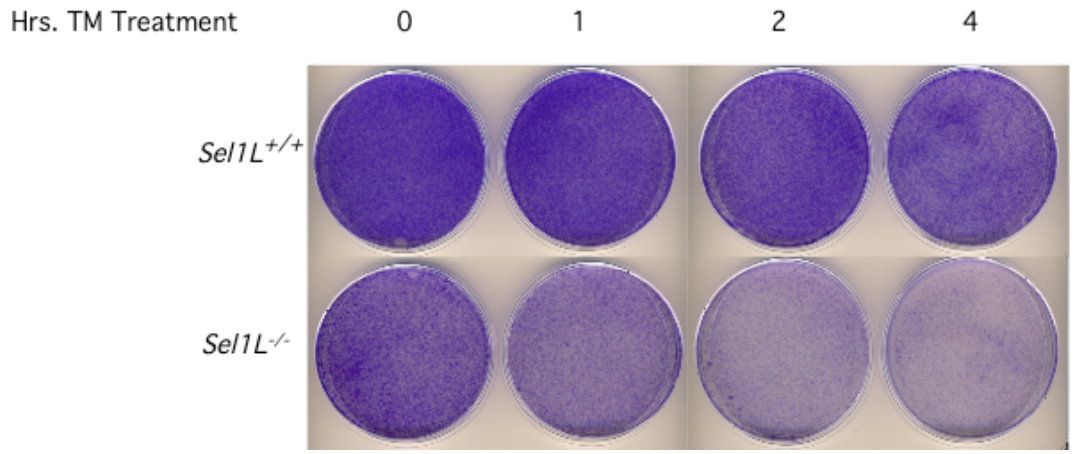

b

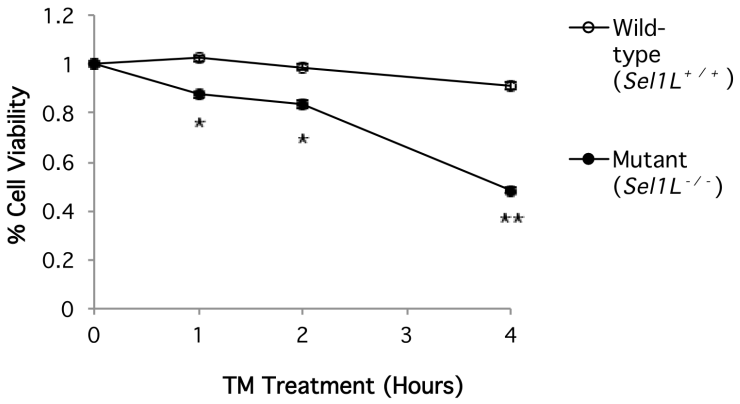

Figure 2.4: *Sel1L*$^{-/-}$ MEFs have decreased cell viability in response to TM. Shown is the response of *Sel1L* MEFs to tunicamycin (TM), with hours of TM treatment (2 μg/ml). (a) An equal number of E12.5 MEFs (2 X 10^5) from each genotype were plated in 6 cm dishes and treated with TM for the indicated periods of time. After incubation with TM, cells were trypsinized and re-plated in 10 cm dishes and grown for 5 days. Then, cells in each plate were stained with the crystal violet stain for viable cell nuclei and (b) quantified after solubilization in 1% SDS and spectrophotometer reading (at 570 nm). Relative cell viability at each time point was calculated as a percentage of the non-TM-treated plates (0 hour time point) for each genotype. *, $p<0.01$, **, $p<0.001$ (n= 3 independent experiments). Seen in Figure 3 of (137).

2.4.4 *Sel1L*$^{-/-}$ MEFs have an impaired ability to degrade misfolded proteins

Null Hong Kong (NHK) is an α_1-antitrypsin variant. As a terminally misfolded protein, it has been well established in literature as a known substrate of ERAD (142). To assess if *Sel1L*$^{-/-}$ cells have a reduced ability to dispose misfolded proteins, we transfected *Sel1L*$^{-/-}$ MEFs with an NHK-GFP expression plasmid and performed cycloheximide-based protein chase (cycloheximide is a translational inhibitor in eukaryotic cells). Western blot analysis indicated that the *Sel1L*$^{-/-}$ MEFs show retention of the misfolded protein, while there was a normal physiological degradation of it in the *Sel1L*$^{+/+}$ MEFs (Figure 2.5a). These results are recapitulated with *Sel1L*$^{-/-}$ MEFs which are co-transfected with either a plasmid expressing a truncated *Sel1L* (dominant-negative) or full-length *Sel1L*. Again, there was an impaired degradation of NHK when it is co-transfected with the truncated construct, but this phenotype is rescued by expression with the full-length construct. Live imaging of the NHK-GFP fluorescence also reinforced this pattern in the *Sel1L*$^{-/-}$ and *Sel1L*$^{+/+}$ MEFs (Figure 2.5b).

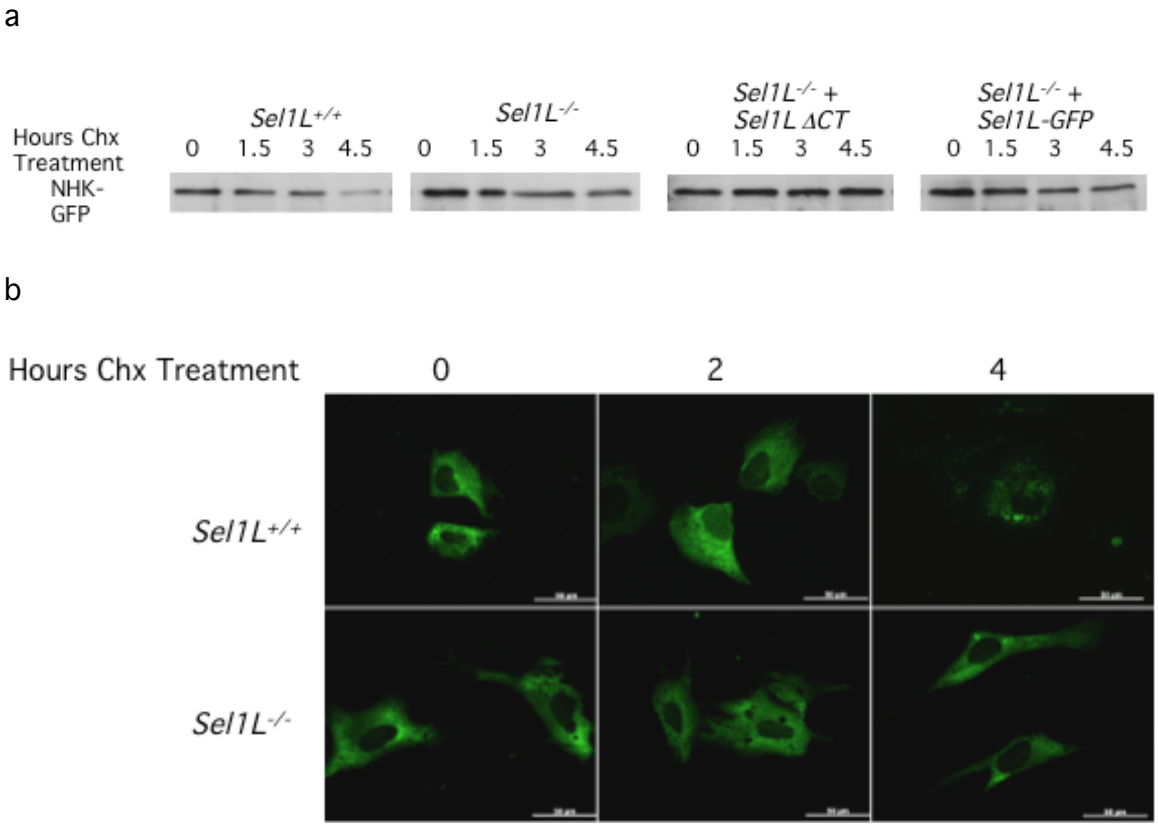

Figure 2.5: *Sel1L*$^{-/-}$ MEFs have an impaired ability to degrade misfolded proteins. (a) From left to right, transfection of NHK-GFP and GFP in wild- type MEFs, mutant MEFs, mutant MEFs co-transfected with a truncated *Sel1L* variant, and mutant MEFs co-transfected with full-length *Sel1L*. (b) Degradation of NHK-GFP in *Sel1L* MEFs, seen with fluorescent microscopy, 40X magnification; NHK = Null Hong Kong Antitrypsin Variant; Chx = Cycloheximide (translational inhibitor)

2.5 Discussion

Here, we report the first *in vivo* functional analysis of SEL1L. Using a gene-trapped mouse model that disrupts gene and protein expression, we find that a homozygous mutation in *Sel1L* causes early gestational lethality. This is the first evidence indicating that *Sel1L* is required for mammalian development. Furthermore, the embryonic deficiency of SEL1L was shown to increase the expression of UPR markers, induce apoptosis in the central nervous system, cause ER stress in the liver, and reduce cell growth and cell viability. The likely

cause of this systemic phenotype is an impaired degradation pathway in embryonic cells, preventing the extrusion of misfolded proteins from the ER lumen. Taken together, these results suggest that SEL1L is necessary for overall ER homeostasis during mouse embryonic development.

This gene trap insertion in *Sel1L* results in the deletion of the carboxyl-terminal end of the SEL1L protein. This mutation eliminates several highly conserved motifs and domains in the protein structure, including the Hrd3p motif (also seen in the yeast ortholog) and the transmembrane domain (106). We predict that the gene trap in this model would disrupt SEL1L's function in ERAD, as the protein can no longer localize to the membrane and facilitate degradation. However, we have not confirmed the deletion of all potential isoforms of SEL1L and recognize the possibility of alternative functions for the truncated *Sel1L* allele. Indeed, it has been reported that several other alternative transcripts are derived from alternative splicing of *Sel1L* mRNA (106). Thus, further studies are necessary to completely understand the functions of *Sel1L*.

SEL1L has been proposed to operate at the translocation step of ERAD. It interacts with several other proteins to remove misfolded proteins from the ER lumen and target them for degradation in the cytosol under normal and ER stress conditions (91, 118). *In vivo* and *in vitro* evidence from our mouse model supports this function. First, we show that the absence of *Sel1L* induces the unfolded protein response and apoptotic pathways. Quantitative real-time PCR data collected by Anish Vani, showed that markers such as *Bip*, *Hrd1*, $p58^{IPK}$, and *Erdj3* are upregulated in whole $Sel1L^{-/-}$ embryos (137). These genes are established markers of ER stress because transcriptional regulators of the UPR induce their expression to alleviate the burden within the ER. Immunohistochemistry

detected increased apoptosis in regions of the central nervous system of the *Sel1L*$^{-/-}$ embryos (Figure 2.1). Neurons in the forebrain and dorsal root ganglia undergo massive growth and differentiation during vertebrate development, and rely on protein synthesis for synaptic formation (143). The presence of ER stress in the central nervous system of the *Sel1L*$^{-/-}$ embryo activates the UPR, yet the UPR is unable to successfully adapt and instead initiates apoptotic pathways. Secondly, we showed that in embryonic liver, *Sel1L* is required for maintaining hepatocyte organelle morphology and function. The liver is another organ with a relatively high biosynthetic load during development (and postnatally). *Sel1L*$^{-/-}$ embryonic livers display evident ER stress in electron micrographs, demonstrating that ERAD dysfunction leads to an accumulation of misfolded proteins (Figure 2.2). Thirdly, we show that in mouse embryonic fibroblasts (MEFs), *Sel1L* is required for growth and cell viability in conditions of exogenous ER stress (Figures 2.3 and 2.4). Finally, we have proven that *Sel1L* is required for proper degradation of unfolded proteins. Using a cycloheximide-chase experiment to detect levels of transfected NHK, a known ERAD substrate, we show that there is reduced degradation of the NHK protein in *Sel1L*$^{-/-}$ MEFs over time (Figure 2.5). In other functional data collected by Adam Francisco, mutant MEFs also exhibit impaired secretion as determined by a Guassia Luciferase reporter assay (137). Overall, the presence of ER stress caused by the lack of *Sel1L* affects cellular survival and function. Further studies would be necessary to determine the specific cause of embryological death in this mouse model.

Mouse models of other ERAD components have yielded similar phenotypes to what we have seen with the *Sel1L* global knockout. For example, complete loss of *Hrd1* and *Derlin1* result in embryonic lethality and systemic ER

stress as well (144, 145). Only the *Derlin1*-deficient mice, however, showed obvious growth retardation during development. Loss of other ERAD proteins, such as Derlin3 and Herp, show no effect on embryogenesis and growth in mice. Despite the lack of an overt ER stress-related phenotype, *Herp*-deficient mice display impaired glucose tolerance and susceptibility to brain ischemic injury. Collectively, these mouse models point to a close link between embryogenesis and the quality control of proteins and reinforce the notion that SEL1L functions through interacting with other ERAD components.

The current mouse model, while proven valuable for understanding the role of *Sel1L* in embryonic development, has limitations in dissecting SEL1L function in adult tissues. SEl1L has high expression in the pancreas and the central nervous system, most likely because of the high capacity for protein secretion in these areas. Therefore, SEl1L may be necessary for cell viability and function in the pancreas and brain. ER stress and insufficient secretion, caused by loss of *Sel1L*, could play a role in neurodegenerative disease or metabolic disorders.

To summarize, studies of the first mouse model has shown that *Sel1L* is critical for development. Embryological, *in vitro*, and *in vivo* data implicate the existence of endogenous ER stress and greater susceptibility to exogenous ER stress in $Sel1L^{-/-}$ mice. There is also severely defective degradation of misfolded proteins, and impaired secretion of proteins in *Sel1L*-deficient cells. Therefore, SEL1L is necessary for ER, cellular, and whole organism homeostasis. Future studies regarding the physiological role of SEL1L will likely be carried out using a conditional mouse model to dissect the tissue-specific functions of SEL1L.

CHAPTER 3: THE ROLE OF *Sel1L* IN PANCREATIC β-CELLS AND GLUCOSE HOMEOSTASIS

3.1 Abstract

Suppressor-enhancer-lin12-1-Like (*Sel1L*) encodes a factor present at high abundance in the mature pancreas. As a type I endoplasmic reticulum (ER) membrane protein, SEL1L has previously been implicated in ERAD, a protein quality control process that is crucial for maintaining ER homeostasis. We have reported the first mouse genetic mutation for *Sel1L*, a hypomorphic allele generated through gene trapping. While homozygous mice ($Sel1L^{-/-}$) are embryonically lethal, heterozygous mice ($Sel1L^{+/-}$) are viable and show a normal glucose metabolic profile when fed with a normal diet. We hypothesize that heterozygosity of *Sel1L* may impair the ability of mature β-cells to functionally adapt to increased insulin demand under the condition of insulin resistance. We first tested this hypothesis in a diet-induced obesity model. Male $Sel1L^{+/-}$ mice and their wild-type littermates (10-weeks of age) were fed with a high-fat diet (HFD) for 24 weeks. $Sel1L^{+/-}$ mice showed progressively higher fasting blood glucose levels than their wild-type control mice after 8 weeks of HFD feeding. At the end of the HFD-feeding period, $Sel1L^{+/-}$ mice were glucose intolerant and had an impaired glucose-stimulated insulin secretion (GSIS) as compared to wild-type mice. Pancreatic morphometry indicated that $Sel1L^{+/-}$ mice had a markedly reduced β-cell mass. No observable increase of β-cell apoptosis but a significant decrease in β-cell proliferation was detected in the pancreas of $Sel1L^{+/-}$ mice. Pancreatic islets isolated from $Sel1L^{+/-}$ mice showed elevated expression of unfolded protein response (UPR) markers, indicative of the presence of ER stress.

In vitro experiments using cultured mouse and rat insulinoma cell lines, ectopically expressing a deletion mutant SEL1L, also confirmed these *in vivo* findings. To further investigate the function of SEL1L in the β-cell, we generated conditional *Sel1L*-defecient mice ($Sel^{lox/lox}$) and crossed them with mice expressing *Cre* under the control of the rat insulin II gene promoter (*RIP-Cre*). Mice with *RIP-Cre*-mediated deletion of *Sel1L* ($Sel^{lox/lox}$; *RIP-Cre*) showed elevated blood glucose levels in comparison to control mice ($Sel^{lox/lox}$ and $Sel^{lox/+}$; *RIP-Cre*) by 2 weeks of age. Additionally, $Sel^{lox/lox}$; *RIP-Cre* mice displayed a metabolic phenotype similar to that seen with HFD-fed $Sel1L^{+/-}$ mice. Immunohistochemical analysis of pancreata in $Sel^{lox/lox}$; *RIP-Cre* mice showed no changes in β-cell mass, but instead a pronounced trafficking defect in the proinsulin secretory pathway. Taken together, our *in vivo* and *in vitro* data strongly suggest that SEL1L has a critical functional role in the mature pancreas, most likely through maintaining normal β-cell proliferation and/or function.

3.2 Introduction

Type 2 diabetes (T2D) is an emerging global epidemic, becoming the major health concern of the 21st century. In the United States, over 25 million Americans are diagnosed with T2D and there are alarming increasing trends in the population and the cost of this disease (3). T2D is understood to be a heterogenous disorder characterized by reduced β-cell mass and reduced insulin secretion in the setting of insulin resistance (146). As such, obesity is a well-defined risk factor of T2D. The underlying mechanisms of β-cell loss and dysfunction in obese individuals, leading to the manifestation of T2D, remain

unknown. Accumulating evidence indicates an intracellular stress, localized at the endoplasmic reticulum (ER), may play a causal role in the development of this disease.

The ER is a highly specialized cytoplasmic organelle in which various metabolic signals and pathways are integrated to regulate protein, glucose, cholesterol, lipid and metabolism (147). As a principal site of protein synthesis, and together with the Golgi apparatus, it facilitates the transport and release of correctly folded proteins. Ribosomes attached to the ER membrane translate de novo peptides into the luminal space. Here, chaperones, glycosylation enzymes, and reductases create an optimal environment for proteins to achieve their native conformation. Non-native proteins are retained in the ER lumen and subject to further folding cycles as directed by a stringent "quality control" system (130). This system ensures that misfolded proteins are retained in the ER for further folding cycles, or targeted for proteasome-mediated degradation in the cytoplasm. Various conditions can disturb ER functions, including inhibition of protein glycosylation, a state of hypoxia, changes in calcium balance, impairment of protein transport from the ER to the Golgi, and overexpression of improperly folded proteins. Alterations in ER homeostasis lead to an accumulation of misfolded or unfolded proteins, a condition termed "ER stress." ER stress elicits the unfolded protein response (UPR) as an adaptive mechanism to restore normal ER function (148).

The UPR integrates three primary transduction pathways that transmit signals from the ER to the nucleus. Three indepedent transmembrane sensors initiate each pathway: PERK, IRE1α, and ATF6. The final outcome of this advanced signaling network is the activation of four distinct cellular responses.

The first is transcriptional activation of chaperones to enhance an essential ER function. The second is translational attenuation to decrease the client load of ER lumen proteins. The third is ER-associated degradation (ERAD), where terminally misfolded proteins are retrotranslocated into the cytosol and tagged for degradation at the proteasome. Finally, in the case where these three adaptive outcomes fail to eliminate ER stress, apoptotic pathways are activated (22).

The UPR is known to play an important role in the basic physiology of several cell types, including B cells, hepatocytes and osteoblasts (149). In fact, it is estimated that misfolded proteins constitute upwards of 30% of newly synthesized proteins as determined by a variety of cell types, confirming the UPR as a fundamental cellular process (150). The β-cell is no exception, with its primary function of producing and secreting insulin in response to secretogogue stimulation. In order to fulfill this function, the β-cell must maintain constant synthesis of insulin and its precursor, proinsulin. Accordingly, the β-cell experiences rapid increases in proinsulin synthesis in response to an influx of nutrients (53). Any increase in the biosynthetic load of the β-cell could potentially result in ER stress, thus hindering proper proinsulin folding in the ER, trafficking of proinsulin to the Golgi, and secretion of mature insulin from secretory granules (55). This is particularly the case in T2D, where a state of insulin resistance imposes a biosynthetic burden on the β-cell.

Several mouse models have shown that ER stress in the β-cell recapitulates characteristics of T2D (61-64). Very few, however, have contributed to our understanding of the particular role of ERAD in glucose homeostasis. We have generated and characterized the first mouse model for *Sel1L*, a gene that

encodes a type I ER membrane protein with high abundance in the vertebrate pancreas and central nervous system (137). It has been proposed that SEL1L facilitates protein-protein interactions and nucleates the ERAD machinery at the interface of the ER and cytoplasm (known as the retrotranslocon) (91, 118). This complex in its entirety is responsible for identification, translocation, ubiquitylation, and ultimate degradation of misfolded proteins. Our global knockout demonstrated that a homozygous mutation in *Sel1L* (*Sel1L*$^{-/-}$) causes early gestational lethality. We have also previously shown that the complete elimination of *Sel1L* is associated with endogenous ER stress, a defective ERAD, and cell death (137). Epithelial cells of the *Sel1L*$^{-/-}$ pancreatic bud are unable to grow and differentiate into β-cells in culture (151). However, heterozygous mice (*Sel1L*$^{+/-}$) show no prominent developmental phenotype, and also no obvious metabolic phenotype on a regular chow diet.

Experimental high-fat diets (HFD) have been used to simulate the "Western" diet that induces obesity and the complications that are associated with it, specifically insulin resistance and T2D. The condition of obesity produces ER stress by a global increase in the synthesis of secretory proteins in the body, mechanical stress, abnormalities in nutrient availability, and lipotoxicity (37). We hypothesize that challenging *Sel1L*$^{+/-}$ mice with a HFD will lead to enhanced ER stress in the β-cell in comparison to the wild-type mice on a HFD.

In addition to using a nutritional stress to investigate the specific role of *Sel1L* in the β-cell, we have also generated a conditional mouse model with a β-cell-specific deletion of *Sel1L*. These mice have been engineered using the cre-lox approach and exhibit *RIP-Cre*-mediated recombination of a floxed *Sel1L* allele. By

using this model, we can gain insight into the tissue-specific function of SEL1L in glucose homeostasis under normal or stressed conditions.

3.3 Materials and Methods

Mice

The *Sel1L* global knockout mice were generated by a gene trap insertion (SA-β-geo-polyA) between exons 14 and 15 of chromosome 12. The gene-trapped mouse embryonic stem cell line, CA0017 (Sanger Institute Gene Trap Resource), was injected into C57BL/6 blastocysts. The resulting chimeric male founders were backcrossed to C57BL/6 females to generate heterozygous mice. After backcrossing for about 5 generations, $Sel1L^{+/-}$ mice were then intercrossed to generate viable $Sel1L^{+/+}$ and $Sel1L^{+/-}$ mice for these studies.

$Sel1L^{lox/+}$ mice were generated by injecting pre-targeted embryonic stem cells into C57BL/6 blastocysts. Mice expressing the target vector were bred to *FLPe* transgenic mice, kindly provided by Dr. Paula Cohen. The resulting $Sel^{lox/+}$ mice were then bred to homozygosity. $Sel^{lox/lox}$ mice were crossed with *RIP-Cre* mice (Jackson Laboratory, B6.Cg-Tg(Ins2-cre)25Mgn/J). $Sel^{lox/+}$; *RIP-Cre* were crossed to $Sel^{lox/lox}$ mice to generate $Sel^{lox/lox}$; *RIP-Cre* mice and littermate controls for experiments. A standard PCR was performed on genomic DNA to confirm Cre-mediated recombination (Appendix B, Figure a).

All animal experiments were performed in accordance with the Cornell Animal Care and Use Guidelines.

In Vivo Physiological Studies

Blood glucose levels were taken at the same time on a weekly basis (random or non-fasting blood glucose) or after 8 hours of overnight fasting (fasting blood glucose). For the glucose tolerance test (GTT), mice were fasted for 8 hours and then given an intraperitoneal injection of a sterile solution of glucose in phosphate-buffered saline (PBS) at a final concentration of 1 g/kg body weight. Blood glucose levels were measured at 0, 15, 30, 60 and 120-minute time points. For the insulin tolerance test (ITT), mice were fasted overnight for 8 hours and given an intraperitoneal (IP) injection of recombinant insulin in PBS (Eli Lilly, 0.75 IU/kg body weight). Blood glucose levels were measured for each mouse at 0, 30, 60, 90, and 120-minute time points. The Ascensia ELITE XL glucometer and accompanying strips were used for the aforementioned studies. Serum insulin was assayed using the ELISA Kit for Rat/Mouse Insulin (Millipore) and Mouse Insulin Ultrasensitive ELISA (ALPCO) according to manufacturer's instructions.

Mice were placed on the research high-fat diet (Harlan Teklad Custom Research Diet), consisting of 60.3% fat, 21.3% carbohydrate, and 18.4% protein (kcal breakdown), at 6 weeks (conditional knockout mice) or 10 weeks (global knockout mice) of age. Food was given *ad libitum*. For pharmacological treatment, 4-phenylbutyric (4-PBA) sodium salt (Scandinavian Formulas) was given once a day by oral gavage at a concentration of 1g/kg (global knockout mice). For water bottle treatment, 4-PBA sodium salt was dissolved in acidified drinking water (1 g/kg/day) and provided to mice starting at 10 weeks of age (conditional knockout mice). Bottles were replaced weekly.

Islet isolations, Ex Vivo and In Vitro Glucose-Stimulated Insulin Secretion (GSIS)

Mouse islet isolations were performed as previously described with minor modifications (152). Briefly, after sacrifice of each mouse, the pancreas was perfused via the common bile duct with 2 mg/ml collagenase (Sigma) in Hank's balanced salt solution (HBSS). The inflated pancreas was excised and incubated at 37 °C for 5-8 minutes. The collagenase-digested pancreas was vigorously shaken, washed 3 times with 10 ml of ice-cold HBSS, and re-suspended in 1 ml of 27% Ficoll 400 (Sigma) in HBSS. Islets were hand-picked and washed three times with ice-cold 1X HBSS before processing for further analysis.

Ex vivo GSIS was performed as described previously (153). Briefly, isolated islets were cultured overnight in RPMI 1640 medium supplemented with 10% FBS, antibiotics, and 10 mM glucose. Approximately 10 islets per well were selected in a 24-well dish with Krebs-Ringer bicarbonate buffer (KRBB) consisting of (in mM): glucose 2.8, NaCl 130, KCl 4.8, $MgSO_4$ 1.2, KH_2PO_4 1.2, $CaCl_2$ 2.5, $NaHCO_3$ 5.0, and HEPES 10, titrated to pH 7.4 with NaOH and supplemented with 1% BSA (Sigma). Islets were cultured for 1 hour at 37°C and 5% CO_2. Islets were then incubated for 30 minutes in either 2.8 and 17.8 mM glucose KRBB, after which the supernatants were collected and stored at -80°C until assayed for insulin concentration using the Mouse Insulin Ultrasensitive ELISA (ALPCO).

In vitro GSIS was conducted in stably infected Min6 cells (see *Insulinoma Cell Lines*) using a previously established protocol (154). Briefly, Min6 cells were plated at a density of 1 X 10^6 cells per well in a 6-well plate with standard culture media. After induction with doxycycline, the media was removed and cells were

washed 2X with KRBB without BSA or glucose. After, cells were equilibrated with KRBH containing 1% BSA and 2.8 mM glucose for 30 minutes at 37°C and 5% CO_2. They were then incubated with either 2.8 mM or 17.8 mM glucose for 30 minutes, after which the supernatants were removed and stored at -80°C until assayed for insulin concentration using the ELISA Kit for Rat/Mouse Insulin (Millipore).

The islets or Min6 from each GSIS treatment were centrifuged, washed, and resuspended in either RIPA buffer for total protein concentration determination or an acid ethanol solution (95% ethanol, 10.2 N HCl in a 50:1 ratio) for insulin content concentration. Secreted insulin was normalized to islet insulin content, which was normalized to the total protein concentration.

Pancreatic Morphology and Immunohistochemistry

Pancreata were removed and fixed in 4% paraformaldehyde (PFA) at 4° overnight, embedded in paraffin blocks, and sectioned at 5-8 μm. For insulin immunostaining, sections were rehydrated, blocked for endogenous peroxidase activity (3% H_2O_2), and permeabilized with 0.1% Triton-100 in PBS. After blocking with 10% normal donkey serum, guinea pig anti-human insulin (Linco, 1:1000) was applied overnight at 4°. An HRP-conjugated donkey anti-guinea pig immunoglobulin (IgG) secondary antibody (Jackson ImmunoResearch Laboratories, 1:500) was applied for 1 hour at room temperature. The ImmPact DAB peroxidase kit (Vector Technologies) was used as the substrate. Slides were counterstained with hematoxylin (Gill's, diluted 1:10). β-cell mass was determined as previously described (155). Briefly, total pancreatic and β-cell

areas were measured using the AxioVision software (Version 4.1). β-cell mass (mg) was calculated by multiplying the percentage of β-cell area identified by insulin immunostaining with the total pancreatic weight. To determine β-cell proliferation, pancreatic sections were co-immunostained with mouse monoclonal anti-Ki67 (Vector Laboratories, 1:500) and anti-insulin antibodies. Cy3-conjugated donkey anti-mouse and Cy2-conjugated donkey anti-guinea pig secondary antibodies (Jackson ImmunoResearch Laboratories, 1:500) were applied. Nuclei were counterstained with DAPI. The percentage of Ki67-positive cells was derived by dividing the number of Ki67-positive nuclei by the total number of counted β-cell nuclei. TUNEL staining was performed according to instructions for the Chemicon International Apoptog Peroxidase *In Situ* Apoptosis Detection Kit S7100 (Millipore Corporation). The ImmPact DAB peroxidase kit (Vector Technologies) was used as the substrate, and a hemotoxylin counterstain (Gill's, diluted 1:10) was applied. Images were acquired using either the Zeiss Axiovert 40 microscope or the Zeiss LSM 510 Meta confocal microscope.

RNA Extraction and Quantitative Real-Time Reverse Transcription PCR

RNA was isolated from relevant tissues by the TRIzol-chloroform method. RNA quality and concentration was measured using the Agilent 2100 Bioanalyzer (Agilent Technologies). First-strand cDNA synthesis was performed using RT Buffer, dNTPs, DTT, RNAout, and SuperScript III Reverse Transcriptase (all Invitrogen). Quantitative PCR was carried out using Power SYBR Green PCR Master Mix or iTaq Universal SYBR Green Supermix (Bio-Rad)

on an ABI Prism 7000 Sequence Detection System or StepOnePlus Real-Time PCR System (Applied Biosystems). PCR primers were designed using the PrimerSelect program of Lasergene 7.1 Sequence Analysis Software (DNAstar). Final quantification and normalization was determined according to the $\Delta\Delta C_q$ calculation method (156).

Insulinoma Cell Lines

Min6 and INS-1 insulinoma cells were maintained in normal media (Min6: Dulbecco's modified Eagle's medium with 10% fetal bovine serum, 1% sodium pyruvate, 1% Glutamax, 1% Pen-Strep, and 2 μl β-mercaptoethanol; INS-1: Roswell Park Memorial Institute medium with 10 % fetal bovine serum, 1% sodium pyruvate, 1% Glutamax, 1% Pen-Strep, and 10 mM HEPES). For generation of stable cell lines, cells were seeded at a confluency of 50% and infected overnight with inducible lentivirus expressing the reverse tetracycline-controlled transactivator (rtTA) or rtTA plus DN-SEL1L-GFP. To induce expression of transgenes, doxycycline (Sigma) was added into the culture medium of Min6 and INS-1 cells (200 μg/ml).

Statistical Analyses

Statistical analysis using the student's T-Test or two-way repeated measures ANOVA with Tukey's HSD post-hoc test where appropriate was performed using STATA (v12).

3.4 Results

3.4.1 *Sel1L*$^{+/-}$ mice are more susceptible to high-fat diet induced hyperglycemia

Wild-type (*Sel1L*$^{+/+}$) and heterozygote (*Sel1L*$^{+/-}$) mice were transitioned from a normal chow diet to a high-fat diet (HFD) at 10 weeks of age. The average body weights of the two genotypes did not significantly differ or diverge throughout the 28-week treatment period (Appendix B, Figure b). However, after 8 weeks on the HFD, the fasting blood glucose levels of the *Sel1L*$^{+/-}$ mice were significantly higher than those of the *Sel1L*$^{+/+}$ mice (Figure 3.1a). Although the *Sel1L*$^{+/+}$ mice displayed a normal response to the HFD with increasing fasting blood glucose levels over time, this rate is higher in the *Sel1L*$^{+/-}$ mice. *Sel1L*$^{+/+}$ and *Sel1L*$^{+/-}$ mice on a HFD also showed a differential metabolic phenotype in other respects. After 20 weeks on a HFD, the glucose tolerance test (GTT) revealed a higher fasting glucose level for the *Sel1L*$^{+/-}$ mice in comparison to their wild-type counterparts (Figure 3.1b). When injected intraperitoneally with glucose (1 g/kg), the heterozygous mice were not as efficient as the wild type mice in blood glucose uptake. As time elapses, the blood glucose level of the *Sel1L*$^{+/-}$ mice remained consistently higher than the *Sel1L*$^{+/+}$ mice. In the *Sel1L*$^{+/+}$ mice, blood glucose levels fell to fasting levels within 2 hours, the blood glucose levels in the *Sel1L*$^{+/-}$ mice remained high at this time point. We reasoned that glucose intolerance could be the result of either insulin resistance or a defect in insulin secretion. When injected intraperitoneally with insulin (1 U/kg), blood glucose levels in the *Sel1L*$^{+/+}$ and *Sel1L*$^{+/-}$ mice, after 24 weeks on the diet, were not significantly different (Figure 3.1c). Interestingly, the fasting serum levels of insulin in *Sel1L*$^{+/-}$ mice on a HFD for 20 weeks were noticeably elevated in comparison with the *Sel1L*$^{+/+}$ mice (Figure 3.1d). This elevation appears to be a

feature of HFD feeding, as there is no difference in fasting serum insulin levels between the two genotypes on normal chow (at the same age as the HFD mice).

We used the glucose-stimulated insulin secretion (GSIS) assay to determine β-cell functionality in *Sel1L*$^{+/+}$ and *Sel1L*$^{+/-}$ mice (Figure 3.1e). Islets were isolated from mice of both genotypes and incubated in a low glucose condition (buffer containing 3 mM glucose) and a high glucose condition (buffer containing 30 mM). A 10-fold glucose concentration difference was used to provide an adequate level of stress to the haploinsufficient islets, similar to a HFD. Basal level and glucose-stimulated insulin secreted into the media were measured to give the fold change in GSIS. This value is greatly reduced in *Sel1L*$^{+/-}$ islets, indicating that an inherent insulin secretion defect could explain elevated fasting blood glucose levels in the *Sel1L*$^{+/-}$ mice.

Figure 3.1: *Sel1L*$^{+/-}$ mice on a HFD exhibit a greater degree of hyperglycemia and impaired insulin secretion. (a) Fasting blood glucose levels were taken once every four weeks for wild-type (n=11) and heterozygote mice (n=17) on a 60% high-fat diet (HFD). Treatment started at 10 weeks of age (Week 0). (b) Glucose tolerance was assessed using a glucose tolerance test (GTT) in both genotypes after 20 weeks of HFD feeding (n=7-8 mice per genotype). (c) Insulin resistance was assessed using an insulin resistance test (ITT) in both genotypes after 24 weeks of HFD feeding, n=7-8 mice per genotype (d) Fasting serum insulin levels in *Sel1L*$^{+/+}$ (n=9) and *Sel1L*$^{+/-}$ mice (n=9) on normal chow (NC) and a HFD for 20 weeks. (e) Fold change in glucose-stimulated insulin secretion (GSIS) in pancreatic islets isolated from *Sel1L*$^{+/+}$ (n=3) and *Sel1L*$^{+/-}$ mice (n=4), then challenged with 30 mM glucose *in vitro*. The fold change represents the ratio between the media insulin concentration with high glucose (30 mM) to the concentration with low glucose (3 mM). *, $p<0.05$; **, $p<0.01$. Seen in Figures 1 and 2 of (157).

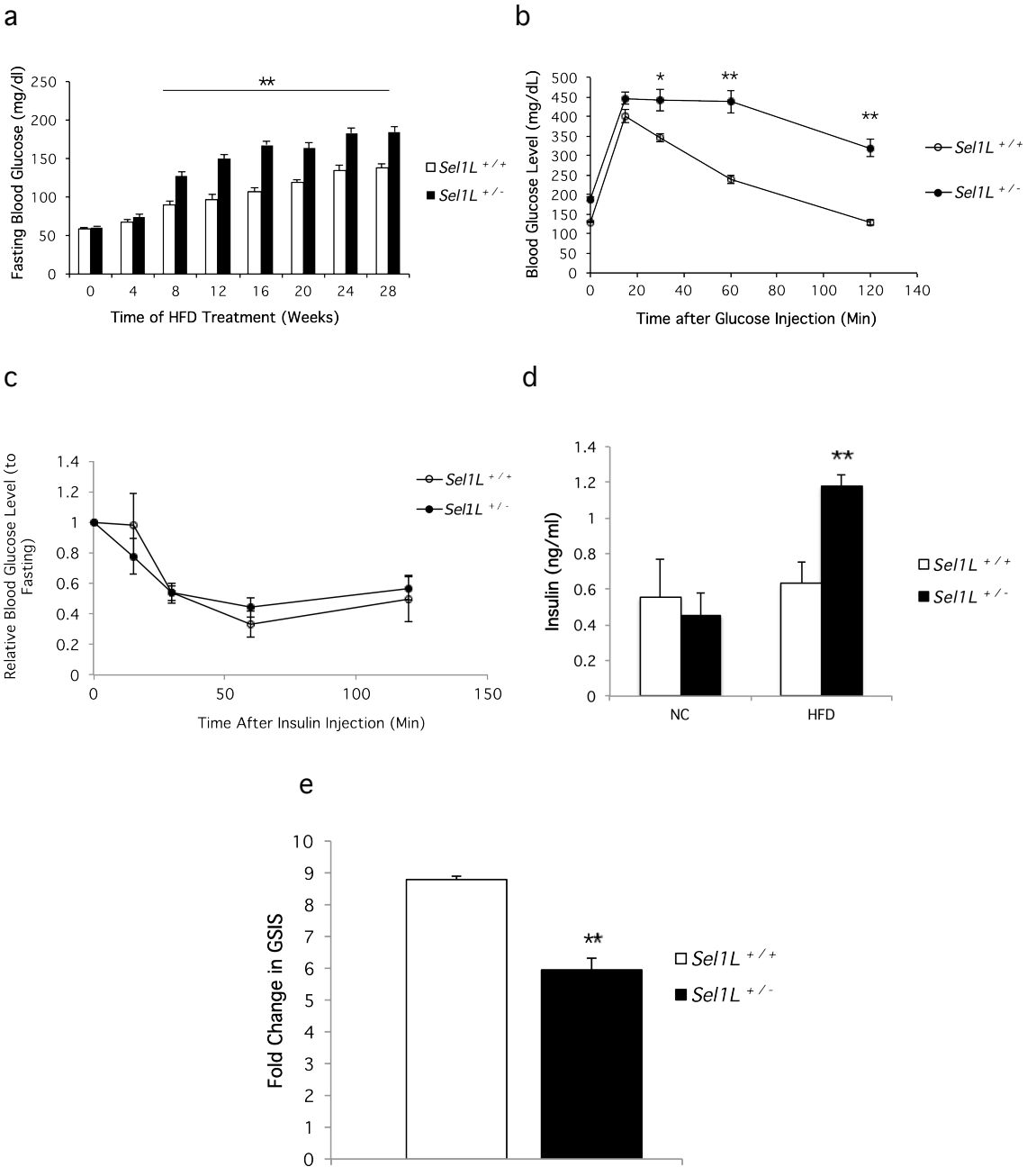
a
Fasting Blood Glucose (mg/dl)
250
200
150
100
50
0
**
0
4
8
12
16
20
24
28
Time of HFD Treatment (Weeks)
Sel1L +/+
Sel1L +/-
b
Blood Glucose Level (mg/dL)
500
450
400
350
300
250
200
150
100
50
0
*
**
**
0
20
40
60
80
100
120
140
Time after Glucose Injection (Min)
Sel1L +/+
Sel1L +/-
c
Relative Blood Glucose Level (to Fasting)
1.4
1.2
1
0.8
0.6
0.4
0.2
0
0
50
100
150
Time After Insulin Injection (Min)
Sel1L +/+
Sel1L +/-
d
Insulin (ng/ml)
1.4
1.2
1
0.8
0.6
0.4
0.2
0
**
NC
HFD
Sel1L +/+
Sel1L +/-
e
Fold Change in GSIS
10
9
8
7
6
5
4
3
2
1
0
**
Sel1L +/+
Sel1L +/-

3.4.2 *Sel1L*$^{+/-}$ mice exhibit a failure to expand β-cell mass in response to a HFD

It is well known that there is an adaptive response to insulin resistance in the β-cell. One result of peripheral insulin resistance is an expansion of β-cell mass and an increase in β-cell proliferation. Insulin immunostaining of pancreatic sections from *Sel1L*$^{+/+}$ and *Sel1L*$^{+/-}$ mice (Figure 3.2a and 3.2b, respectively) demonstrated that islets are particularly smaller in the *Sel1L*$^{+/-}$ mice on a HFD (for 20 weeks). The calculated β-cell mass (Figure 3.2c) affirmed that it is significantly lower in *Sel1L*$^{+/-}$ mice. To determine the fundamental cause of this, we performed TUNEL staining for apoptosis and Ki67 immunostaining for proliferation. The TUNEL analysis revealed no major difference in apoptosis in pancreatic sections from each genotype (data not shown). However, we did discover that there were less Ki67-positive β-cells in the pancreatic sections from HFD-fed *Sel1L*$^{+/-}$ mice (Figure 3.2e) versus the HFD-fed *Sel1L*$^{+/+}$ mice (Figure 3.2d). Co-staining with insulin and counterstaining with DAPI in these sections allowed us to identify proliferating β-cells and quantify them for each genotype (Figure 3.2f). These results indicate that *Sel1L*$^{+/-}$ mice are incapable of expanding their β-cell mass in response to peripheral insulin resistance, as seen in wild-type mice.

Figure 3.2: *Sel1L*$^{+/-}$ mice on a HFD have less β-cell mass due to reduced proliferation of β-cells. These images show insulin staining of islets, indicated in brown, in representative pancreatic sections from (a) *Sel1L*$^{+/+}$ and (b) *Sel1L*$^{+/-}$ mice after 20 weeks on a HFD (10X magnification). (c) β-cell mass at this time point was calculated by using the ratio of the positively stained insulin areas to the area of the pancreatic section, then multiplying by the weight of the whole pancreas (n= 7 mice per genotype). Immunostaining for Ki67 (red), insulin (green) and DAPI (blue) is seen in representative pancreatic sections from (d) *Sel1L*$^{+/+}$ and (e) *Sel1L*$^{+/-}$ mice after 20 weeks on a HFD (40X magnification). The white arrows indicate staining of Ki67 β-cells as a marker of proliferation. (f) Quantification of the percentage of Ki67-positive β-cells in pancreatic sections from *Sel1L*$^{+/+}$ and *Sel1L*$^{+/-}$ mice (n=3 mice per genotype) on a HFD (20 weeks). *, $p<0.05$, **, $p<0.01$. Seen in Figure 2 of (157).

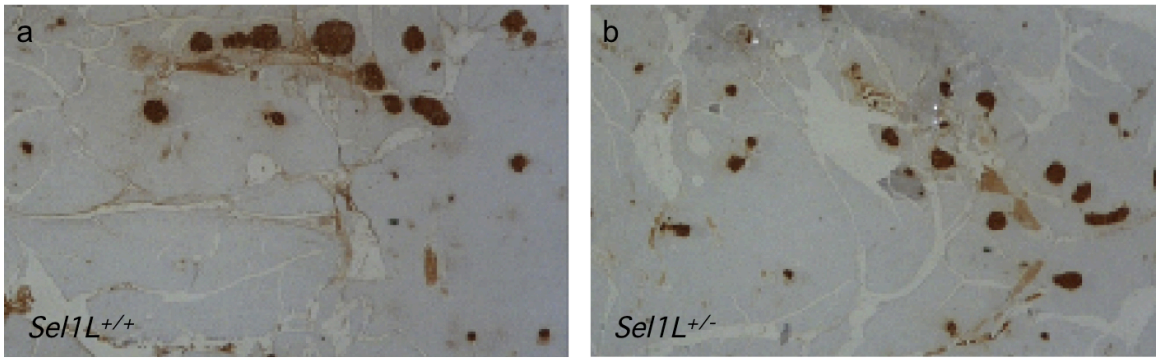
a
Sel1L+/+
b
Sel1L+/-

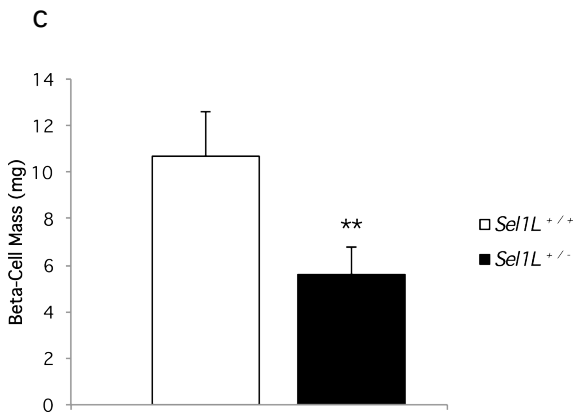
c
Beta-Cell Mass (mg)
14
12
10
8
6
4
2
0
**
Sel1L+/+
Sel1L+/-

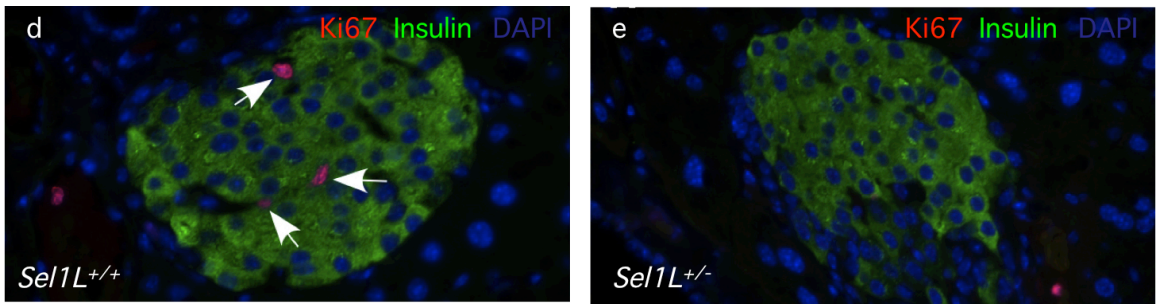
d
Ki67 Insulin DAPI
Sel1L+/+
e
Ki67 Insulin DAPI
Sel1L+/-

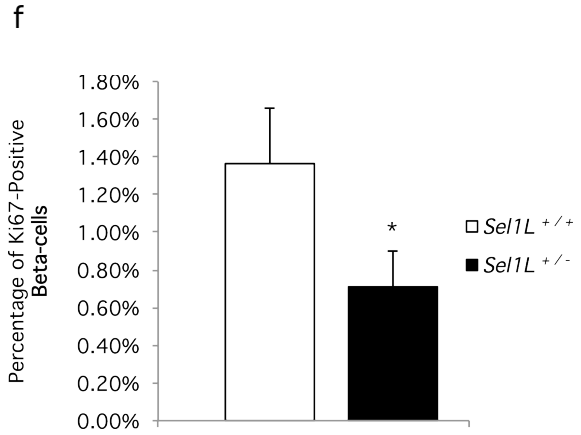
f
Percentage of Ki67-Positive Beta-cells
1.80%
1.60%
1.40%
1.20%
1.00%
0.80%
0.60%
0.40%
0.20%
0.00%
*
Sel1L+/+
Sel1L+/-

3.4.3 Endoplasmic reticulum stress is present in pancreatic islets and other peripheral tissues of HFD-fed *Sel1L*$^{+/-}$ mice

We previously reported that the complete loss of *Sel1L* in mice (*Sel1L*$^{-/-}$) causes ER stress throughout the organism (137). We therefore evaluated the possible presence of ER stress in the tissues of HFD-fed *Sel1L*$^{+/-}$ mice that are most affected by the onset of obesity. In islets isolated from *Sel1L*$^{+/+}$ and *Sel1L*$^{+/-}$ mice and cultured overnight under low glucose conditions (10 mM), there was no significant difference in gene expression of UPR markers such as *Bip*, *Herp*, *Chop*, and *p58*^{IPK} (Figure 3.3a). However, a high glucose condition (30 mM) resulted in a marked upregulation of UPR markers in the islets of *Sel1L*$^{+/-}$ mice, in comparison to wild-type controls (Figure 3.3b). To verify the evident ER stress, we asked whether a chemical chaperone known as 4-PBA (0.02 M) can promote proper protein folding. Islets isolated from *Sel1L*$^{+/-}$ mice were incubated with either 4-PBA or DMSO in high glucose, and gene expression was again assessed and compared between the two samples (Figure 3.3c). The presence of 4-PBA significantly reduced ER stress in *Sel1L*$^{+/-}$ islets. To demonstrate an *in vivo* effect, Adam Francisco orally administered 4-PBA or PBS daily to *Sel1L*$^{+/+}$ and *Sel1L*$^{+/-}$ mice (HFD, 20 weeks) for one week. By the end of the treatment period, the 4-PBA-treated *Sel1L*$^{+/-}$ mice showed a significant reduction in their fasting blood glucose levels in comparison to the PBS-treated controls (157). Together, these results imply that the hyperglycemia in HFD-treated *Sel1L*$^{+/-}$ mice is dependent on ER stress.

ER stress has also been implicated in the development of insulin resistance in diet-induced obesity models. Although the insulin tolerance test showed no significant difference in response to exogenous insulin administration, the fasting

serum insulin levels of *Sel1L*$^{+/-}$ mice on a HFD were higher than those seen in the *Sel1L*$^{+/+}$ mice (Figure 3.1d). This points to some degree of insulin resistance in the heterozygotes challenged with a HFD. Therefore, in collaboration with Dr. Haibo Sha from Dr. Ling Qi's lab, we prepared protein lysates from the livers of *Sel1L*$^{+/+}$ and *Sel1L*$^{+/-}$ mice after 20 weeks on the HFD. Through western blotting, we observed markedly increased expression of UPR markers such as BIP, CALNEXIN, and EIF2α in the livers of the HFD-fed *Sel1L*$^{+/-}$ mice (157). Therefore, ER stress is pervasive in many tissues of the *Sel1L*$^{+/-}$ mice on a HFD.

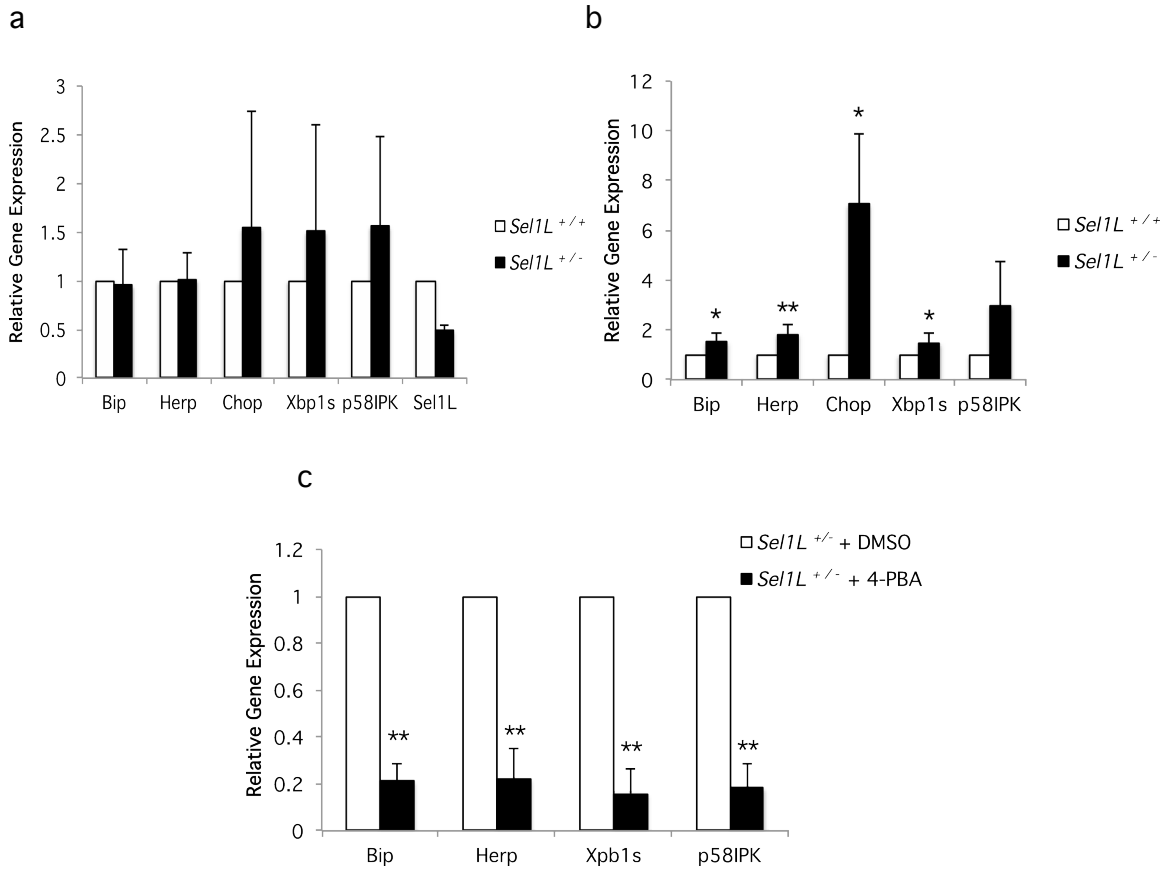

Figure 3.3: Key UPR markers are upregulated in the islets of *Sel1L*$^{+/-}$ mice on a HFD. Quantitative real-time PCR (qPCR) was used to assess the expression of UPR markers in cDNA from islets isolated from *Sel1L*$^{+/+}$ and *Sel1L*$^{+/-}$ mice (n=3 sets of islets per genotype) and cultured in (a) 10 mM glucose and (b) 30 mM glucose overnight. In (c), qPCR analysis of UPR markers in islets isolated from *Sel1L*$^{+/-}$ mice and treated in high glucose conditions with a chemical chaperone, 4-PBA (0.02 M), or DMSO as a control (n=3 sets of islets per treatment). *, $p<0.05$; **, $p<0.01$. Seen in Figure 3 of (157).

3.4.4 Interference of SEL1L function *in vitro* results in impaired glucose-stimulated insulin secretion and proliferation

To further address the mechanism by which *Sel1L* maintains β-cell homeostasis, we developed a tetracycline-inducible lentivirus that expresses a dominant negative form of SEL1L (DN-SEL1L). This construct contains a deletion at the C-terminal end of the SEL1L protein and a GFP tag. We used this lentivirus in the insulinoma cell lines, MIN6 (mouse-derived) and INS-1 (rat-

derived). In Min6 cells that are stably infected with DN-SEL1L-GFP, the addition of doxycycline (dox) to the media promotes the expression of the deletion mutant, seen in Figure 3.4a. After confirming the expression of the construct through western blotting and fluorescence microscopy, we used the stably infected Min6 cells cultured with and without dox to determine the effects of SEL1L disruption on β-cell function. *In vitro* GSIS confirms that there was a failure to completely respond to a high glucose concentration (stimulated) in Min6 cells expressing DN-SEL1L (Figure 3.4b).

We also evaluated the role of *Sel1L* in β-cell proliferation using INS-1 cells. We generated INS-1 cell lines stably expressing the rtTA regulatory proteins (as a virus control) and rtTA and DN-SEL1L. In the cells expressing rtTA and DN-SEL1L (+), there was increased protein expression of the chaperone BIP within 12 hours of dox incubation versus the control cells (-) (Figure 3.4c). Throughout the dox treatment, BIP levels remained consistently higher in cells expressing DN-SEL1L. Furthermore, Adam Francisco used cell counting and thymidine incorporation to assess cell proliferation in these cell lines (157). The proliferation rate of the INS-1 cells stably infected with DN-SEL1L was significantly lower than that of INS-1 cells infected with rtTA alone (both cell lines incubated with dox in the media).

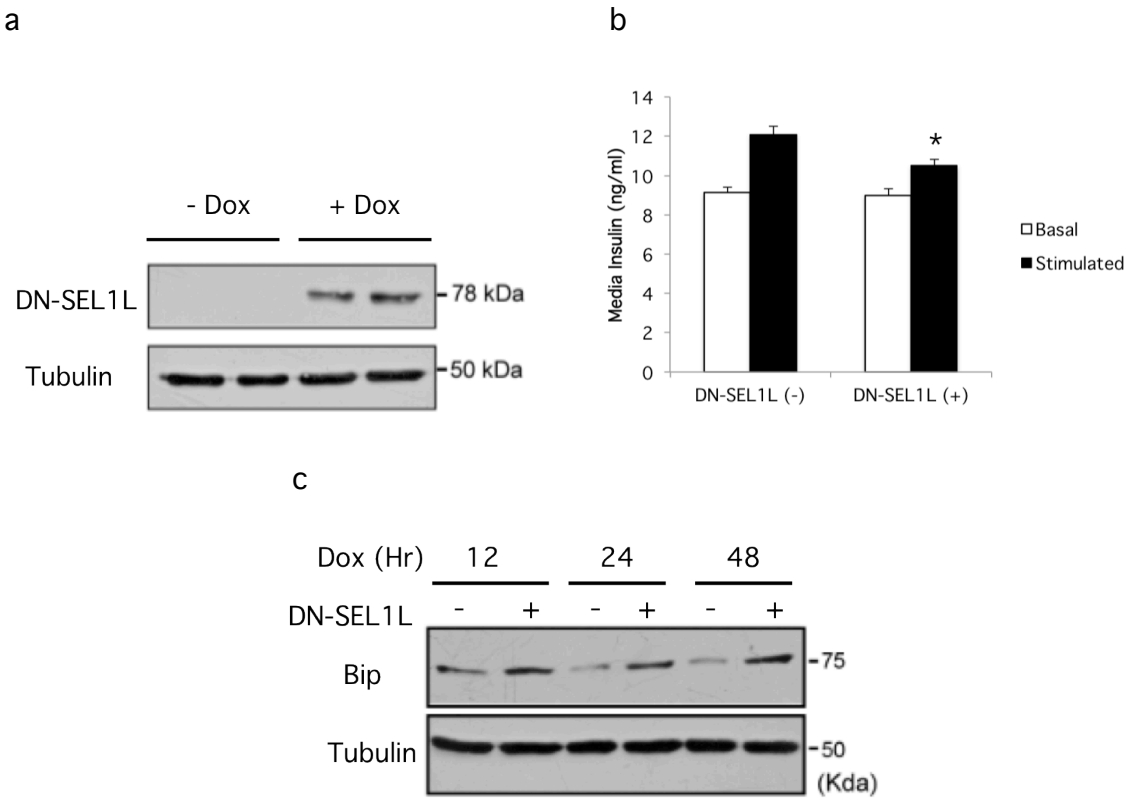

Figure 3.4: Insulinoma cell lines ectopically expressing a dominant-negative form of SEL1L show evidence of defective insulin secretion and ER stress. Min6 cells were stably infected with a tetracycline-inducible lentivirus expressing a dominant negative form of SEL1L (DN-SEL1L) tagged to GFP. (a) Western blot analysis of infected Min6 cells in the absence and presence of doxycycline (Dox), and probed for GFP and tubulin as a loading control. (b) In vitro glucose-stimulated insulin secretion in Min6 cells without DN-SEL1L and with DN-SEL1L (n=3 independent experiments). The basal condition was low glucose (2.8 mM) and the stimulated condition was high glucose (17.8 mM). (c) Western blot of protein lysate from INS-1 cells with and without stable expression of the dox-inducible lentiviral transgene, DN-SEL1L-GFP. The BIP protein was probed for after 12, 24, and 48 hours of dox induction. Tubulin is shown as a loading control. *, $p<0.05$. Seen in Figure 4 of (157).

3.4.5 Selective deletion of *Sel1L* in β-cells leads to early-onset hyperglycemia in mice

Although using a diet-induced obesity model with the *Sel1L* heterozygous mice was insightful, we wanted to further investigate the physiological role of *Sel1L* in β-cells. To address this, we generated mice with floxed *Sel1L* alleles (loxP

sites flanking exon 6 of the *Sel1L* gene). Mice homozygous for this floxed allele ($Sel^{lox/lox}$) were then crossed to mice expressing the *Cre* recombinase, driven by the rat insulin promoter (*RIP-Cre*). Using this line of *Cre* mice, genetic deletion of *Sel1L* would be expected primarily in β-cells of these mutant mice ($Sel^{lox/lox}$; *RIP-Cre*) (158).

The metabolic phenotype of $Sel^{lox/lox}$; *RIP-Cre* mice were characterized in comparison to their $Sel^{lox/lox}$ and $Sel^{lox/+}$; *RIP-Cre* littermate controls. Random blood glucose levels were consistently higher in $Sel^{lox/lox}$; *RIP-Cre* mice, starting as early as 2 weeks of age (Figure 3.5a). This trend is sustained into adulthood and the difference is evident even in the absence of a nutrient or chemical stress on these mice. Similarly, fasting blood glucose levels were elevated in $Sel^{lox/lox}$; *RIP-Cre* mice as early as 6 weeks of age (Figure 3.5b). To measure the *in vivo* response of β-cells to glucose, we performed a glucose tolerance test (GTT) at various ages. The GTT at 6 weeks of age revealed that mutant mice are severely glucose intolerant, as seen by their reduced ability to clear the injected glucose as efficiently as the control mice (Figure 3.5c). At 12 weeks of age, the GTT indicated that $Sel^{lox/lox}$; *RIP-Cre* mice reach higher blood glucose levels post-injection than seen in the 6-week GTT (Figure 3.5d). The $Sel^{lox/+}$; *RIP-Cre* mice at this age appear to exhibit a similar response to the glucose injection at both ages. This evidence suggests that glucose intolerance is exacerbated over time in $Sel^{lox/lox}$; *RIP-Cre* mice.

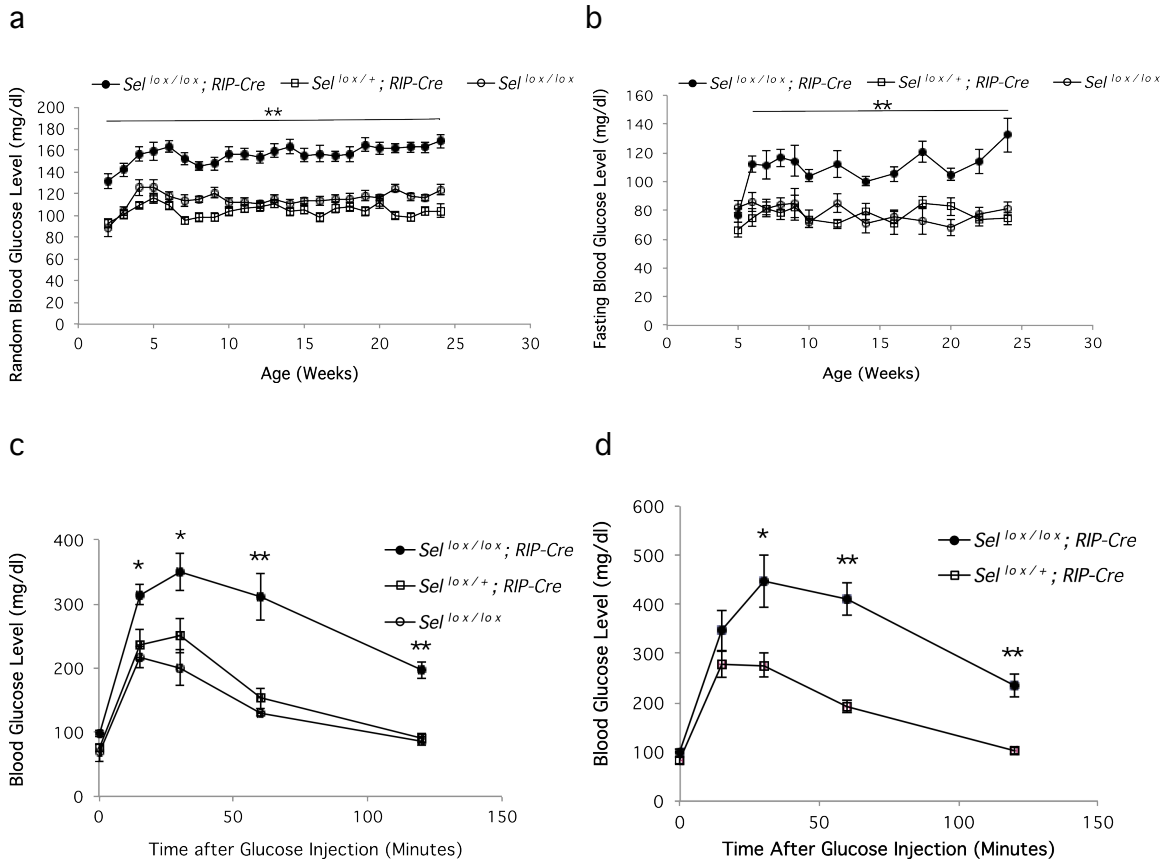

Figure 3.5: Mice with the conditional deletion of *Sel1L* in β-cells display early onset hyperglycemia and glucose intolerance. (a) Random blood glucose levels of wild-type (*Sel*$^{lox/lox}$), heterozygote (*Sel*$^{lox/+}$*; RIP-Cre*), and mutant (*Sel*$^{lox/lox}$*; RIP-Cre*) mice were measured on a weekly basis between 2 and 24 weeks of age (n=18-23 mice per genotype). (b) Fasting blood glucose levels were measured for *Sel*$^{lox/lox}$ and *Sel*$^{lox/lox}$*; RIP-Cre* mice on a weekly basis between 5 and 24 weeks of age (n=5 mice per genotype). Glucose tolerance was assessed using a glucose tolerance test (GTT) in *Sel*$^{lox/lox}$ (n=4), *Sel*$^{lox/+}$*; RIP-Cre* (n=7) and *Sel*$^{lox/lox}$*; RIP-Cre* (n=8) mice at (c) 6 weeks of age and (d) 12 weeks of age. *, p<0.05; **, p<0.01.

3.4.6 A high-fat diet exacerbates hyperglycemia and glucose intolerance in *Sel*$^{lox/lox}$*; RIP-Cre* mice

In our earlier studies, the high-fat diet (HFD) was used as an exogenous stress on the *Sel1L*$^{+/-}$ mice. Administering a diet high in fat content leads to obesity. Obesity is associated with insulin resistance, and insulin resistance prompts insulin production in β-cells. We reasoned that in mice with a β-cell-

specific deletion of *Sel1L*, a high-fat diet would be particularly detrimental to β-cell function. Indeed, a high-fat diet, started at 6 weeks of age, caused a substantial increase in fasting blood glucose levels in *Sel*$^{lox/lox}$; *RIP-Cre* mice. This was seen just after one week of treatment (Figure 3.6a). Over the course of the treatment period, the glucose levels increased steadily to values averaging close to 300 mg/dl in the mutant mice at the 14-week termination point. Furthermore, the GTT in *Sel*$^{lox/lox}$ and *Sel*$^{lox/lox}$; *RIP-Cre* mice, after 6 weeks on the HFD, showed a significant difference in glucose tolerance between the two genotypes. The *Sel*$^{lox/lox}$; *RIP-Cre* mice reached higher blood glucose levels post-injection, and fail to clear this blood glucose over the course of the 2-hour period (Figure 3.6b).

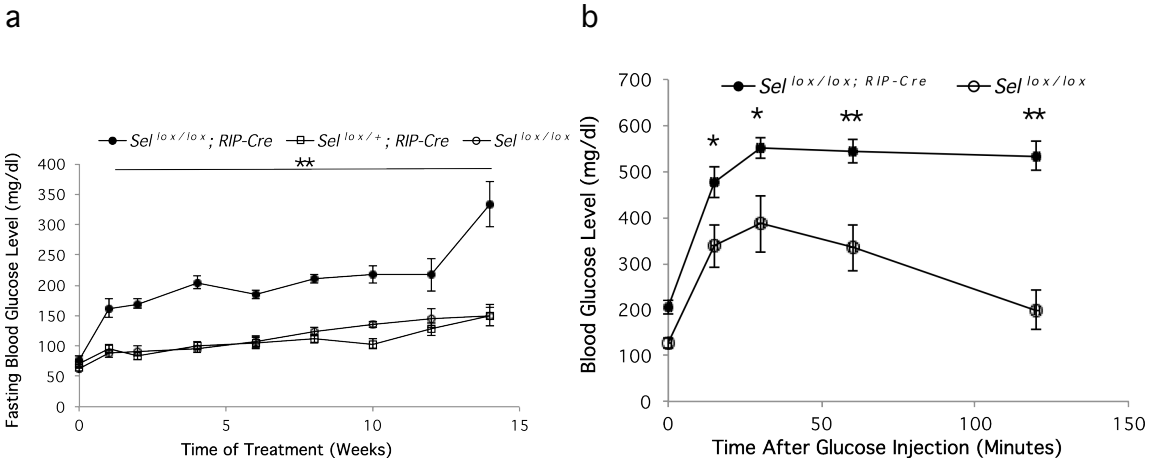

Figure 3.6: A HFD worsens the metabolic phenotype in *Sel*$^{lox/lox}$; *RIP-Cre* mice. Wild-type (*Sel*$^{lox/lox}$, n=8), heterozygote (*Sel*$^{lox/+}$; *RIP-Cre*, n=11), and mutant (*Sel*$^{lox/lox}$; *RIP-Cre*, n=10) mice were started on a 60% high-fat diet at 6 weeks of age (Week 0). (a) Fasting blood glucose levels were taken for each genotype throughout the 14-week treatment period. (b) Glucose tolerance was assessed with a glucose tolerance test (GTT) in *Sel*$^{lox/lox}$ (n=4) and *Sel*$^{lox/lox}$; *RIP-Cre* (n=5) mice after 6 weeks on a HFD. *, $p<0.05$; **, $p<0.01$.

3.4.7 The absence of *Sel1L* in β-cells causes improper trafficking and secretion of insulin

Loss of β-cell mass was partially responsible for the greater degree of hyperglycemia observed in *Sel1L*$^{+/-}$ mice on a HFD. To determine if a similar observation could be made in *Sel*$^{lox/lox}$*; RIP-Cre* mice, we used insulin immunostaining of pancreatic sections from *Sel*$^{lox/lox}$ and *Sel*$^{lox/lox}$*; RIP-Cre* mice (Figure 3.7a and 3.7b, respectively). This illustrated that there was no obvious change in β-cell mass due to the loss of *Sel1L*. Quantification of β-cell mass in each genotype (Figure 3.7c) confirmed there was no significant difference at 6 weeks of age. Immunohistochemical analysis using TUNEL assay revealed that there are no detectable differences in β-cell apoptosis at this age (data not shown). Furthermore, Ki67 immunostaining of pancreatic sections from each genotype also indicated that β-cell proliferation is normal in *Sel*$^{lox/lox}$*; RIP-Cre* mice (see Figure 4.4e).

Since there is no β-cell loss or defect in the ability of β-cells to proliferate in *Sel*$^{lox/lox}$*; RIP-Cre* mice, we next wanted to investigate the functionality of β-cells. Islets were isolated from *Sel*$^{lox/lox}$ and *Sel*$^{lox/lox}$*; RIP-Cre* mice and cultured *in vitro* in a low glucose concentration condition (2.8 mM) and a high glucose concentration condition (17.8 mM). Even in the low glucose condition, islets from *Sel*$^{lox/lox}$*; RIP-Cre* mice secreted less insulin in comparison to wild-type islets. While islets from *Sel*$^{lox/lox}$ mice showed a normal increase in insulin secretion in response to the high glucose concentration, islets from *Sel*$^{lox/lox}$*; RIP-Cre* mice failed to respond.

To further understand this marked insulin secretion defect, we used co-immunostaining of pancreatic sections to localize proinsulin to cellular

compartments. In both wild-type and mutant islets, proinsulin co-localizes with GM130, a member of the Golgin family of proteins and a component of the Golgi apparatus (Figure 3.7e and 3.7f) (159). However, mutant islets displayed more intense proinsulin staining (Figure 3.7f), suggesting that there was greater expression in comparison to wild-type islets. This accumulation of proinsulin was not confined to the Golgi, as proinsulin also co-localized with the ER marker calnexin in mutant but not wild-type β-cells (Figure 3.7h and 3.7g, respectively). Together, the intensity and localization of proinsulin expression in mutant islets indicates that the anterograde trafficking of this precursor is stymied due to the loss of *Sel1L*.

Figure 3.7: *Sel$^{lox/lox}$; RIP-Cre* mice have significantly reduced glucose-stimulated insulin secretion due to a proinsulin trafficking defect. These images show insulin staining of islets, indicated in brown, in representative pancreatic sections from (a) *Sel$^{lox/lox}$* and (b) *Sel$^{lox/lox}$; RIP-Cre* mice at 6 weeks of age (10X magnification). (c) β-cell mass at this time point was calculated by using the ratio of the positively stained insulin areas to the area of the pancreatic section, then multiplying by the weight of the whole pancreas (n= 5 mice per genotype). (d) Glucose-stimulated insulin secretion was assayed using an insulin ELISA for islets isolated from *Sel$^{lox/lox}$* (n=4) and *Sel$^{lox/lox}$; RIP-Cre* (n=4) mice and cultured *in vitro*. Immunostaining of a representative pancreatic section are pictured from (e) *Sel$^{lox/lox}$* and (f) *Sel$^{lox/lox}$; RIP-Cre* mice; from left to right, proinsulin (green), GM130 (red), and the merged image with DAPI (nuclei, blue). Similarly, immunostaining of representative islets from (g) *Sel$^{lox/lox}$* and (h) *Sel$^{lox/lox}$; RIP-Cre* mice; from left to right, proinsulin (green), calnexin (red), and the merged image with DAPI (nuclei, blue). p *, $p<0.05$; **, $p<0.01$.

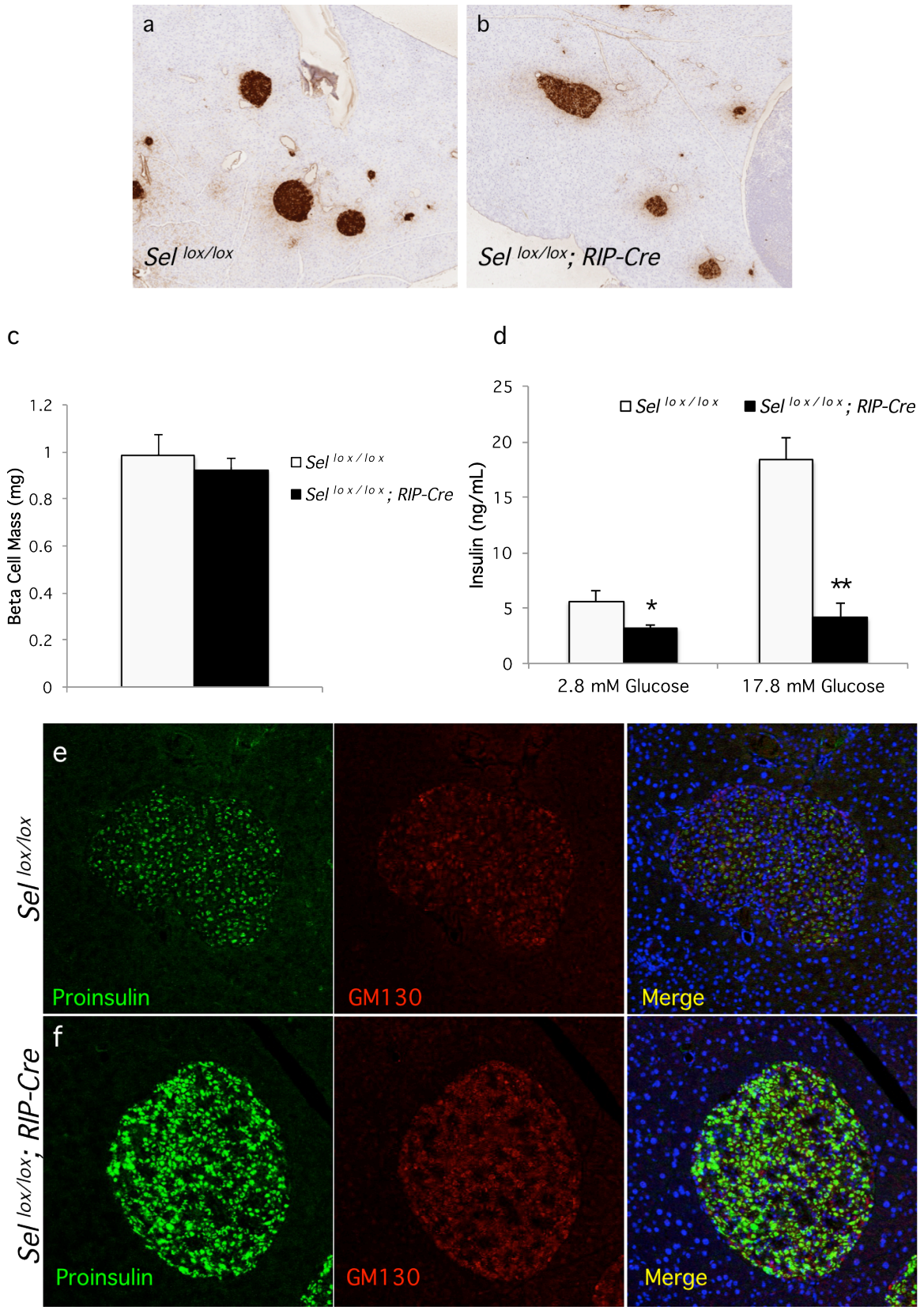
a
Sel lox/lox
b
Sel lox/lox; RIP-Cre
c
Beta Cell Mass (mg)
1.2
1
0.8
0.6
0.4
0.2
0
Sel lox/lox
Sel lox/lox; RIP-Cre
d
Insulin (ng/mL)
25
20
15
10
5
0
Sel lox/lox
Sel lox/lox; RIP-Cre
*
**
2.8 mM Glucose
17.8 mM Glucose
e
Sel lox/lox
Proinsulin
GM130
Merge
f
Sel lox/lox; RIP-Cre
Proinsulin
GM130
Merge

Figure 3.7, Continued:

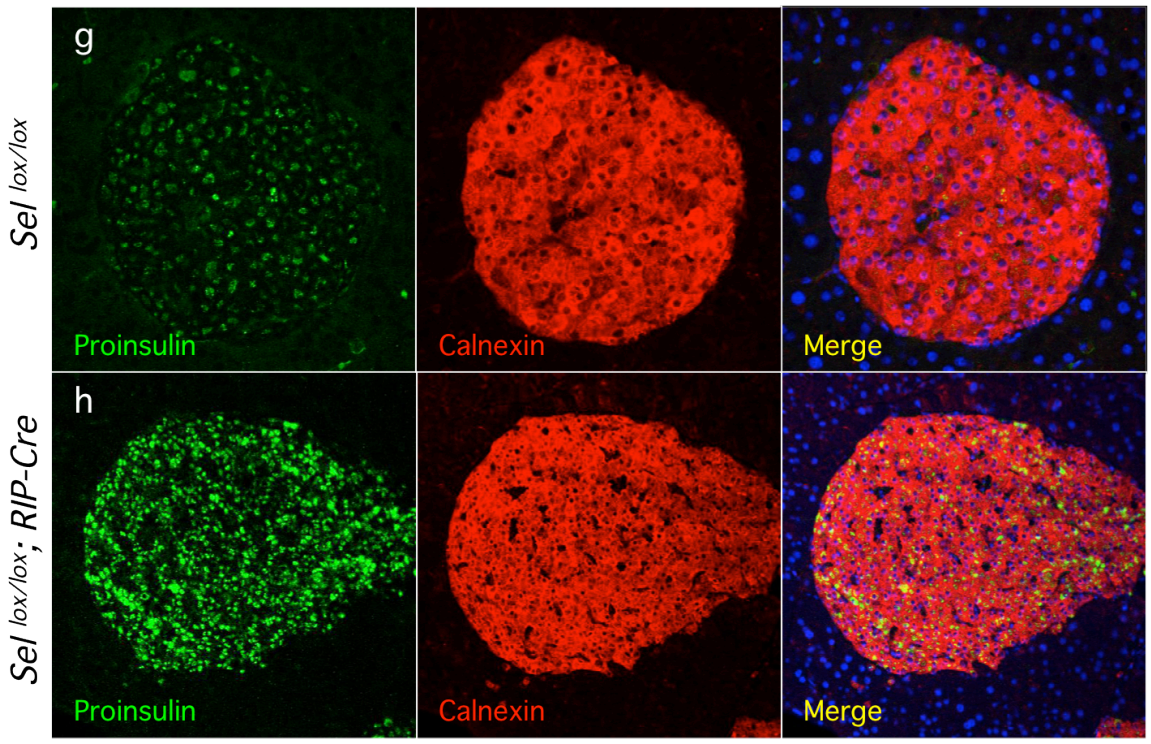

3.4.8 Administration of 4-PBA promotes reduction of hyperglycemia in *Sel*$^{lox/lox}$; *RIP-Cre* mice.

We first affirmed the presence of ER stress in β-cells lacking *Sel1L* by using quantitative real-time RT- PCR of UPR markers in isolated islets from *Sel*$^{lox/lox}$ and *Sel*$^{lox/lox}$; *RIP-Cre* mice (Figure 3.8a). This expression analysis revealed a consistent upregulation of UPR markers, such as *Erdj3*, *Chop*, and *Xbp1s* in the islets of the mutant mice.

This observation indicated that β-cells lacking *Sel1L* are subject to ER stress. We wanted to use an *in vivo* approach to determine if the ER stress is causing elevated blood glucose levels. To test this, we placed wild-type and mutant mice on a 4-PBA water bottle treatment (1 g/kg B.W.) at 10 weeks of age.

4-PBA is a chemical chaperone that has been previously reported to promote intracellular protein folding, trafficking, and secretion in conditions of ER stress. The 4-PBA treatment was effective in lowering fasting blood glucose levels in *Sel*$^{lox/lox}$*; RIP-Cre* mice after 10 weeks. As 4-PBA has been established to mitigate ER stress *in vivo* and *in vitro*, and 4-PBA can reduce fasting blood glucose levels in our mutant mice, we speculate that ER stress is responsible for the hyperglycemic phenotype in *Sel*$^{lox/lox}$*; RIP-Cre* mice.

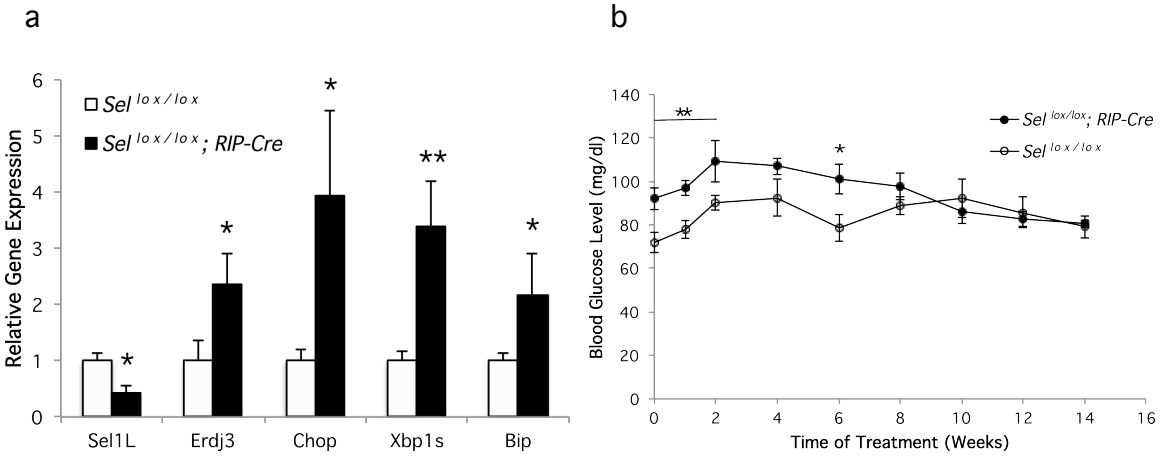

Figure 3.8: 4-PBA can rescue hyperglycemia in *Sel*$^{lox/lox}$*; RIP-Cre* mice. (a) Quantitative real-time PCR (qPCR) was used to assess the expression of UPR markers in cDNA from islets isolated from *Sel*$^{lox/lox}$ and *Sel*$^{lox/lox}$*; RIP-Cre* mice (n=4-5 sets of islets per genotype). In (b), fasting blood glucose levels during water bottle administration of the chemical chaperone 4-PBA (1 g/kg) to *Sel*$^{lox/lox}$ and *Sel*$^{lox/lox}$*; RIP-Cre* mice (n=5 mice per genotype), were observed starting at 10 weeks of age (Week 0). *, $p<0.05$; **, $p<0.01$.

3.5 Discussion

It is abundantly clear that abnormalities in insulin sensitivity and β-cell function contribute to hyperglycemia in T2D. The HFD and conditional mouse models for *Sel1L* insufficiency implicate that defective ER-associated degradation may play a critical role in susceptibility to this metabolic disorder. Haploid

insufficiency of SEL1L and obesity, caused by a HFD, contribute to the development of metabolic characteristics of diabetes. *Sel1L*$^{+/-}$ mice on a HFD display elevated blood glucose levels, in comparison to HFD-fed wild-type mice, starting at 8 weeks of HFD treatment. They also exhibit a greater degree of glucose intolerance and reduced *in vitro* glucose-stimulated insulin secretion (GSIS) from islets. Interestingly, *Sel1L*$^{+/-}$ mice on a HFD have reduced β-cell mass at later stages of HFD treatment (20 weeks) in comparison to controls. This reduction in mass was found to be the result of inadequate proliferative capacity of β-cells in response to insulin resistance. In the presence of high glucose, islets isolated from *Sel1L*$^{+/-}$ mice show evident upregulation of UPR markers compared to wild-type islets. Correspondingly, incubation with the chemical chaperone 4-PBA reverses induction of the UPR in *Sel1L*$^{+/-}$ islets in a high glucose condition. *In vitro* studies in insulinoma cell lines expressing a dominant-negative form of SEL1L reinforce the impaired GSIS and reduced proliferation observed *in vivo*.

The selective deletion of *Sel1L* in β-cells (*Sel*$^{lox/lox}$*; RIP-Cre*) also confirms an integral role for SEL1L in β-cell function. *Sel*$^{lox/lox}$*; RIP-Cre* mice exhibit hyperglycemia (on a normal diet) and severely impaired glucose intolerance that worsens over time. These metabolic parameters are exacerbated when *Sel*$^{lox/lox}$*; RIP-Cre* mice are administered a high-fat diet. While there is no observable difference in β-cell mass between *Sel*$^{lox/lox}$*; RIP-Cre* mice and *Sel*$^{lox/lox}$ mice (up to 12 weeks of age), defective GSIS and glucose intolerance are observed in the *Sel*$^{lox/lox}$*; RIP-Cre* mice. Further, β-cells of *Sel*$^{lox/lox}$*; RIP-Cre* mice have an accumulation of proinsulin in the ER which obstructs the insulin secretory pathway. UPR markers are upregulated in the islets of *Sel*$^{lox/lox}$*; RIP-Cre* mice, and administration of 4-PBA

in drinking water can reduce fasting blood glucose levels over time, suggesting ER stress is the presumable cause of this cellular and metabolic phenotype.

Various mouse and human genetic models have demonstrated that increased ER stress induces β-cell dysfunction and T2D. For example, mutations in *Perk*, *Eif2α*, *p58^{IPK}*, and *Wfs1* in mice lead to hyperglycemia due to defective intracellular trafficking of ER cargo proteins, insufficient insulin secretion, and/or β-cell death (61, 62, 160, 161). These studies substantiate the role of the UPR in β-cell function and survival. While many of these models focus on the regulation of proinsulin and insulin synthesis and translational attenuation, the importance of the ERAD mechanism in pancreatic β-cells has not been extensively studied. However, two mouse models support the function of ERAD in normal β-cell physiology. The *Akita* mouse, characterized by expression of misfolded insulin, exhibits hyperglycemia, decreased insulin secretion, and progressive apoptosis of β-cells over time (57). With regard to ERAD components, *Akita* mice have been observed to have relatively higher transcript levels of *Bip*, *Hrd1*, and *Sel1L* in the pancreatic islets compared to their wild-type counterparts (117). Also, transgenic mice for the *human islet amyloid polypeptide (hIAPP)* gene provide critical insight into the failure of the UPR to prevent intracellular oligomerization of this amyloidogenic protein. Male mice exhibit a diabetic phenotype beginning between 4 to 8 weeks of age, and death around 16 weeks. This diabetic phenotype includes β-cell death associated with decreased circulating insulin levels, hyperglycemia, and abnormal intracellular aggregates of hIAPP (162). An impaired ubiquitin-proteasomal pathway in the β-cells

contributes to the apoptosis in this mouse model (163). Furthermore, islets from patients with T2D show dysfunctional ubiquitin-proteasomal degradation, due in part to overexpression of misfolded human islet amyloid polypeptide (hIAPP) (164). This dysfunction was found to be mediated by a deficiency in ubiquitin carboxyl-terminal hydrolase L1 (UCH-L1) protein levels.

Interestingly, phenotypic similarities were observed between ERAD-deficient and autophagy-deficient mice. Autophagy is the engulfment of misfolded proteins or protein aggregates within double-membrane vesicles that subsequently fuse to a lysosome, containing the proper enzymes for degrading the contents (103). Knockout of autophagy-related protein 7 (ATG7), a factor for autophagy, in β-cells of mice results in a level of hyperglycemia that is comparable to what we observe in our conditional mouse model. Moreover, there is decreased β-cell mass, compromised β-cell function, and an accumulation of ubiquitylated aggregates in the *Atg7*-β-cell-deficient mice (165). When challenged with a high-fat diet, these mice fail to expand β-cell mass due to increased apoptosis and degeneration of β-cells (166).

Intriguingly, although the *Sel1L*$^{+/-}$ mice on a HFD and *Sel*$^{lox/lox}$*; RIP-Cre* mice both display an apparent defect in insulin secretion in response to glucose, they both also have elevated serum insulin levels (Figure 3.1a and 4.4a). Hyperinsulinemia is typically an indication of insulin resistance. It has been reported that an increase in JNK activity (through nutrient-induced ER stress in mice) causes an increase in serine phosphorylation of insulin receptor substrate-1 (IRS-1), which in turn reduces insulin receptor signaling and contributes to insulin resistance in peripheral tissues (37). Essentially, ER stress may provide an

important link between obesity and T2D. Although the insulin tolerance test (ITT) in heterozygote mice on a HFD indicates that there is no significant change in insulin sensitivity, we did see an upregulation of UPR markers at the protein level in their livers. Further biochemical and molecular studies would be required to determine what role SEL1L has in regulating insulin sensitivity in peripheral tissues.

One notable difference between the HFD and conditional mouse models for *Sel1L* is related to β-cell mass. *Sel1L*$^{+/-}$ mice on a HFD have a markedly reduced β-cell mass in comparison to wild-type mice on a HFD. This is attributed to a decrease in proliferation of β-cells and not to an increase in apoptosis. In *Sel*$^{lox/lox}$*; RIP-Cre* mice, there is no change in β-cell mass due to the genetic loss of *Sel1L*. Instead, there is a striking defect in GSIS in the β-cells. This differential phenotype at the level of the β-cell points to diverse roles for SEL1L in β-cell function and proliferation. β-cell mass is not altered at 8 weeks of age for HFD-fed *Sel1L*$^{+/-}$ mice, but fasting blood glucose levels are significantly elevated. This leads to the possibility that the observed hyperglycemia is due to an inherent secretion defect. Only at later stages of the HFD treatment do we observe insufficient expansion of β-cell mass. A HFD has been shown to have lipotoxic effects in β-cells *in vivo* and *in vitro*. Chronically elevated levels of circulating free fatty acids (FFAs) are putative mediators of β-cell dysfunction and death in T2D (167, 168). Palmitate, a saturated long-chain FFA, induces ER stress in both clonal and primary murine and human β-cells, and preferentially activates both PERK and IRE1α pathways (72, 169). Several studies indicate that palmitate triggers ER

stress in β-cells through perturbations in ER Ca^{2+} balance and disruption of secretory pathways (71, 170). Therefore, in the condition of long-term overnutrition, haploinsuffieciency of SEL1L function generates some level of ER stress to affect β-cell proliferation. However, increased β-cell death is not seen in *Sel1L*$^{+/-}$ mice on a HFD, indicating that adaptive mechanisms in the cells must be preventing the initiation of apoptotic pathways. ER stress can decrease β-cell proliferation via induction of the UPR, when translational attenuation limits cell growth capabilities. IRE1α activity is known to mediate apoptotic pathways in response to ER stress, but has also recently been shown to inhibit proliferation through downregulation polo-like kinase 1 (PLK1), an early trigger for G2/M transition (171). β-cell mass is known to be modulated by several factors, including by increased signaling by insulin and/or insulin-like growth factor-1 (IGF-1) (146). SEL1L could be a direct or indirect participant in regulating insulin signaling to influence β-cell proliferation. Perhaps certain proteins in these signaling pathways are regulated by ERAD, which is presumably compromised in our heterozygote mouse model for *Sel1L*.

Trafficking of proteins from the ER to the Golgi apparatus is required for efficient ERAD (172). Conversely, it seems that an intact ERAD is necessary for proper protein folding and trafficking. In yeast, mutations in ERAD components such as Der1p and Hrd3p lead to morphological changes in the ER and Golgi and a slower maturation rate of wild-type secretory proteins (173). In *Sel1L*$^{+/-}$ mice on a HFD and *Sel*$^{lox/lox}$*; RIP-Cre* mice, loss of *Sel1L* contributes to an inability to secrete insulin and this in turn contributes to hyperglycemia. A defective ERAD complex in the β-cells of these mice causes an accumulation of proinsulin

within the ER and delayed maturation of insulin. Both of these models also have reduced total pancreatic insulin content in comparison to their respective controls (Appendix B, Figures f and g). A similar observation was made in islets and insulinoma cell lines with loss of *Perk* function. These cells are reported to have impaired anterograde protein trafficking and are unable to retrotranslocate and degrade known ERAD substrates. In our *Sel1L*-deficient models, impaired trafficking could be a consequence of or a cause of ER stress. Although 4-PBA is able to rescue hyperglycemia in both the $Sel1L^{+/-}$ mice on a HFD and $Sel^{lox/lox}$; *RIP-Cre* mice, this chemical compound has properties that improve both ER stress and secretory protein trafficking. Therefore, further studies would be required to dissect the general role of SEL1L in ER homeostasis and a potential more specific role in ER to Golgi trafficking.

Taken together, these data reinforce an instrumental role for *Sel1L* in ER and β-cell homeostasis. SEL1L is required for maintaining normal glucose tolerance. At a cellular level, SEL1L is necessary for secretion of insulin in response to glucose and for expansion of β-cell mass in response to HFD-induced insulin resistance. Therefore, the ERAD process is indispensible for glucose homeostasis. Our data demonstrates that ER stress has an important causal role in the pathogenesis of T2D. Administration of 4-PBA, to mitigate ER stress in the β-cell, could be an effective therapy to enhance insulin secretion and improve β-cell survival in this disease.

CHAPTER 4: THE ROLE OF *Sel1L* IN HYPOTHALAMIC NEURONS AND ENERGY HOMEOSTASIS

4.1 Abstract

The hypothalamus is a major site of integration of peripheral and central signals to maintain energy balance. Inaction of hypothalamic neurons to leptin and insulin (leptin/insulin resistance) is the cause of obesity. Cellular and molecular evidence points to an emerging role for endoplasmic reticulum (ER) stress in mediating leptin resistance in the hypothalamus. To further address this potential role, we investigated the contribution of an ER-specific pathway, known as ER-associated degradation (ERAD), in energy homeostasis. The *mouse Suppressor-enhancer-lin 12-1-Like* (*Sel1L*) gene encodes an ER transmembrane protein known to nucleate the ERAD translocation machinery at the interface of the ER and cytosol. We have previously reported that global disruption of *Sel1L* leads to early embryonic lethality in mice. As discussed in Chapter 3, we generated conditional knockout mice with selective deletion of *Sel1L* in β-cells. The RIP-*Cre* transgene, however, was also found to be expressed in the hypothalamus. Starting at around 12 weeks of age, the male mutant mice ($Sel^{lox/lox}$; *RIP-Cre*), showed a pronounced increase in body weight, food intake, and adiposity over time in comparison to control mice ($Sel^{lox/lox}$ and $Sel^{lox/+}$; *RIP-Cre*). Furthermore, $Sel^{lox/lox}$; *RIP-Cre* mice had elevated fasting leptin and insulin levels and an impaired response to the administration of exogenous leptin, suggestive of leptin resistance. ER stress was present in the hypothalami of $Sel^{lox/lox}$; *RIP-Cre* mice, particularly in the arcuate nucleus and paraventricular nucleus, as

determined by quantitative RT-PCR of UPR markers. The arcuate nucleus also showed increased expression of the *Pomc* transcript and unchanged expression of *Npy* transcript. Starting at 10 weeks of age, ongoing administration of the chemical chaperone 4-PBA in drinking water prevented weight gain in $Sel^{lox/lox}$; *RIP-Cre* mice. Finally, administration of 4-PBA via the intracerebroventricular (ICV) route reduced food intake and body weight in $Sel^{lox/lox}$; *RIP-Cre* mice at 23 weeks of age, indicating that ER stress is mediating the hyperphagic obesity in these mice. Taken together, these data strongly suggest that *Sel1L* has a crucial role in the central nervous system to regulate energy homeostasis. Further investigations are needed to elucidate the molecular mechanisms that underlie the observed SEL1L action in the brain.

4.2 Introduction

Obesity has become a major global public health concern in recent decades. Currently, over one-third of adults in the US are obese and the rate at which both adults and children worldwide are becoming overweight or obese is staggering (174). Mortality rates associated with being overweight and obese have also seen an upward trend due to related risks such as hypertension, diabetes and hypercholesterolemia. Manifestation of obesity and weight gain has been shown to be multifaceted, ranging from genetic predisposition to socioeconomic status to age. The genetic determinants of body weight regulation in humans, however, still remain poorly understood.

Weight balance in mammals involves the integration of signals from the pancreas, adipose tissue, gastrointestinal tract, and brain, among several other organs. The brain, in particular, controls food intake and energy expenditure

through leptin signaling in the hypothalamus. Leptin, a hormone secreted from adipose tissue, enters the brain and acts on its receptors in the mediobasal hypothalamus to exert its anorexigenic effects. In particular, the arcuate nucleus (ARC) has high expression of Ob-Rb (the predominant long-form of the leptin receptor) in two distinct neuronal populations: NPY/AGRP and POMC/CART. NPY/AGRP co-expressing neurons promote food intake while POMC/CART co-expressing neurons inhibit food intake through melanocortin signaling in secondary neurons (175). Leptin and insulin behave reciprocally on these neurons so their effect in response to nutritional status is decreased energy intake and increased energy expenditure to produce a sense of satiety.

An obese state is characterized by overconsumption and an expansion of adipose tissue, leading to hyperleptinemia. Despite this elevation of leptin in the blood and consequently in cerebrospinal fluid, the aforementioned hypothalamic neurons cannot respond appropriately to restore energy balance. This condition is referred to as "leptin resistance," and is a main target for unraveling the cellular and molecular basis of obesity. The two hypotheses that have received the most attention in this regard are the impairment of leptin transport to its targets in the brain or a defect in the intracellular Ob-Rb signaling cascade (46, 176). High-fat diet (HFD) murine models have been used to resolve the interaction between polygenic and environmental factors that contribute to leptin resistance. Diet-induced obese (DIO) mice are also systems to explore leptin function and compromised leptin and insulin signaling in obesity. Evidence from several HFD studies has implicated a critical role for endoplasmic reticulum (ER) stress in the pathogenesis of diet-induced obesity (47, 48, 50).

Disequilibrium in misfolded or unfolded proteins and the folding capacity of the ER generates "ER stress." ER stress elicits the UPR as an adaptive mechanism to restore normal ER function (148). The UPR is a signaling network that integrates 3 distinct branches, each initiated by an ER-localized "stress sensor": PERK, IRE1α, and ATF6. Together, the UPR regulates the expression of various genes to maintain homeostasis in the ER or induce apoptosis in conditions where ER stress cannot be mitigated. Homeostatic mechanisms of the UPR include an attenuation of protein translation and increased ERAD to remove toxic proteins from the ER lumen. ER stress has been implicated as a causal factor in many pathologies, including metabolic disease, inflammation, neurodegeneration, and cancer (177).

Although previous studies have described ER stress as a principle mediator of central insulin and leptin resistance in the context of a HFD and overnutrition, they have not addressed ER stress as it relates to the genetic component of obesity. Compelling scientific evidence has led to the belief that the propensity to become obese is largely genetically determined (178, 179). This is supported by the fact that weight loss in obese individuals is often met with compensatory genetic responses, leading to an increase in hunger and decrease in activity. For this reason, most people who lose weight by dieting eventually regain it within a short period of time (180, 181).

In the present study, we explore the contribution of the UPR and specifically ERAD in the regulation of weight balance. We developed a conditional mouse model for *Suppressor-enhancer-lin 12-1-Like* (*Sel1L*), a gene that encodes a multimodular protein with an established role in ERAD. SEL1L is speculated to function in protein-protein interactions at the interface of the ER

lumen and cytosol, where it facilitates the ubiquitylation and extrusion of misfolded proteins. In the first mouse model for *Sel1L*, we have previously shown an essential role for this ERAD factor in development and glucose homeostasis (137, 157). With our current conditional knockout mice, we were able to effectively delete *Sel1L* in the hypothalamus. Here, we reveal for the first time a novel mechanism by which ERAD regulates energy homeostasis and by which ER stress contributes to the pathogenesis of obesity.

4.3 Materials and Methods

Mice

For the conditional deletion of *Sel1L*, embryonic stem cells were purchased by the UC Davis KOMP repository and injected into C57BL/6 blastocysts. Mice expressing the target vector were bred to *FLPe* transgenic mice, kindly provided by Dr. Paula Cohen. The resulting $Sel^{lox/+}$ mice were bred to homozygosity. $Sel^{lox/lox}$ mice were crossed with *RIP-Cre* mice (Jackson Laboratory, B6.Cg-Tg(Ins2-cre)25Mgn/J). $Sel^{lox/+}$*; RIP-Cre* were crossed to $Sel^{lox/lox}$ mice to generate $Sel^{lox/lox}$*; RIP-Cre* mice and littermate controls for experiments. A standard PCR was performed on genomic DNA to confirm Cre-mediated recombination (Appendix C, Figure a).

All animal experiments were performed in accordance with the Cornell Animal Care and Use Guidelines.

In vivo physiological studies

Body weights of mice were recorded on a weekly basis starting one week after birth. For the insulin tolerance test (ITT), mice were fasted overnight for 8 hours and given an intraperitoneal (IP) injection of recombinant insulin in PBS (Eli Lilly, 0.75 IU/kg B.W.). Blood glucose levels were measured for each mouse at 0, 30, 60, 90, and 120-minute time points. The Ascensia ELITE XL glucometer and accompanying strips were used for blood glucose measurement. For the leptin resistance test, recombinant leptin (A.F. Parlow, National Hormone & Peptide Program, 3 mg/kg B.W.) was delivered to mice via IP injection at 9 A.M. and 6 P.M. for 4 days. Body weight, food intake and random blood glucose were measured each day. Serum insulin and serum leptin were assayed using the Mouse Insulin Ultrasensitive ELISA (ALPCO) and the Leptin (Mouse/Rat) ELISA (ALPCO), respectively, according to manufacturer's instructions.

For 4-PBA treatment, 4-phenylbutyric sodium salt (Scandinavian Formulas) was dissolved in acidified drinking water (1 g/kg/day) and provided to mice starting at 10 weeks of age. Bottles were replaced weekly.

Intracerebroventricular (ICV) cannulation was performed as previously described (182, 183). Following implantation of the cannulas, mice recovered for 5 days. Baseline measurements were taken for 3 days prior to injections with 4-PBA (1 μl of 10 mg/ml or 10 μg). Body weight and food intake were recorded daily.

For activity (energy expenditure) data collection, the Oxymax Comprehensive Lab Animal Monitoring System (CLAMS) for Rats and Mice (Columbus Instruments) was used (courtesy of Dr. Ling Qi and the Department of Animal Science). Pair-feeding was performed with individually housed *Sel*$^{lox/lox}$

and *Sel*$^{lox/lox}$*; RIP-Cre* mice between 16 and 18 weeks of age. *Sel*$^{lox/lox}$ mice were fed *ad libitum* and their food intake was measured every 24 hours. The same amount of food was provided to age- and weight-matched *Sel*$^{lox/lox}$*; RIP-Cre* mice. Body weights were measured each day.

All physiological studies used male mice.

Adiposity and Micro computed tomography (Micro CT) analysis

Adiposity was measured at 6 weeks and 32 weeks of age by dissecting and weighing the paired epididymal, subcutaneous, and retroperitoneal white adipose depots for each mouse. The adiposity percentage for each mouse represents the collective weight of these depots as a ratio to the total body weight.

Micro CT scans of 1-year old *Sel*$^{lox/lox}$ and *Sel*$^{lox/lox}$*; RIP-Cre* mice were performed at the Cornell Micro CT and Nano CT Imaging Facility using the GE eXplore CT120 (50 μM resolution). Analysis was performed as described previously (184). OsiriX (v5.5) imaging software was used for the 3D rendering and quantification of regions of interest. Total fat volume was determined as an absolute value and not a percentage.

Immunohistochemistry

To determine β-cell proliferation, pancreatic sections were co-immunostained with mouse monoclonal anti-Ki67 (Vector Laboratories, 1:500) and anti-insulin antibodies. Cy3-conjugated donkey anti-mouse and Cy2-

conjugated donkey anti-guinea pig secondary antibodies (Jackson ImmunoResearch Laboratories, 1:500) were applied. Nuclei were counterstained with DAPI. The percentage of Ki67-positive cells was derived by dividing the number of Ki67-positive nuclei by the total number of counted β-cell nuclei.

RNA Extraction and Quantitative Real-Time Reverse Transcription PCR

For isolation of the whole hypothalamus, mice were decapitated and their brains were quickly extracted and stored on dry ice for 5 minutes. A mouse brain slicer matrix (Zivic Instruments) was used to separate the hypothalamus from other brain tissue. For the isolation of hypothalamic regions, brains were extracted, immediately embedded in OCT, frozen on dry ice, and stored at -80 until further use. Specific regions were isolated using a crystat and cylindrical brain punchers based on the Mouse Brain Stereotaxic Atlas (Academic Press, Second edition). For these isolations, punches from each region were pooled from two independent mice per sample. RNA was isolated from hypothalamic regions and the hypothalamus by the TRIzol-chloroform method. RNA quality and concentration was measured using the Agilent 2100 Bioanalyzer (Agilent Technologies). First-strand cDNA synthesis was performed using RT Buffer, dNTPs, DTT, RNAout, and SuperScript III Reverse Transcriptase (all Invitrogen). Quantitative PCR was carried out using Power SYBR Green PCR Master Mix or iTaq Universal SYBR Green Supermix (Bio-Rad) on an ABI Prism 7000 Sequence Detection System or StepOnePlus Real-Time PCR System (Applied Biosystems). PCR primers were designed using the PrimerSelect program of Lasergene 7.1

Sequence Analysis Software (DNAstar). Final quantification and normalization was determined according to the $\Delta\Delta C_q$ calculation method (156).

Statistical Analyses

Statistical analysis using the student's T-Test or two-way repeated measures ANOVA with Tukey's HSD post-hoc test where appropriate was performed using STATA (v12).

4.4 Results

4.4.1 The hypothalamus-specific deletion of *Sel1L* contributes to the increased weight gain over time on a normal chow diet

Body weights were monitored on a weekly basis in the three genotypes (*Sel*$^{lox/lox}$, *Sel*$^{lox/+}$; *RIP-Cre*, and *Sel*$^{lox/lox}$; *RIP-Cre*) starting at 2 weeks of age. For both males and females, there appeared to be relatively normal fluctuations in body weight between the three genotypes, while maintained on a normal chow diet, for the first 12 weeks of age (Figure 4.1a and 4.1b). However, after this time point there was a steady increase in the body weights of the *Sel*$^{lox/lox}$; *RIP-Cre* mice. The divergence was slower in males than in females, with the body weights of the male mice reaching significantly higher values at 18 weeks of age, and female mice at 13 weeks of age ($p<0.05$). By 32 weeks of age, *Sel*$^{lox/lox}$; *RIP-Cre* mice continued to gain weight in comparison to their control littermates (Figure 4.1c). This difference is exemplified in Figure 4.1d and 4.1e. At 12 months of age, the discrepancy in mass is exceptional, as depicted through Micro CT imaging and computer-assisted analysis of adiposity (Figure 4.1f and 4.1g). The body weights

of *Sel*$^{lox/lox}$*; RIP-Cre* mice at this age are, on average, about 73% higher than *Sel*$^{lox/lox}$ mice.

Figure 4.1: *Sel$^{lox/lox}$; RIP-Cre* mice gain significant weight over time on a normal chow diet. Shown here are the body weights of (a) male and (b) female mice of each genotype (n=8-12 mice per genotype per sex) from 2 to 24 weeks of age ($p<0.05$ after week 18 for males and week 13 for females). (c) Body weights were measured for each sex at 32 weeks of age. (d) and (e) Pictures representing an average *Sel$^{lox/lox}$; RIP-Cre* (left) and *Sel$^{lox/lox}$* (right) mouse were taken at 32 weeks of age. Micro CT images show visceral and subcutaneous fat depots highlighted in red for (f) *Sel$^{lox/lox}$* and (g) *Sel$^{lox/lox}$; RIP-Cre* mice at approximately 12 months of age. (h) Quantification (to be added). *, $p<0.05$; **, $p<0.01$.

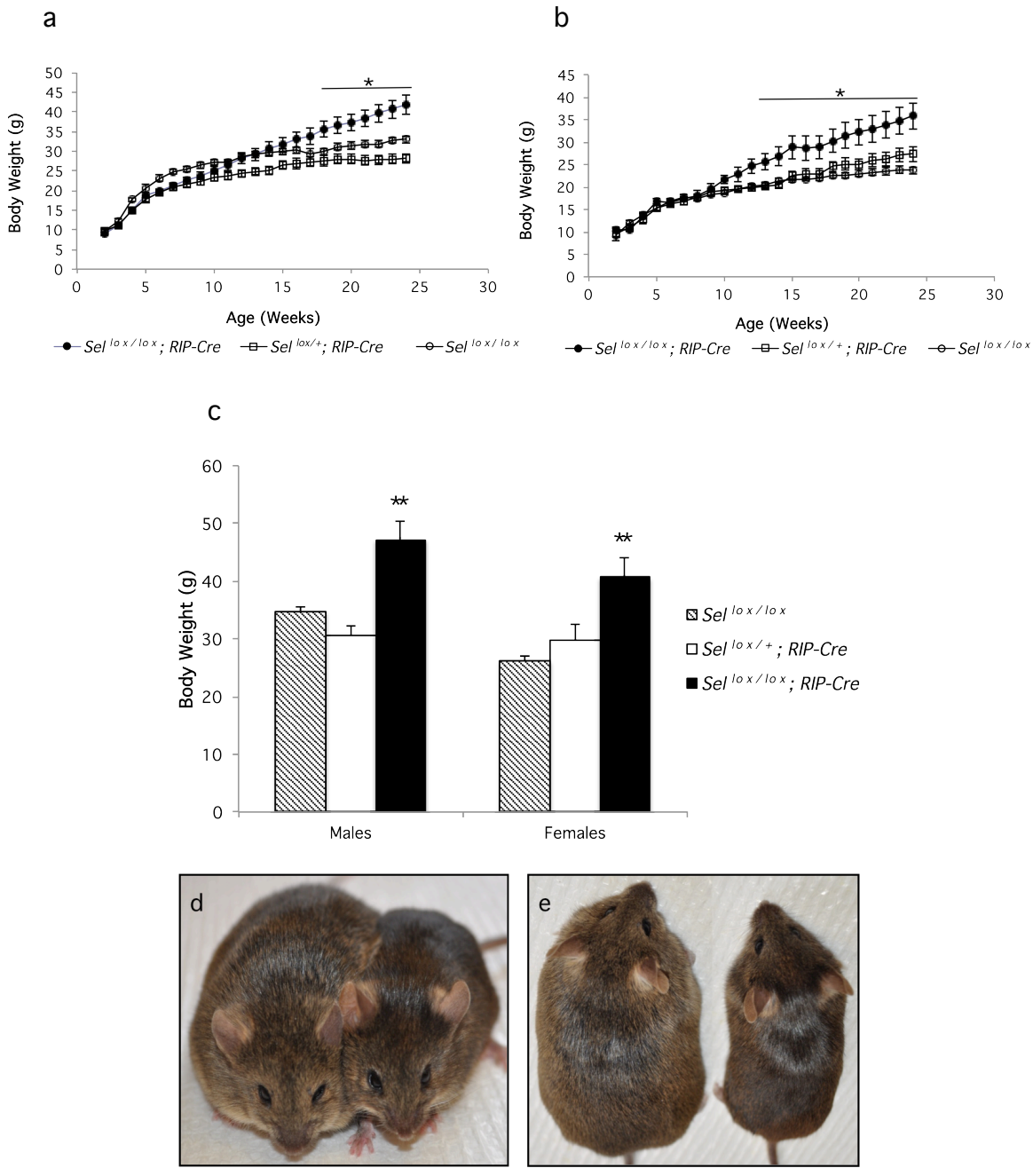
a
Body Weight (g)
Age (Weeks)
*
Sel lox/lox; RIP-Cre
Sel lox/+; RIP-Cre
Sel lox/lox
b
Body Weight (g)
Age (Weeks)
*
Sel lox/lox; RIP-Cre
Sel lox/+; RIP-Cre
Sel lox/lox
c
Body Weight (g)
**
**
Males
Females
Sel lox/lox
Sel lox/+; RIP-Cre
Sel lox/lox; RIP-Cre
d
e

Figure 4.1, Continued:

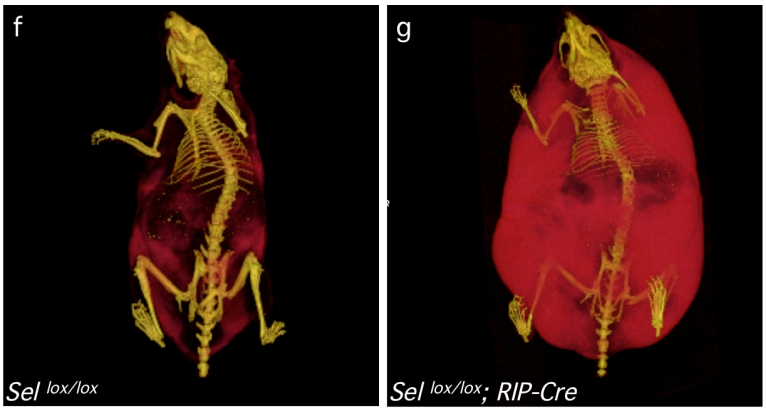

4.4.2 Increased adiposity in *Sel*$^{lox/lox}$*; RIP-Cre* mice is due to hyperphagia

To quantify adiposity at 32 weeks of age for the *Sel*$^{lox/lox}$*; RIP-Cre* mice versus the controls (collectively *Sel*$^{lox/lox}$ and *Sel*$^{lox/+}$*; RIP-Cre* mice), various white fat depots were isolated from each mouse and weighed (Figure 4.2a). Adiposity was also quantified at 6 weeks of age for each genotype, and no significant difference was observed (data not shown). The mutant mice, on average, displayed adiposity that was nearly twice greater than that seen in the control mice. The expansion of subcutaneous, retroperitoneal, epicardial (Figure 4.2a and 4.2b), and epididymal fat depots was clearly seen in *Sel*$^{lox/lox}$*; RIP-Cre* mice. Histological analysis of subcutaneous adipose tissue in *Sel*$^{lox/lox}$ and *Sel*$^{lox/lox}$*; RIP-Cre* mice (Figure 4.2e and 4.2f, respectively) indicated that there are enlarged adipocytes in the mutant mice.

Increased adiposity led us to investigate feeding behavior and energy expenditure as possible sources of this deviance. Mice between the ages of 7 and 11 weeks, when the body weights are similar between the genotypes, did not

show a genotype-dependent difference in food intake (Figure 4.2g). However, *Sel*$^{lox/lox}$*; RIP-Cre* mice between the ages of 12 and 16 weeks had significantly higher food intake in comparison to their littermate controls (Figure 4.3h). Energy expenditure was assessed using a lab animal monitoring system for *Sel*$^{lox/lox}$ and *Sel*$^{lox/lox}$*; RIP-Cre* mice at 12 weeks of age, prior to the divergence in body weights. Oxygen consumption and the respiratory exchange ratio (RER), as indicators of gas exchange and therefore energy expenditure, were not significantly different between the genotypes (Figure 4.2i). Therefore, only hypothalamic feeding circuits are altered in *Sel*$^{lox/lox}$*; RIP-Cre* mice, and the increase in body weight is primarily attributed to hyperphagia. Pair-feeding studies with mice at 16 weeks of age also confirmed this finding (Appendix C, Figure b).

Figure 4.2: Obesity in *Sel$^{lox/lox}$; RIP-Cre* mice is due to hyperphagia. (a) Various white fat depots were excised and their collective weight as a percentage of the total body weight per mouse was used to assess adiposity in *Sel$^{lox/lox}$; RIP-Cre* mice and control (*Sel$^{lox/lox}$* and *Sel$^{lox/+}$; RIP-Cre*) mice at 32 weeks of age (n=7-8 mice/genotype). Pictures of the thoracic cavity are seen for a (b) wild-type and (c) mutant mouse at 32 weeks of age, as well as (d) epididymal fat pads from a wild-type (left) and mutant (right) mouse. Next, H&E staining of subcutaneous fat pad sections from a (e) *Sel$^{lox/lox}$; RIP-Cre* and (f) *Sel$^{lox/lox}$* mouse are depicted (10X magnification). (g) Food intake per day was measured in mice of each genotype between the ages of 7 and 11 weeks and (h) between the ages of 12 and 16 weeks (n=6-7 cages per genotype). (i) Metabolic cages were used to determine oxygen consumption (VO_2, seen above) as a reflection of energy expenditure in the mice at 12 weeks of age (n=4 cages per genotype).

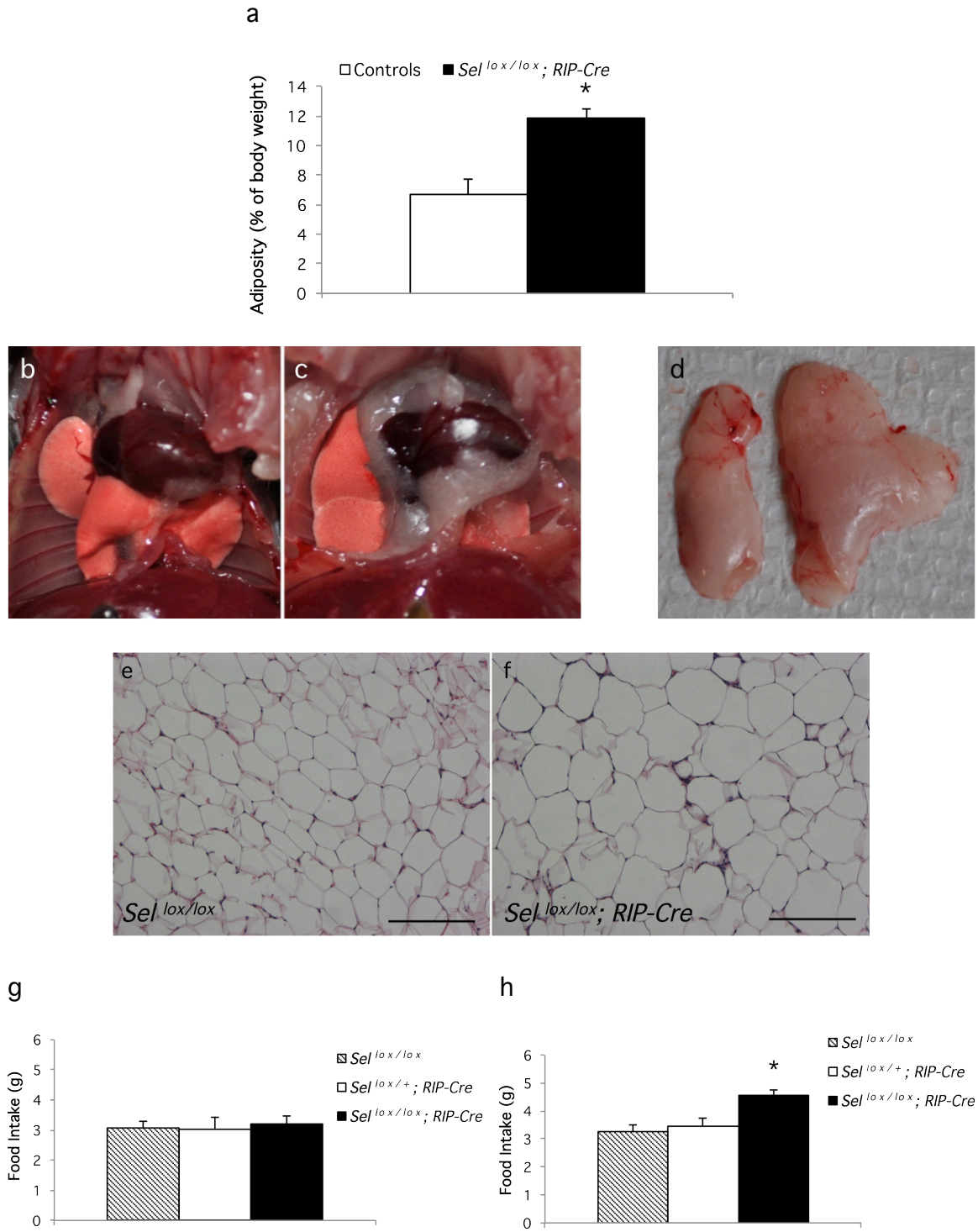
a
Controls
Sel lox/lox; RIP-Cre
Adiposity (% of body weight)
14
12
10
8
6
4
2
0
*
b
c
d
e
f
Sel lox/lox
Sel lox/lox; RIP-Cre
g
h
Food Intake (g)
6
5
4
3
2
1
0
Sel lox/lox
Sel lox/+; RIP-Cre
Sel lox/lox; RIP-Cre
*

Figure 4.2, Continued:

i

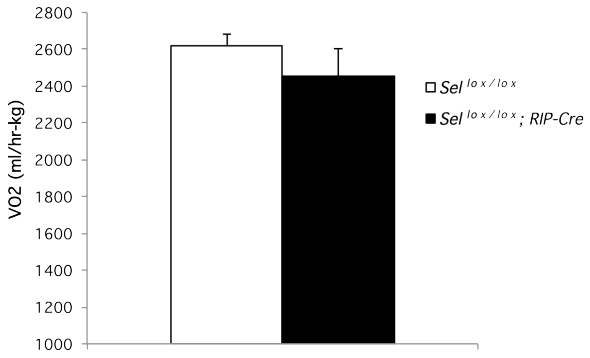

4.4.3 *Sel*$^{lox/lox}$*; RIP-Cre* mice are leptin resistant prior to weight gain

Leptin plays a key role in regulating energy intake and expenditure. Its presence in the central nervous system, specifically the mediobasal hypothalamus, is proportional to its plasma concentration. We therefore examined fasting serum leptin levels in *Sel*$^{lox/lox}$ and *Sel*$^{lox/lox}$*; RIP-Cre* mice at various ages (Figure 4.3a). A normal increase in serum leptin levels was observed in *Sel*$^{lox/lox}$ mice, due to a correlated increase in adiposity with age. Serum leptin levels in *Sel*$^{lox/lox}$*; RIP-Cre* mice were significantly higher than those seen in *Sel*$^{lox/lox}$ mice at each age. At 6 and 12 weeks of age, there was no significant difference in body weights between the genotypes, yet still elevated serum leptin levels in *Sel*$^{lox/lox}$*; RIP-Cre* mice. By 32 weeks of age, an accumulation of adipose tissue contributed to serum leptin levels that are on average about 2.5 times higher in *Sel*$^{lox/lox}$*; RIP-Cre* mice than in control mice.

To further assess leptin resistance, we administered leptin (I.P., 2.5 mg/kg B.W.) twice daily to *Sel*$^{lox/+}$*; RIP-Cre* and *Sel*$^{lox/lox}$*; RIP-Cre* mice and measured body weight and food intake each day. Administration of a supraphysiological dose of recombinant leptin caused reductions in weight and food consumption in control mice over a 2 to 3 day period. As seen in Figure 4.3b and 4.3c, *Sel*$^{lox/lox}$*; RIP-Cre* mice had a blunted response to the exogenous leptin versus the *Sel*$^{lox/+}$*; RIP-Cre* mice. Together, hyperleptinemia and a diminished response to leptin constitute a state of leptin resistance in *Sel*$^{lox/lox}$*; RIP-Cre* mice.

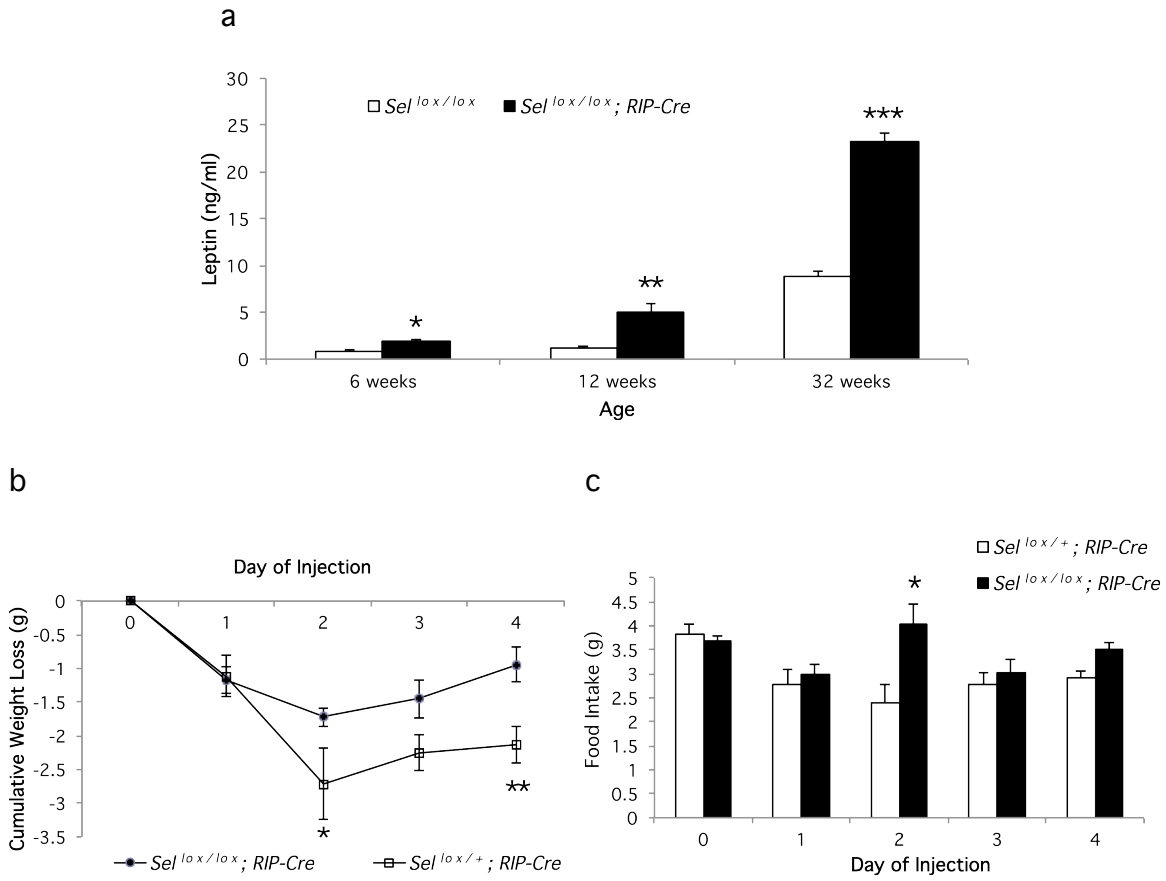

Figure 4.3: *Sel*$^{lox/lox}$*; RIP-Cre* mice have severe leptin resistance. (a) Serum from fasting *Sel*$^{lox/lox}$ and *Sel*$^{lox/lox}$*; RIP-Cre* mice at various ages was collected and assayed for leptin concentration using an ELISA (n=6-8 mice per genotype). Mice of each genotype (*Sel*$^{lox/+}$*; RIP-Cre* and mutants, n=7-8 mice per genotype) were given I.P. injections leptin (2.5 mg/kg B.W.) twice daily for 4 days. Changes in (b) weight and (c) food intake were monitored over this time. *, $p<0.05$; **, $p<0.01$, ***, $p<0.001$.

4.4.4 Increased fat content manifests in apparent insulin resistance in *Sel*$^{lox/lox}$*; RIP-Cre* mice

The *RIP-Cre* transgene is also expressed in the pancreatic β-cells of mice. Therefore *Sel1L* is deleted in the β-cells of *Sel*$^{lox/lox}$*; RIP-Cre* mice. As discussed previously in Chapter 3, *Sel*$^{lox/lox}$*; RIP-Cre* mice are hyperglycemic and their β-cells have a conspicuous defect in glucose-stimulated insulin secretion. Furthermore,

Sel1L$^{+/-}$ mice (global knockout) have reduced proliferation of β-cells in response to HFD-induced insulin resistance. Since insulin is an important adiposity signal in the central nervous system, and since *Sel1L* deletion is expected in β-cells, we wanted to determine the degree of insulin resistance and its effect in the β-cells of *Sel*$^{lox/lox}$; *RIP-Cre* mice.

As with leptin, fasting serum insulin levels were assayed in *Sel*$^{lox/lox}$ and *Sel*$^{lox/lox}$; *RIP-Cre* mice at 6, 12 and 32 weeks of age (Figure 4.4a). Whereas the serum insulin concentration in control mice remained relatively constant with age, the serum insulin concentration in *Sel*$^{lox/lox}$; *RIP-Cre* mice was increased with age. Again, as seen with the serum leptin levels, there was elevated serum insulin at 6 and 12 weeks of age, which is prior to the period of weight gain in *Sel*$^{lox/lox}$; *RIP-Cre* mice. To physiologically assess insulin resistance, we performed an insulin tolerance test on mice at 24 weeks of age (Figure 4.4b). Mice were injected with recombinant insulin (IP, 0.75 IU/kg B.W.) and blood glucose levels were monitored at intervals within a 2-hour post-injection period. *Sel*$^{lox/lox}$ mice and *Sel*$^{lox/+}$; *RIP-Cre* mice responded normally to the exogenous insulin with a modest decline in blood glucose levels. *Sel*$^{lox/lox}$; *RIP-Cre* mice displayed an anomalous response to the insulin injecton, with average relative blood glucose levels that significantly increased during the post-injection period.

Given that the ITT revealed severe insulin resistance in *Sel*$^{lox/lox}$; *RIP-Cre* mice, we expected there would be an expansion of β-cell mass in response to this resistant state. Insulin immunostaining of pancreatic sections from *Sel*$^{lox/lox}$ and *Sel*$^{lox/lox}$; *RIP-Cre* mice demonstrated that β-cell mass was significantly higher in the *Sel*$^{lox/lox}$; *RIP-Cre* mice at 32 weeks of age (Appendix C, Figure d). We also

performed Ki67 and insulin co-immunostaining on pancreatic sections from each genotype at this same age to evaluate proliferation of β-cells. There were significantly more Ki67-positive, and thus proliferating, β-cells in the *Sel*$^{lox/lox}$*; RIP-Cre* pancreata (Figure 4.4d) than in the *Sel*$^{lox/lox}$ pancreata (Figure 4.4c). Quantification of Ki67-positive β-cells in each genotype at 6 weeks of age indicated that there was no significant difference in proliferative cells between the genotypes at this time (Figure 4.4e). At 32 weeks of age, the percentage of Ki67-positive β-cells in the *Sel*$^{lox/lox}$*; RIP-Cre* pancreata was comparable to that seen at 6 weeks of age (for both genotypes). While wild-type mice show a normal decline in β-cell proliferation with age, the development of insulin resistance does indeed prompt β-cell replication in the mutant. Therefore, the absence of *Sel1L* in β-cells of *Sel*$^{lox/lox}$*; RIP-Cre* does not hinder β-cell proliferation in response to insulin resistance.

Figure 4.4: *Sel*$^{lox/lox}$*; RIP-Cre* mice maintain a normal response to insulin resistance in the β-cell. (a) Serum from fasting *Sel*$^{lox/lox}$ and *Sel*$^{lox/lox}$*; RIP-Cre* mice at various ages was collected and assayed for insulin concentration using an ELISA (n=6-8 mice per genotype). (b) At 24 weeks of age, insulin tolerance was assessed in *Sel*$^{lox/lox}$, *Sel*$^{lox/+}$*; RIP-Cre* and *Sel*$^{lox/lox}$*; RIP-Cre* mice through an ITT (n=5-8 mice per genotype). Immunostaining for Ki67 (red), insulin (green) and DAPI (blue) is seen in representative pancreatic sections from (c) *Sel*$^{lox/lox}$ and (d) *Sel*$^{lox/lox}$*; RIP-Cre* mice at 32 weeks of age (40X magnification). (e) Quantification of the percentage of Ki67-positive β-cells in pancreatic sections from *Sel*$^{lox/lox}$ and *Sel*$^{lox/lox}$*; RIP-Cre* mice (n=4 mice per genotype) at 6 and 32 weeks of age. *, $p<0.05$, **, $p<0.01$, ***, $p<0.001$.

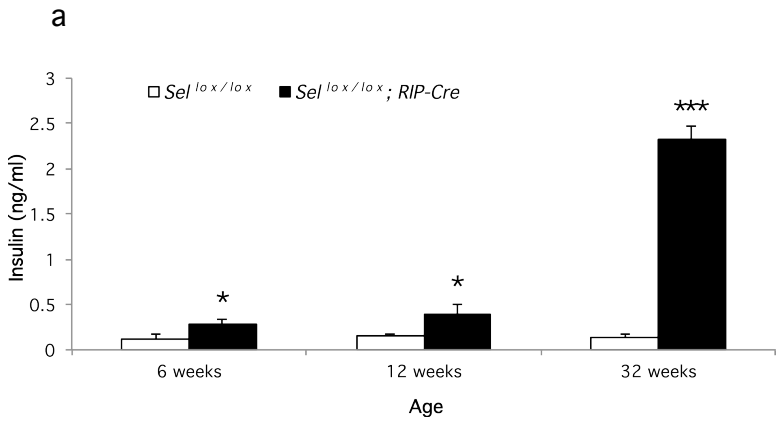
a
Sel lox/lox
Sel lox/lox; RIP-Cre
Insulin (ng/ml)
3
2.5
2
1.5
1
0.5
0
*
*
***
6 weeks
12 weeks
32 weeks
Age

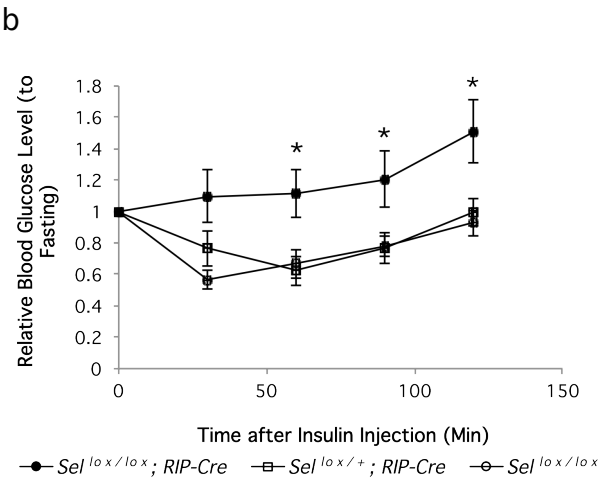
b
Relative Blood Glucose Level (to Fasting)
1.8
1.6
1.4
1.2
1
0.8
0.6
0.4
0.2
0
*
*
*
0
50
100
150
Time after Insulin Injection (Min)
Sel lox/lox; RIP-Cre
Sel lox/+; RIP-Cre
Sel lox/lox

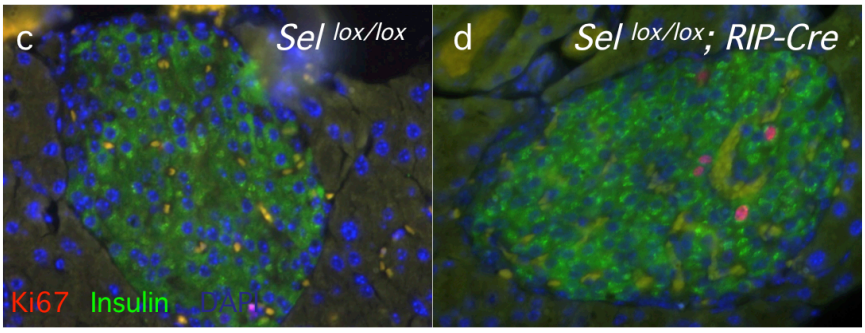
c
Sel lox/lox
Ki67
Insulin
DAPI
d
Sel lox/lox; RIP-Cre

Figure 4.4, Continued:

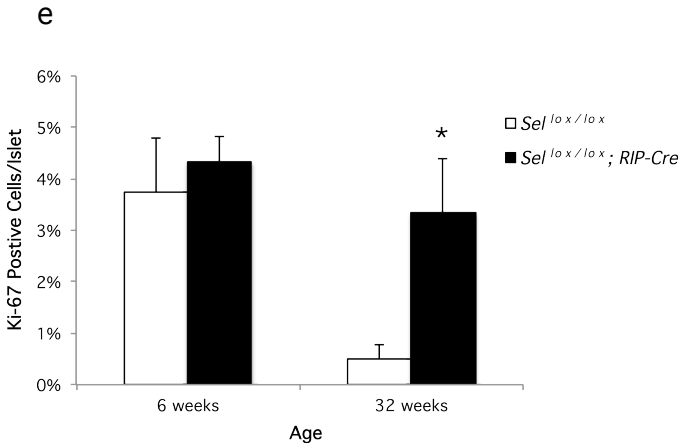

4.4.5 ER stress in the hypothalami of *Sel*$^{lox/lox}$; *RIP-Cre* mice causes weight gain

We hypothesized that ER stress, caused by defective ERAD, may be responsible for the impaired hypothalamic function. To understand the molecular basis of peripheral leptin and insulin resistance in *Sel*$^{lox/lox}$; *RIP-Cre* mice, we utilized quantitative real-time PCR (qPCR) to evaluate the expression of UPR markers in hypothalami excised from *Sel*$^{lox/lox}$ and *Sel*$^{lox/lox}$; *RIP-Cre* mice at 12 weeks of age (Figure 4.5a). There was an expected reduction in the expression of *Sel1L* in the mutant mice, yet a significant increase in the relative expression of *Erdj3*, *Chop*, *Xbp1s* and *Bip*. These genes are classified as UPR markers because they are upregulated in response to ER stress and collectively play an important role in restoration of ER homeostasis.

In collaboration with Dr. Colin Young from Dr. Robin Davisson's lab, we extracted specific regions of the hypothalamus and performed qPCR in order to characterize and localize the metabolic functions of *Sel1L*. In analyzing the arcuate nucleus (ARC) of each genotype, the relative gene expression of *Pomc*

(which is ultimately processed posttranslationally to α-MSH) was significantly higher in the mutants than in the wild-type controls (Figure 4.5b). Expression of the orexigenic neurotransmitter *Npy* was unchanged while the expression of the UPR marker *Erdj3* was highly upregulated in the ARC of mutant mice (Figure 4.5b). In comparing gene expression in the paraventricular nucleus (PVN) of each genotype, *Erdj3*, *Xbp1s*, and *Chop* were significantly higher in mutant mice than in the control mice (Figure 4.5c). These data altogether suggest that there is evident ER stress in key regions of the hypothalamus that are likely responsible for modulating energy balance through leptin signaling.

We next assessed whether ER stress is causing leptin resistance and ultimately weight gain. To test this, we placed wild-type and mutant mice on a 4-PBA water bottle treatment (1 g/kg B.W.) at 10 weeks of age. 4-PBA in drinking water has previously been shown to ameliorate ER stress in various brain regions of rodents and therefore has the ability to cross the blood brain barrier (185). In our study, treatment with 4-PBA in the drinking water effectively prevented weight gain in $Sel^{lox/lox}$; *RIP-Cre* mice (Figure 4.5d). The significant divergence in weights between the genotypes was normally seen around 18 weeks of age (corresponding to 8 weeks of 4-PBA treatment). The body weights of the mutant mice were similar to those of the wild-type mice throughout the course of the treatment, and this trend is sustained until the termination point (14 weeks).

Also in collaboration with Dr. Colin Young, intracerebroventricular (ICV) cannulas were instrumented into $Sel^{lox/lox}$ and $Sel^{lox/lox}$; *RIP-Cre* mice at 22 weeks of age. At this age, the body weights of mutant mice are on average 15 g more than that of wild-type mice. Daily ICV injections of 4-PBA (20 μg) resulted in modest weight reduction (3 to 4 g) in $Sel^{lox/lox}$; *RIP-Cre* mice, and no effect on the body

weights of the *Sel*$^{lox/lox}$ mice throughout the 12-day injection period (Figure 4.5e). *Sel*$^{lox/lox}$*; RIP-Cre* mice also showed a reduction in food intake (data not shown), indicating that relief of ER stress can partially rescue the energy imbalance in *Sel*$^{lox/lox}$*; RIP-Cre* mice.

Figure 4.5: ER stress causes disturbances in energy balance in *Sel$^{lox/lox}$; RIP-Cre* mice. (a) Gene expression of *Sel1L* and various UPR markers was analyzed using quantitative real-time PCR (qPCR) on total hypothalamic cDNA from *Sel$^{lox/lox}$* and *Sel$^{lox/lox}$; RIP-Cre* mice (n=4 per genotype). UPR marker and neuropeptide expression in each genotype (n=6 per genotype), specifically in the (b) arcuate nucleus and the (c) paraventricular nucleus, was also examined using qPCR. In (d), body weight during water bottle administration of the chemical chaperone 4-PBA (1 g/kg) to *Sel$^{lox/lox}$* and *Sel$^{lox/lox}$; RIP-Cre* mice (n=5 mice per genotype), was observed starting at 10 weeks of age (Week 0). (e) 4-PBA (10 μg) was also administered daily through an intracerebroventricular (ICV) cannula in wild-type and control mice (n=4 mice per genotype) at 23 weeks of age and changes in body weight were measured over an 8 day period. *, $p<0.05$; **, $p<0.01$.

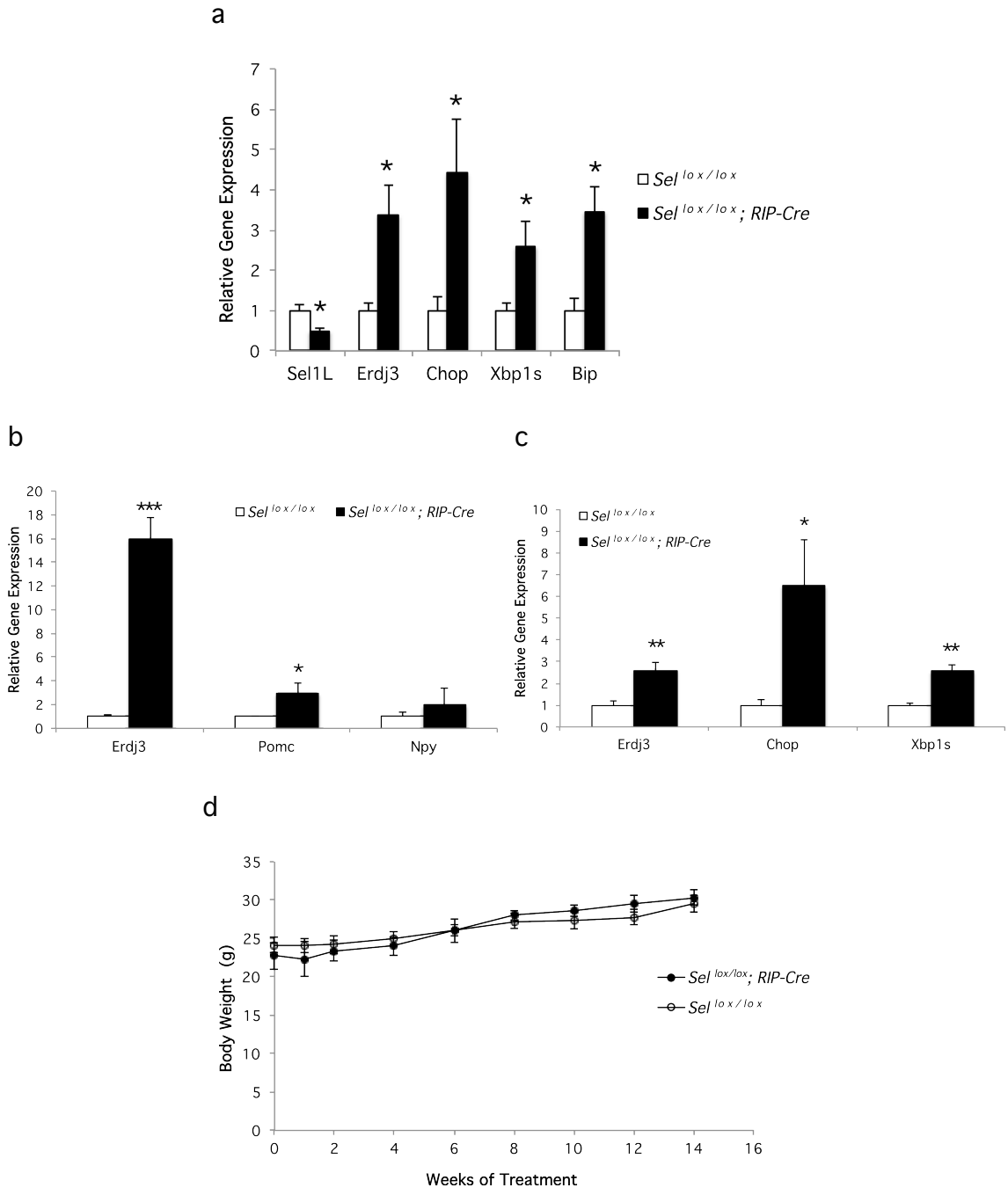
a
Relative Gene Expression
Sel1L
Erdj3
Chop
Xbp1s
Bip
Sel lox/lox
Sel lox/lox; RIP-Cre
b
Relative Gene Expression
Erdj3
Pomc
Npy
c
Relative Gene Expression
Erdj3
Chop
Xbp1s
d
Body Weight (g)
Weeks of Treatment
Sel lox/lox; RIP-Cre
Sel lox/lox

e

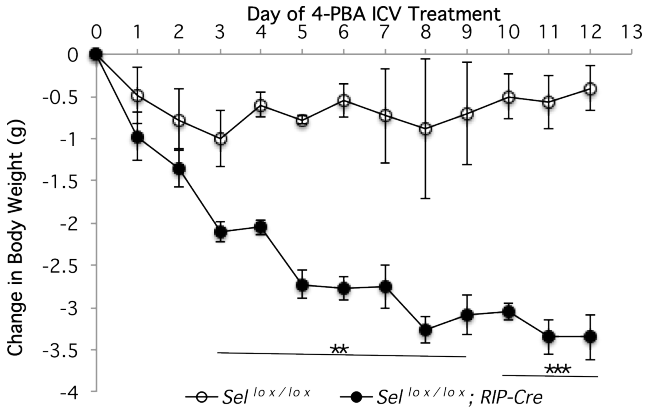

4.5 Discussion

Obesity coincides with a state of central and peripheral insulin and leptin resistance. The fundamental causes of this pathophysiological state are unknown. Our data from the hypothalamus-specific deletion of *Sel1L* in mice collectively suggest a plausible genetic predisposition that manifests in obesity and related disorders. *Sel$^{lox/lox}$; RIP-Cre* mice develop robust obesity over time. Prior to significant weight gain, *Sel$^{lox/lox}$; RIP-Cre* mice are hyperleptinemic and hyperinsulinemic, and resistant to the anorexigenic effects of exogenous leptin. Furthermore, the leptin resistance appears to only affect food intake, as energy expenditure is not significantly different between *Sel$^{lox/lox}$; RIP-Cre* mice and wild-type mice. Analysis of UPR gene expression, also prior to phenotypic changes in weight, confirms the presence of ER stress in the hypothalamus of *Sel$^{lox/lox}$; RIP-Cre* mice. Administration of 4-PBA, a chemical chaperone, in drinking water prevents the onset of weight gain in *Sel$^{lox/lox}$; RIP-Cre* mice, implicating a preventative role for this drug in our mouse model for obesity. Additionally,

delivery of 4-PBA directly to hypothalamic areas (ICV route) results in the reduction of body mass in overweight *Sel*$^{lox/lox}$*; RIP-Cre* mice, suggesting a potential therapeutic use for this drug.

The elevated serum insulin and leptin levels at 6 weeks of age in *Sel*$^{lox/lox}$*; RIP-Cre* mice are of particular interest (Figure 4.4a and Figure 4.3a, respectively). First, the insulin tolerance test (ITT) reveals that at this stage, mutant mice have a normal response to insulin (Appendix B, Figure d). Second, assessment of adiposity in the *Sel*$^{lox/lox}$*; RIP-Cre* mice at 6 weeks of age is comparable to that seen in age-matched *Sel*$^{lox/lox}$ mice (appendix). As previously elaborated on (Chapter 3), *Sel1L* is also deleted in β-cells of *Sel*$^{lox/lox}$*; RIP-Cre* mice, leading to hyperglycemia and reduced insulin secretion. Due to elevated blood glucose levels at an early age, *Sel*$^{lox/lox}$*; RIP-Cre* mice may maintain higher circulating levels of insulin as a physiological adaptation. Although higher levels of leptin are typically associated with an increase in fat mass, leptin secretion may be alternatively affected in this hyperinsulinemic state. Altered glucose metabolism and serum insulin have been shown to be important determinants of leptin secretion *in vivo* (186, 187). Alternatively, discrete changes in adiposity that are undetectable by our method of measurement may account for elevated leptin levels. Further studies at the level of the adipocyte or the use of a more sensitive method to assess adiposity are needed to explain these phenomena.

The administration of 4-PBA to *Sel*$^{lox/lox}$*; RIP-Cre* mice implicates a causal role for ER stress in the hypothalamus as a key mediator of the development of leptin resistance and obesity. The absence of SEL1L function throughout the hypothalamus causes inadequate ERAD and compromises the UPR's adaptive

capabilities. This is the likely mechanism of sustained ER stress. As alluded to in the introduction, several previous studies in diet-induced and genetic models for obesity demonstrated that there is a link between ER stress and leptin resistance. HFD-fed mice as well as *ob*/*ob* mice show increased ER stress is in their hypothalami in comparison to lean controls (47). ER stress in the hypothalamus causes leptin resistance in lean mice, as assessed by a decrease in downstream markers of leptin signaling such as STAT3 phophorylation and neuropeptide expression. In accordance with this, chemical chaperones such as 4-PBA and tauroursodeoxycholic acid (TUDCA), are able to decrease ER stress and improve leptin signaling *in vitro* and *in vivo*. Overnutrition caused by a HFD has also been shown to lead to activation of the IKK/NFκB inflammatory pathway, which is mediated by diet-induced hypothalamic ER stress (50). Furthermore, IKK/NFκB activation contributes to central leptin and insulin resistance by promoting the expression of *Socs3*, an inhibitor of leptin and insulin signaling.

The *Sel1L*-deficient mice phenocopy, to a certain degree, mice with disrupted autophagy. Autophagy is the engulfment of misfolded proteins or protein aggregates within double-membrane vesicles that subsequently fuse to a lysosome, containing the proper enzymes for degrading the contents (103). Knockout of ATG7, a factor for autophagy, in POMC neurons results in hyperphagia, increased body weight, and glucose intolerance (188, 189). All of these parameters are exacerbated when these mice are challenged with a HFD. The loss of autophagy in POMC neurons is associated with perturbed axonal projections and impaired α-MSH production and secretion, both of which are proposed mechanisms for perturbed energy balance in these mice. These results reinforce the importance of the protein quality control in hypothalamic neurons.

Our qPCR results showing gene expression in the ARC (Figure 4.5b) suggest that leptin signaling in this region is not compromised, as *Pomc* mRNA levels are upregulated in the mutant mice. This observation suggests that leptin signaling is mostly retained in first-order neurons of the ARC. This does not, however, exclude the possibility that the POMC protein could be affected posttranslationally by ER stress. The POMC protein undergoes cleavage in secretory vesicles to generate several nascent hormones. Although α-MSH has an established role in regulating feeding behavior, other hypothalamic POMC products (ACTH, β-endorphin) have important roles in the immune, integumentary and reproductive systems (190). We did not observe any dysfunctions related to these systems in $Sel^{lox/lox}$; *RIP-Cre* mice, providing some evidence that POMC processing is unaffected.

The use of *RIP-Cre* transgenic mice contributes a level of complexity in determining the molecular basis of disease in $Sel^{lox/lox}$; *RIP-Cre* mice. Various reporter lines have confirmed that *Cre*-mediated recombination occurs throughout the hypothalamus in addition to β-cells (158). The absolute neuronal populations that are affected by this recombination have not yet been elucidated. Several mouse lines in the *RIP-Cre* background are characterized by the development of obesity, often with altered β-cell morphology and function. These models include those for *Irs2*, *Stat3*, and *Tsc1* (191-193). Together, these studies substantiate the expression of *RIP-Cre* in neurons essential for nutrient homeostasis.

Therefore, the fact that *Sel1L* is deleted throughout the hypothalamus precludes our ability to identify a specific mechanism and site for energy

imbalance in *Sel*$^{lox/lox}$*; RIP-Cre* mice. Our results, however, provide some basis for focusing on the PVN. Because immediate leptin signaling in the ARC leads to elevated *Pomc* expression in accordance with elevated circulating leptin in mutant mice, it is reasonable to assume a secondary neuron defect is responsible for leptin resistance. The relative expression of *Sel1L* in the PVN and ventromedial hypothalamus (VMH) are the lowest amongst several brain regions we examined in *Sel*$^{lox/lox}$*; RIP-Cre* mice compared to their wild-type counterparts (Appendix C, Figure c). This implies these regions could be important sites of dysfunction in our mutant mouse model. Lesions in the PVN and VMH of rodents independently and synergistically produce hyperphagic obesity while on normal chow or a HFD (194). Neurons of the PVN synthesize and secrete several neuropeptides that have been shown to reduce food intake and body weight, such as corticotropin-releasing hormone (CRH), thyrotropin-releasing hormone (TRH), and oxytocin (195-197). Similarly, brain-derived neurotrophic factor (BDNF) in the VMH acts downstream of melanocortin-4 receptor (MC4R) signaling to inhibit food intake (198). These positive mediators of weight balance could be disrupted in the presence of ER stress to produce this increased energy intake and obesity in *Sel*$^{lox/lox}$*; RIP-Cre* mice.

It is notable that *Sel*$^{lox/lox}$*; RIP-Cre* mice have elevated food intake, but unaffected energy expenditure (Figure 4.2i). This may also reflect a PVN-specific defect. Mice heterozygous for *Sim1*, encoding a transcription factor, are hyperphagic with unaltered energy expenditure (199). These mice also have less neuronal cell mass particularly in the PVN. Therefore, loss of functional neuronal cells in the PVN predominantly increases appetite and does not influence energy expenditure in this model for obesity.

It has also been demonstrated through cre-lox engineering that MC4Rs in the PVN control food intake, and that MC4Rs elsewhere control energy expenditure (200). Several studies implicate that MC4R could be another probable candidate for susceptibility to ER stress in *Sel*$^{lox/lox}$; *RIP-Cre* mice. To date, MC4R variants are the most common genetic cause of human obesity described (17). Humans and mouse models with MC4R deficiency experience increased appetite and develop severe obesity over time (201). In childhood obesity-associated heterozygous MC4R variants, there is intracellular retention of the receptor and less cell surface expression (202). These obesity-linked variants of MC4R are also retained in the ER when ectopically expressed in immortalized neurons, causing an increase in the expression of ER chaperones, increased ER-associated degradation, and decreased expression of the receptor at the plasma membrane (52). Treatment with 4-PBA *in vitro* restores the receptor to the cell surface and is also able to rescue the function of one variant.

It is noteworthy that *SEL1L* may confer susceptibility to obesity in humans. The *SEL1L* gene in humans is located on chromosome 14q24.3-31 in what is referred to as a "genome desert." Previous genome-wide association studies (GWAS) have reported chromosome 14q31 as a locus harboring a single-nucleotide polymorphism (SNP) associated with increased abdominal fat (and therefore weight circumference) in obese populations (203, 204). Although these studies have identified the gene at this locus as Neurexin 3 (*NRXN3*), other GWAS and molecular studies have not been able to confirm *NRXN3* as an obesity-associated variant (205). *SEL1L* is located in close proximity to *NRXN3* on chromosome 14. More importantly, our studies indicate that *SEL1L* is a more feasible candidate gene in this chromosomal region, particularly associated with

excess abdominal fat in obese individuals. Interestingly, in addition to the locus at chromosome 14q31, *MC4R* has also been identified as a locus associated with weight circumference.

In summary, we have identified SEL1L as a novel regulator of energy homeostasis. SEL1L and ERAD are imperative for leptin signaling in the hypothalamus. In the absence of SEL1L, the development of ER stress contributes to dysregulation of energy balance and ultimately results in hyperphagic obesity. ER stress could be an important therapeutic target for obesity in the future. Further studies are required, especially in the paraventricular nucleus, to determine the mechanisms by which SEL1L affects the degradation, secretion, and localization of factors related to energy balance.

CHAPTER 5: GENERAL DISCUSSION

5.1 Working Model

The broad goal of this dissertation is to determine the physiological role of SEL1L in the whole organism, with an emphasis in glucose and energy homeostasis. This was based on the hypothesis that the loss of ERAD in β-cells and hypothalamic neurons can causes ER stress and cellular dysfunction in T2D. In Chapter 2, we show evidence from our *Sel1L* global knockout mouse model that attests to the essential role for SEL1L in development. Our embryological and *in vitro* data show that *Sel1L* is required for ER homeostasis, cell growth and viability, efficient ERAD, and secretion. We use this as the cellular and molecular basis for understanding the more tissue-specific functions of SEL1L. Specifically, we explore these functions in tissues that are known to participate in the pathogenesis of T2D: the pancreas and brain. In Chapter 3, studies with heterozygous mice on a HFD as well as mice with a β-cell-specific deletion of *Sel1L* demonstrate that *Sel1L* is required for normal glucose tolerance and glucose-stimulated insulin secretion. In the HFD model, *Sel1L* is necessary for proliferation of β-cells in response to diet-induced insulin resistance. In the conditional knockout mouse model, it is clear that *Sel1L* plays an important role in ER to Golgi trafficking of proinsulin. Finally, our conditional knockout model also features the hypothalamus-specific deletion of *Sel1L*. In Chapter 4, our data suggests that *Sel1L* is necessary for the hypothalamic regulation of body mass, and in particular leptin signaling. Taken together we have developed a general working model to illustrate the potential consequences of loss of *Sel1L* on metabolic homeostasis (Figure 5.1):

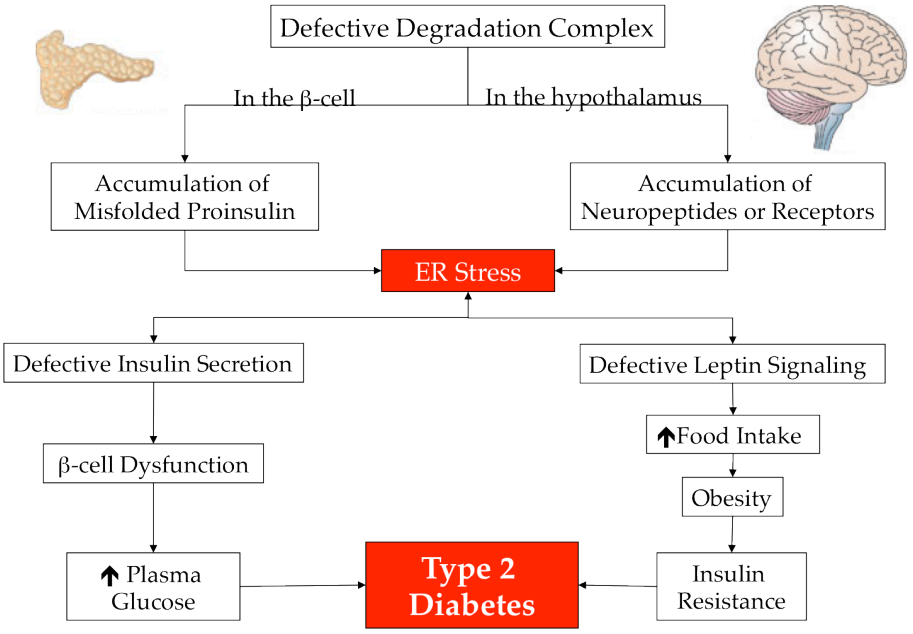

Figure 5.1: Loss of *Sel1L* and the pathogenesis of T2D. A working model linking the absence of *Sel1L* and ERAD complex to the pathogenesis of Type 2 Diabetes through cellular defects at the level of the β-cell and hypothalamic neurons in $Sel^{lox/lox}$; *RIP-Cre* mice.

Previous investigations point to several other diverse mechanisms of β-cell failure. Potential causes include glucolipotoxicity, mitochondrial dysfunctions (and reactive oxygen species), amyloid deposition, and inflammation. Literature also provides evidence for a substantial cellular and molecular influence on insulinemia and insulin resistance. Lipotoxicity, cortisol and inflammation, and alterations in glucose transporter type 4 (GLUT4), along with overnutrition, are associated with a failure to respond to insulin. Overall, this dissertation supports a causal role for ER stress in both β-cell dysfunction and the development of insulin resistance. As Figure 5.1 depicts, our data consistently reinforces that the lack of *Sel1L* is associated with defective ERAD and ER stress. This is evident in our studies with the whole embryo, β-cells and hypothalamic neurons. In the β-cell, ER stress arises from a decreased capacity of

the ER to respond to glucose stimulation and maintain proinsulin production. This manifests in impaired insulin secretion, which constitutes β-cell dysfunction and ultimately leads to a failure to control blood glucose levels. In the hypothalamus, ER stress ultimately leads to leptin resistance and contributes to increased fat content and insulin resistance. As described in the first introductory chapter, insulin resistance coinciding with reduced β-cell secretion or mass leads to T2D.

5.2 Future Directions

Sel$^{lox/lox}$*; RIP-Cre* mice represent a novel model for T2D. However, given the brain and pancreas expression of the *Cre* transgene, it is difficult to dissect glucose and energy phenotypes. An adipoinsular axis has been described, in which insulin and leptin are involved in a hormonal feedback loop (206). This axis can perpetuate obesity and diabetes when dysregulated. Insulin, as an anabolic hormone, increases body fat and stimulates the production of leptin. Leptin suppresses insulin secretion by its action in the hypothalamus as well as in β-cells, and improves insulin sensitivity in peripheral tissues (207). Hypothalamic insulin signaling can also decrease food intake and increase energy expenditure, and has also been shown to inhibit hepatic glucose production (208, 209). In order to distinguish the cell-specific roles of *Sel1L*, *Cre* lines that are mostly β-cell-specific and hypothalamus-specific must be used. For example, *MIP-Cre* and *POMC-Cre* mice would be plausible options.

Our current 4-PBA rescue experiments have not been able to confirm that the deletion of *Sel1L* in β-cells contributes primarily to the glucose phenotype,

and the deletion of *Sel1L* in the hypothalamus to the weight phenotype. However, daily ICV administration of 4-PBA did not significantly alter fasting or non-fasting blood glucose levels in mutant mice over the 8-day period (data not shown). Injections for a longer period of time or perhaps at a higher dose may eventually affect whole body metabolism. This will have to be determined in future experiments where serum leptin and insulin levels, as well as tissue composition, can be assessed following 4-PBA ICV treatment. Although we have focused exclusively on the pancreas and brain for these studies, we must still consider the original model for T2D (Figure 1.1), in which several organs are interconnected in the manifestation of this disease state.

Many questions still remain regarding the role of *Sel1L* and ERAD in glucose and energy homeostasis, especially at a molecular and mechanistic level. Do other factors contributing to diabetes and obesity, such as ageing, feature a downregulation of ERAD components in the pancreas and other peripheral organs? What is the interplay between ERAD, autophagy, and other UPR pathways in this condition of chronic ER stress? How is *Sel1L* regulated (transcriptional, translational, epigenetic) in normal and abnormal physiology? What other hormonal or developmental factors influence the expression of *Sel1L* and ERAD components in disease states? More specific to our mouse model, what are specific substrates of the *Sel1L*-ERAD machinery in each tissue? Or is pathogenesis the result of general ER stress in the absence of *Sel1L*?

Candidate-gene studies and GWAS studies have greatly advanced our current understanding of the genetics of T2D. Together, several novel gene regions and variants that confer susceptibility to this disease have been identified. One gene, Potassium inwardly-rectifying channel, subfamily J,

member 11 (*KCNJ11*), encodes a channel with an important function in insulin secretion and is currently the target of the sulphonylurea class of drugs (210). Another, Peroxisome proliferator-activated receptor-γ (*PPARG*) encodes a transcription factor that is involved in adipocyte differentiation and is a target of the thiazodinedione class of drugs (211). The fat mass and obesity-associated gene (*FTO*) region has emerged as a commonly seen variation associated with fat mass (BMI) in the general population, but the mechanism is unknown (212). As mentioned previously (Chapter 4), *SEL1L* may be located within a locus associated with increased abdominal adiposity in obese individuals. Our research should encourage clinical and basic research scientists to further investigate and fine-map this region, especially in populations with a high prevalence of T2D (for example, South Asian and Mexican-American).

It is increasingly clear that the UPR and ER stress have critical physiological and pathophysiological roles in β-cells and the hypothalamus. Although the mechanisms that cause organ dysfunction in T2D are variable and complex, a genetic predisposition is one of several key contributing factors. Elucidating the role of *SEL1L* and the overall understanding of ER stress in diabetes represents one step closer to the development of new clinical approaches in the treatment of this fatal and costly disease. Again, GWAS studies could substantiate *SEL1L* as a disease variant. Screening for *SEL1L* in patients with T2D could lead to a pharmacogenetic, personalized treatment. It is conceivable that drugs that can ameliorate existing ER stress, such as 4-PBA, would prove to be significant remedies for not only the symptoms of diabetes, but also the central cause of it. Additionally, targeted expression of ERAD

components to the pancreas or brain would facilitate protein processing and thus enhance secretion of insulin or MC4R. Finally, the generation of induced pluripotent stem cells and the clinical implementation of gene therapy are promising tools for translating our basic research into viable cures for T2D.

APPENDIX A

Chapter 2 Supplemental Data

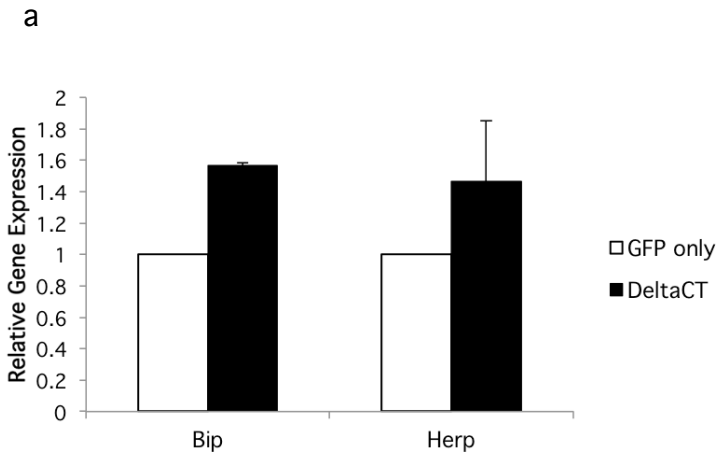

Confirmation of ER stress in HEK cells transfected with a plasmid encoding a truncated, dominant-negative *Sel1L* (DeltaCT)

APPENDIX B

Chapter 3 Supplemental Data

a

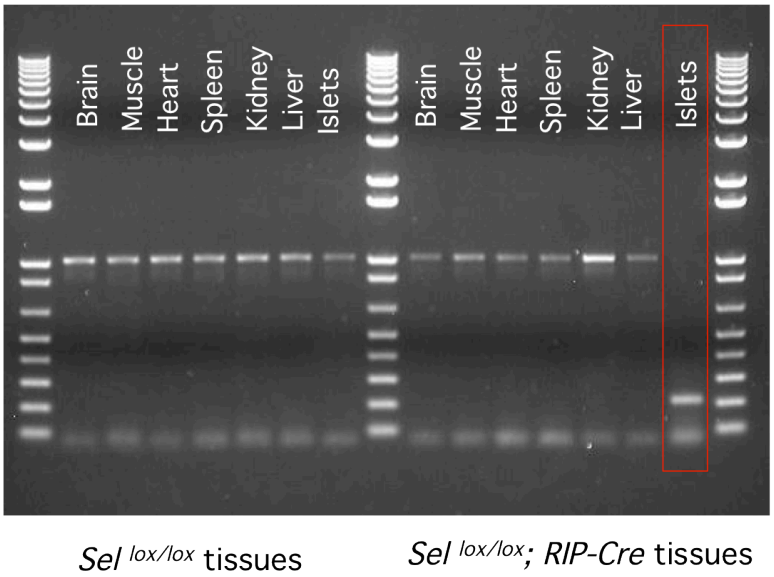

Confirmation of the β-cell-specific deletion (recombination) of *Sel1L* in tissues of *Sel*$^{lox/lox}$ and *Sel*$^{lox/lox}$*; RIP-Cre* mice using genomic PCR

b

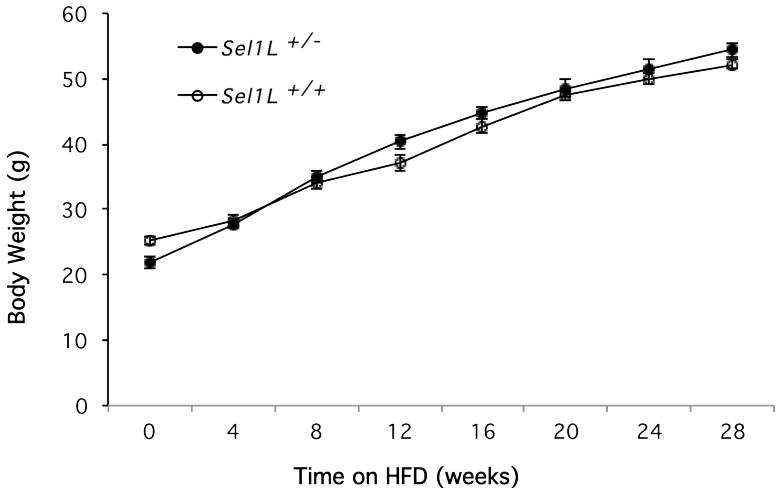

Body weight of HFD-fed *Sel1L*$^{+/+}$ and *Sel1L*$^{+/-}$ mice over the 28-week feeding period

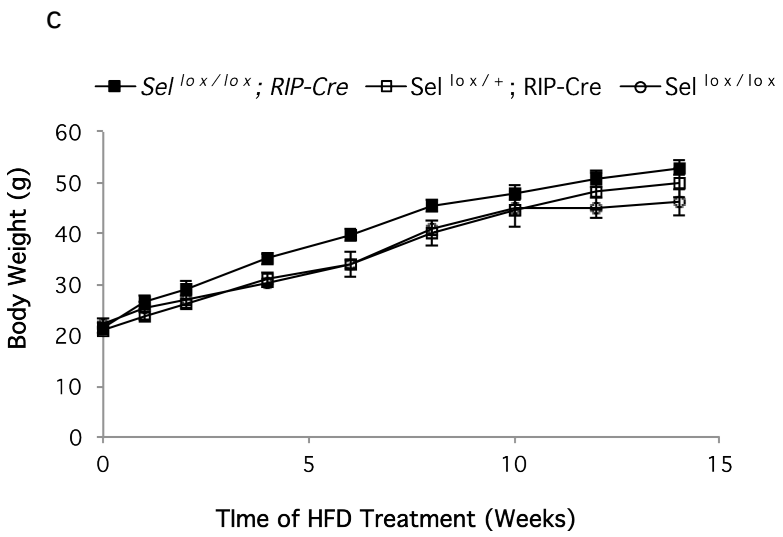

Body weight of HFD-fed *Sel*$^{lox/lox}$, *Sel*$^{lox/+}$*; RIP-Cre,* and *Sel*$^{lox/lox}$*; RIP-Cre* mice over a 14-week feeding period

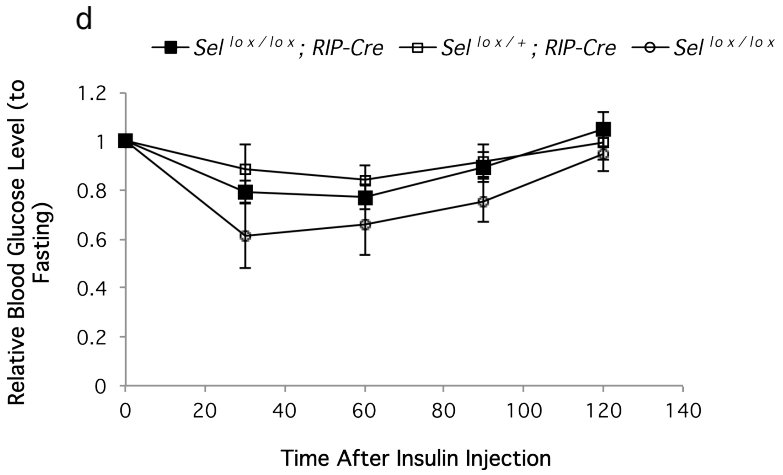

Insulin tolerance test (ITT) in *Sel*$^{lox/lox}$, *Sel*$^{lox/+}$*; RIP-Cre,* and *Sel*$^{lox/lox}$*; RIP-Cre* mice at 6 weeks of age

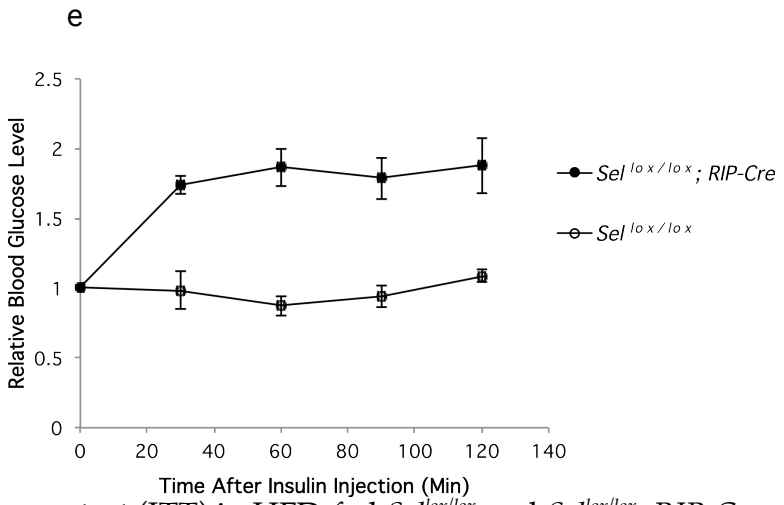

Insulin tolerance test (ITT) in HFD-fed *Sel*$^{lox/lox}$ and *Sel*$^{lox/lox}$*; RIP-Cre* mice after 10 weeks on the diet

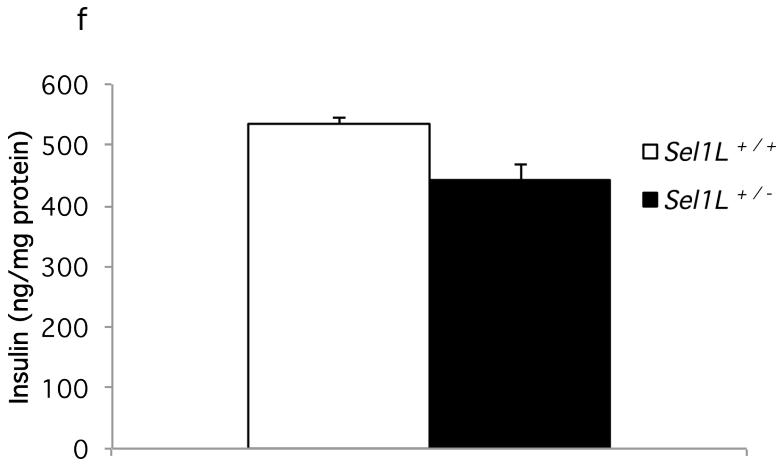

Total pancreatic insulin content in HFD-fed *Sel1L*$^{+/+}$ and *Sel1L*$^{+/-}$ mice after 20 weeks on the diet

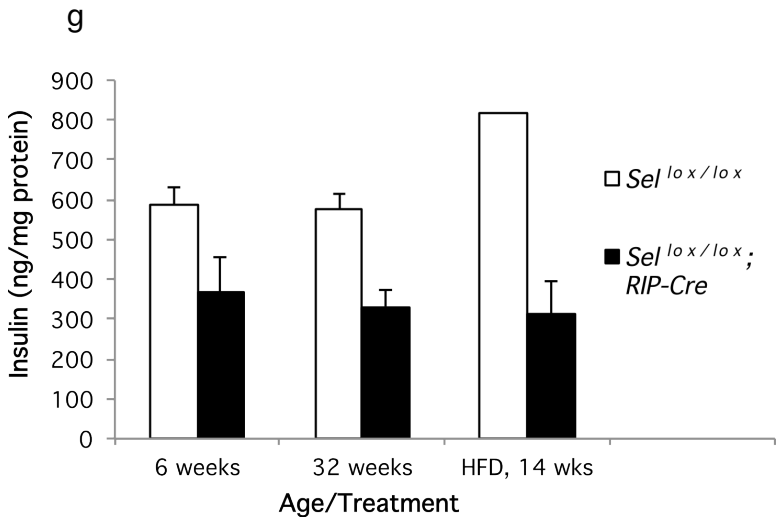

Total pancreatic insulin content in *Sel*$^{lox/lox}$ and *Sel*$^{lox/lox}$*; RIP-Cre* mice at various ages and with HFD treatment

APPENDIX C

Chapter 4 Supplemental Data

a

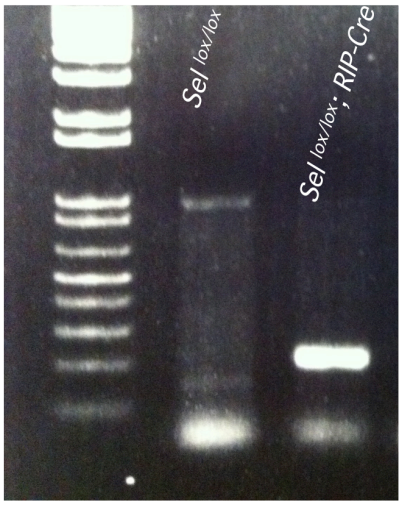

Confirmation of the hypothalamus-specific deletion (recombination) of *Sel1L* in *Sel*$^{lox/lox}$ and *Sel*$^{lox/lox}$*; RIP-Cre* mice using genomic PCR

b

Pair-feeding between the ages and 16 and 18 weeks for *Sel*$^{lox/lox}$ and *Sel*$^{lox/lox}$*; RIP-Cre* mice

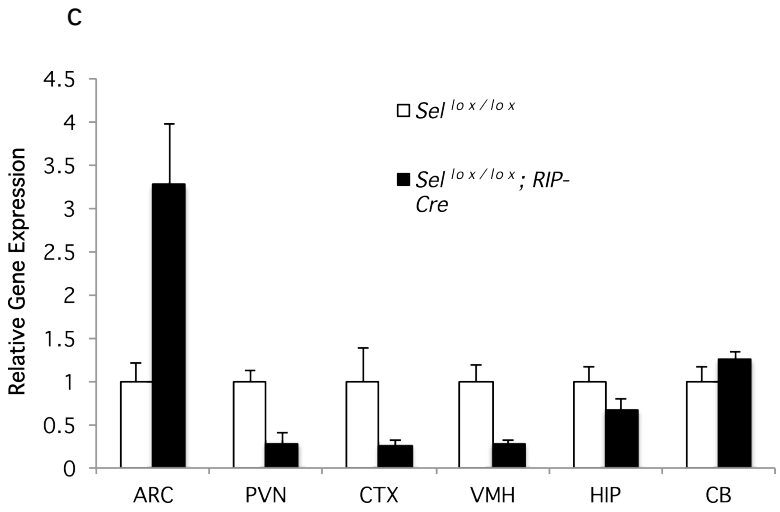

Expression of *Sel1L* in various brain regions of *Sel*$^{lox/lox}$ and *Sel*$^{lox/lox}$*; RIP-Cre* mice; ARC, arcuate; PVN, paraventricular nucleus; CTX, cortex; VMH, ventromedial hypothalamus; HIP, hippocampus; CB, cerebellum

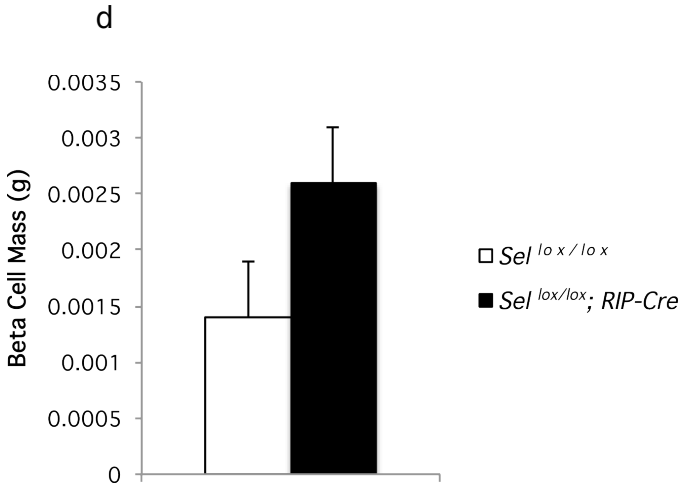

β-cell mass in *Sel*$^{lox/lox}$ and *Sel*$^{lox/lox}$*; RIP-Cre* mice at 32 weeks of age, quantified by insulin staining of pancreatic sections

REFERENCES

1. World Health Organization. Diabetes. WHO Fact Sheet. Geneva, Switzerland: WHO Media Centre; August 2012. Report No.: N°312.

2. Hellman B, Gylfe E, Grapengiesser E, Dansk H, Salehi A. Insulin oscillations--clinically important rhythm. antidiabetics should increase the pulsative component of the insulin release. Lakartidningen. 2007 Aug 8-21;104(32-33):2236-9.

3. Centers for Disease Control and Prevention. National diabetes fact sheet: General information and national estimates on diabetes in the united states, 2011. Atlanta, GA: U.S. Department of Health and Human Services, Centers for Disease Control and Prevention; 2011.

4. Kahn SE, Hull RL, Utzschneider KM. Mechanisms linking obesity to insulin resistance and type 2 diabetes. Nature. 2006 Dec 14;444(7121):840-6.

5. Butler AE, Janson J, Soeller WC, Butler PC. Increased beta-cell apoptosis prevents adaptive increase in beta-cell mass in mouse model of type 2 diabetes: Evidence for role of islet amyloid formation rather than direct action of amyloid. Diabetes. 2003 Sep;52(9):2304-1.

6. Balkau B, Valensi P, Eschwege E, Slama G. A review of the metabolic syndrome. Diabetes Metab. 2007 Dec;33(6):405-13.

7. Shoelson SE, Lee J, Goldfine AB. Inflammation and insulin resistance. J Clin Invest. 2006 Jul;116(7):1793-801.

8. Friedman JM, Halaas JL. Leptin and the regulation of body weight in mammals. Nature. 1998 Oct 22;395(6704):763-70.

9. Elmquist JK, Bjorbaek C, Ahima RS, Flier JS, Saper CB. Distributions of leptin receptor mRNA isoforms in the rat brain. J Comp Neurol. 1998 Jun 15;395(4):535-47.

10. Cheung CC, Clifton DK, Steiner RA. Proopiomelanocortin neurons are direct targets for leptin in the hypothalamus. Endocrinology. 1997 Oct;138(10):4489-92.

11. Elias CF, Lee C, Kelly J, Aschkenasi C, Ahima RS, Couceyro PR, et al. Leptin activates hypothalamic CART neurons projecting to the spinal cord. Neuron. 1998 Dec;21(6):1375-8.

12. Elias CF, Aschkenasi C, Lee C, Kelly J, Ahima RS, Bjorbaek C, et al. Leptin differentially regulates NPY and POMC neurons projecting to the lateral hypothalamic area. Neuron. 1999 Aug;23(4):775-86.

13. Elmquist JK, Elias CF, Saper CB. From lesions to leptin: Hypothalamic control of food intake and body weight. Neuron. 1999 Feb;22(2):221-32.

14. Jequier E. Leptin signaling, adiposity, and energy balance. Ann N Y Acad Sci. 2002 Jun;967:379-88.

15. Tao YX. The melanocortin-4 receptor: Physiology, pharmacology, and pathophysiology. Endocr Rev. 2010 Aug;31(4):506-43.

16. Montague CT, Farooqi IS, Whitehead JP, Soos MA, Rau H, Wareham NJ, et al. Congenital leptin deficiency is associated with severe early-onset obesity in humans. Nature. 1997 Jun 26;387(6636):903-8.

17. Farooqi IS, Yeo GS, Keogh JM, Aminian S, Jebb SA, Butler G, et al. Dominant and recessive inheritance of morbid obesity associated with melanocortin 4 receptor deficiency. J Clin Invest. 2000 Jul;106(2):271-9.

18. Krude H, Biebermann H, Luck W, Horn R, Brabant G, Gruters A. Severe early-onset obesity, adrenal insufficiency and red hair pigmentation caused by POMC mutations in humans. Nat Genet. 1998 Jun;19(2):155-7.

19. Van Heek M, Compton DS, France CF, Tedesco RP, Fawzi AB, Graziano MP, et al. Diet-induced obese mice develop peripheral, but not central, resistance to leptin. J Clin Invest. 1997 Feb 1;99(3):385-90.

20. Hundal RS, Krssak M, Dufour S, Laurent D, Lebon V, Chandramouli V, et al. Mechanism by which metformin reduces glucose production in type 2 diabetes. Diabetes. 2000 Dec;49(12):2063-9.

21. Levine T, Rabouille C. Endoplasmic reticulum: One continuous network compartmentalized by extrinsic cues. Curr Opin Cell Biol. 2005 Aug;17(4):362-8.

22. Sundar Rajan S, Srinivasan V, Balasubramanyam M, Tatu U. Endoplasmic reticulum (ER) stress & diabetes. Indian J Med Res. 2007 Mar;125(3):411-24.

23. Ellgaard L, Molinari M, Helenius A. Setting the standards: Quality control in the secretory pathway. Science. 1999 Dec 3;286(5446):1882-8.

24. Rutkowski DT, Kaufman RJ. A trip to the ER: Coping with stress. Trends Cell Biol. 2004 Jan;14(1):20-8.

25. Cyr DM, Hebert DN. Protein quality control--linking the unfolded protein response to disease. conference on 'from unfolded proteins in the endoplasmic reticulum to disease'. EMBO Rep. 2009 Nov;10(11):1206-10.

26. Lai E, Teodoro T, Volchuk A. Endoplasmic reticulum stress: Signaling the unfolded protein response. Physiology (Bethesda). 2007 Jun;22:193-201.

27. Bertolotti A, Zhang Y, Hendershot LM, Harding HP, Ron D. Dynamic interaction of BiP and ER stress transducers in the unfolded-protein response. Nat Cell Biol. 2000 Jun;2(6):326-32.

28. Shen J, Chen X, Hendershot L, Prywes R. ER stress regulation of ATF6 localization by dissociation of BiP/GRP78 binding and unmasking of golgi localization signals. Dev Cell. 2002 Jul;3(1):99-111.

29. Lee AH, Iwakoshi NN, Glimcher LH. XBP-1 regulates a subset of endoplasmic reticulum resident chaperone genes in the unfolded protein response. Mol Cell Biol. 2003 Nov;23(21):7448-59.

30. Ron D. Translational control in the endoplasmic reticulum stress response. J Clin Invest. 2002 Nov;110(10):1383-8.

31. Haze K, Yoshida H, Yanagi H, Yura T, Mori K. Mammalian transcription factor ATF6 is synthesized as a transmembrane protein and activated by proteolysis in response to endoplasmic reticulum stress. Mol Biol Cell. 1999 Nov;10(11):3787-99.

32. Movassagh M, Foo RS. Simplified apoptotic cascades. Heart Fail Rev. 2008 Jun;13(2):111-9.

33. Oyadomari S, Mori M. Roles of CHOP/GADD153 in endoplasmic reticulum stress. Cell Death Differ. 2004 Apr;11(4):381-9.

34. Puthalakath H, O'Reilly LA, Gunn P, Lee L, Kelly PN, Huntington ND, et al. ER stress triggers apoptosis by activating BH3-only protein bim. Cell. 2007 Jun 29;129(7):1337-49.

35. Szegezdi E, Fitzgerald U, Samali A. Caspase-12 and ER-stress-mediated apoptosis: The story so far. Ann N Y Acad Sci. 2003 Dec;1010:186-94.

36. Oyadomari S, Koizumi A, Takeda K, Gotoh T, Akira S, Araki E, et al. Targeted disruption of the chop gene delays endoplasmic reticulum stress-mediated diabetes. J Clin Invest. 2002 Feb;109(4):525-32.

37. Ozcan U, Cao Q, Yilmaz E, Lee AH, Iwakoshi NN, Ozdelen E, et al. Endoplasmic reticulum stress links obesity, insulin action, and type 2 diabetes. Science. 2004 Oct 15;306(5695):457-61.

38. Shimomura I, Bashmakov Y, Horton JD. Increased levels of nuclear SREBP-1c associated with fatty livers in two mouse models of diabetes mellitus. J Biol Chem. 1999 Oct 15;274(42):30028-32.

39. Ota T, Gayet C, Ginsberg HN. Inhibition of apolipoprotein B100 secretion by lipid-induced hepatic endoplasmic reticulum stress in rodents. J Clin Invest. 2008 Jan;118(1):316-32.

40. Zhou Y, Lee J, Reno CM, Sun C, Park SW, Chung J, et al. Regulation of glucose homeostasis through a XBP-1-FoxO1 interaction. Nat Med. 2011 Mar;17(3):356-65.

41. Zhang K, Shen X, Wu J, Sakaki K, Saunders T, Rutkowski DT, et al. Endoplasmic reticulum stress activates cleavage of CREBH to induce a systemic inflammatory response. Cell. 2006 Feb 10;124(3):587-99.

42. Lee MW, Chanda D, Yang J, Oh H, Kim SS, Yoon YS, et al. Regulation of hepatic gluconeogenesis by an ER-bound transcription factor, CREBH. Cell Metab. 2010 Apr 7;11(4):331-9.

43. Boden G, Duan X, Homko C, Molina EJ, Song W, Perez O, et al. Increase in endoplasmic reticulum stress-related proteins and genes in adipose tissue of obese, insulin-resistant individuals. Diabetes. 2008 Sep;57(9):2438-44.

44. Alhusaini S, McGee K, Schisano B, Harte A, McTernan P, Kumar S, et al. Lipopolysaccharide, high glucose and saturated fatty acids induce endoplasmic reticulum stress in cultured primary human adipocytes: Salicylate alleviates this stress. Biochem Biophys Res Commun. 2010 Jul 2;397(3):472-8.

45. Jiao P, Ma J, Feng B, Zhang H, Diehl JA, Chin YE, et al. FFA-induced adipocyte inflammation and insulin resistance: Involvement of ER stress and IKKbeta pathways. Obesity (Silver Spring). 2011 Mar;19(3):483-91.

46. Munzberg H, Myers MG,Jr. Molecular and anatomical determinants of central leptin resistance. Nat Neurosci. 2005 May;8(5):566-70.

47. Ozcan L, Ergin AS, Lu A, Chung J, Sarkar S, Nie D, et al. Endoplasmic reticulum stress plays a central role in development of leptin resistance. Cell Metab. 2009 Jan 7;9(1):35-51.

48. Milanski M, Degasperi G, Coope A, Morari J, Denis R, Cintra DE, et al. Saturated fatty acids produce an inflammatory response predominantly through the activation of TLR4 signaling in hypothalamus: Implications for the pathogenesis of obesity. J Neurosci. 2009 Jan 14;29(2):359-70.

49. Akira S, Takeda K. Toll-like receptor signalling. Nat Rev Immunol. 2004 Jul;4(7):499-511.

50. Zhang X, Zhang G, Zhang H, Karin M, Bai H, Cai D. Hypothalamic IKKbeta/NF-kappaB and ER stress link overnutrition to energy imbalance and obesity. Cell. 2008 Oct 3;135(1):61-73.

51. Ropelle ER, Flores MB, Cintra DE, Rocha GZ, Pauli JR, Morari J, et al. IL-6 and IL-10 anti-inflammatory activity links exercise to hypothalamic insulin and leptin sensitivity through IKKbeta and ER stress inhibition. PLoS Biol. 2010 Aug 24;8(8):e1000465.

52. Granell S, Mohammad S, Ramanagoudr-Bhojappa R, Baldini G. Obesity-linked variants of melanocortin-4 receptor are misfolded in the endoplasmic reticulum and can be rescued to the cell surface by a chemical chaperone. Mol Endocrinol. 2010 Sep;24(9):1805-21.

53. Straub SG, Sharp GW. Glucose-stimulated signaling pathways in biphasic insulin secretion. Diabetes Metab Res Rev. 2002 Nov-Dec;18(6):451-63.

54. Rhodes CJ. Processing of the insulin molecule. In: LeRoith D, Taylor SI, Olefsky JM, editors. Diabetes Mellitus: A Fundamental and Clinical Text. Philadelphia, PA: Lippincott Williams & Wilkins; 2004. p. 27-50.

55. Rhodes CJ, Shoelson S, Halban PA. Insulin biosynthesis, processing, and chemistry. In: Kahn CR, Weir GC, King GL, Jacobson AM, Moses AC, Smith RJ, editors. Joslin's Diabetes Mellitus. Fourteenth ed. Boston, MA: Joslin Diabetes Center; 2005. p. 65-82.

56. Colombo C, Porzio O, Liu M, Massa O, Vasta M, Salardi S, et al. Seven mutations in the human insulin gene linked to permanent neonatal/infancy-onset diabetes mellitus. J Clin Invest. 2008 Jun;118(6):2148-56.

57. Ron D. Proteotoxicity in the endoplasmic reticulum: Lessons from the akita diabetic mouse. J Clin Invest. 2002 Feb;109(4):443-5.

58. Wang J, Takeuchi T, Tanaka S, Kubo SK, Kayo T, Lu D, et al. A mutation in the insulin 2 gene induces diabetes with severe pancreatic beta-cell dysfunction in the mody mouse. J Clin Invest. 1999 Jan;103(1):27-3.

59. Inoue H, Tanizawa Y, Wasson J, Behn P, Kalidas K, Bernal-Mizrachi E, et al. A gene encoding a transmembrane protein is mutated in patients with diabetes mellitus and optic atrophy (wolfram syndrome). Nat Genet. 1998 Oct;20(2):143-8.

60. Delepine M, Nicolino M, Barrett T, Golamaully M, Lathrop GM, Julier C. EIF2AK3, encoding translation initiation factor 2-alpha kinase 3, is mutated in patients with wolcott-rallison syndrome. Nat Genet. 2000 Aug;25(4):406-9.

61. Zhang W, Feng D, Li Y, Iida K, McGrath B, Cavener DR. PERK EIF2AK3 control of pancreatic beta cell differentiation and proliferation is required for postnatal glucose homeostasis. Cell Metab. 2006 Dec;4(6):491-7.

62. Scheuner D, Song B, McEwen E, Liu C, Laybutt R, Gillespie P, et al. Translational control is required for the unfolded protein response and in vivo glucose homeostasis. Mol Cell. 2001 Jun;7(6):1165-76.

63. Back SH, Scheuner D, Han J, Song B, Ribick M, Wang J, et al. Translation attenuation through eIF2alpha phosphorylation prevents oxidative stress and maintains the differentiated state in beta cells. Cell Metab. 2009 Jul;10(1):13-26.

64. Lipson KL, Ghosh R, Urano F. The role of IRE1alpha in the degradation of insulin mRNA in pancreatic beta-cells. PLoS One. 2008 Feb 20;3(2):e1648.

65. Lipson KL, Fonseca SG, Ishigaki S, Nguyen LX, Foss E, Bortell R, et al. Regulation of insulin biosynthesis in pancreatic beta cells by an endoplasmic reticulum-resident protein kinase IRE1. Cell Metab. 2006 Sep;4(3):245-54.

66. Seo HY, Kim YD, Lee KM, Min AK, Kim MK, Kim HS, et al. Endoplasmic reticulum stress-induced activation of activating transcription factor 6 decreases insulin gene expression via up-regulation of orphan nuclear receptor small heterodimer partner. Endocrinology. 2008 Aug;149(8):3832-41.

67. Kahn SE, D'Alessio DA, Schwartz MW, Fujimoto WY, Ensinck JW, Taborsky GJ,Jr, et al. Evidence of cosecretion of islet amyloid polypeptide and insulin by beta-cells. Diabetes. 1990 May;39(5):634-8.

68. Haataja L, Gurlo T, Huang CJ, Butler PC. Islet amyloid in type 2 diabetes, and the toxic oligomer hypothesis. Endocr Rev. 2008 May;29(3):303-16.

69. Hoppener JW, Ahren B, Lips CJ. Islet amyloid and type 2 diabetes mellitus. N Engl J Med. 2000 Aug 10;343(6):411-9.

70. Lin CY, Gurlo T, Kayed R, Butler AE, Haataja L, Glabe CG, et al. Toxic human islet amyloid polypeptide (h-IAPP) oligomers are intracellular, and vaccination to induce anti-toxic oligomer antibodies does not prevent h-IAPP-induced beta-cell apoptosis in h-IAPP transgenic mice. Diabetes. 2007 May;56(5):1324-32.

71. Jeffrey KD, Alejandro EU, Luciani DS, Kalynyak TB, Hu X, Li H, et al. Carboxypeptidase E mediates palmitate-induced beta-cell ER stress and apoptosis. Proc Natl Acad Sci U S A. 2008 Jun 17;105(24):8452-7.

72. Bachar E, Ariav Y, Ketzinel-Gilad M, Cerasi E, Kaiser N, Leibowitz G. Glucose amplifies fatty acid-induced endoplasmic reticulum stress in pancreatic beta-cells via activation of mTORC1. PLoS One. 2009;4(3):e4954.

73. Boslem E, MacIntosh G, Preston AM, Bartley C, Busch AK, Fuller M, et al. A lipidomic screen of palmitate-treated MIN6 beta-cells links sphingolipid metabolites with endoplasmic reticulum (ER) stress and impaired protein trafficking. Biochem J. 2011 Apr 1;435(1):267-76.

74. Goh TT, Mason TM, Gupta N, So A, Lam TK, Lam L, et al. Lipid-induced beta-cell dysfunction in vivo in models of progressive beta-cell failure. Am J Physiol Endocrinol Metab. 2007 Feb;292(2):E549-60.

75. Lloyd DJ, Wheeler MC, Gekakis N. A point mutation in Sec61alpha1 leads to diabetes and hepatosteatosis in mice. Diabetes. 2010 Feb;59(2):460-7.

76. Sachdeva MM, Claiborn KC, Khoo C, Yang J, Groff DN, Mirmira RG, et al. Pdx1 (MODY4) regulates pancreatic beta cell susceptibility to ER stress. Proc Natl Acad Sci U S A. 2009 Nov 10;106(45):19090-5.

77. Hampton RY. ER-associated degradation in protein quality control and cellular regulation. Curr Opin Cell Biol. 2002 Aug;14(4):476-82.

78. Vembar SS, Brodsky JL. One step at a time: Endoplasmic reticulum-associated degradation. Nat Rev Mol Cell Biol. 2008 Dec;9(12):944-57.

79. Helenius A, Aebi M. Roles of N-linked glycans in the endoplasmic reticulum. Annu Rev Biochem. 2004;73:1019-4.

80. Bukau B, Weissman J, Horwich A. Molecular chaperones and protein quality control. Cell. 2006 May 5;125(3):443-51.

81. Suh K, Gabel CA, Bergmann JE. Identification of a novel mechanism for the removal of glucose residues from high mannose-type oligosaccharides. J Biol Chem. 1992 Oct 25;267(30):21671-7.

82. Ellgaard L, Ruddock LW. The human protein disulphide isomerase family: Substrate interactions and functional properties. EMBO Rep. 2005 Jan;6(1):28-32.

83. Nishikawa SI, Fewell SW, Kato Y, Brodsky JL, Endo T. Molecular chaperones in the yeast endoplasmic reticulum maintain the solubility of proteins for retrotranslocation and degradation. J Cell Biol. 2001 May 28;153(5):1061-70.

84. Sriram M, Osipiuk J, Freeman B, Morimoto R, Joachimiak A. Human Hsp70 molecular chaperone binds two calcium ions within the ATPase domain. Structure. 1997 Mar 15;5(3):403-14.

85. Molinari M, Galli C, Piccaluga V, Pieren M, Paganetti P. Sequential assistance of molecular chaperones and transient formation of covalent complexes during protein degradation from the ER. J Cell Biol. 2002 Jul 22;158(2):247-5.

86. Stronge VS, Saito Y, Ihara Y, Williams DB. Relationship between calnexin and BiP in suppressing aggregation and promoting refolding of protein and glycoprotein substrates. J Biol Chem. 2001 Oct 26;276(43):39779-87.

87. Hosokawa N, Kamiya Y, Kamiya D, Kato K, Nagata K. Human OS-9, a lectin required for glycoprotein endoplasmic reticulum-associated degradation, recognizes mannose-trimmed N-glycans. J Biol Chem. 2009 Jun 19;284(25):17061-8.

88. Hosokawa N, Wada I, Hasegawa K, Yorihuzi T, Tremblay LO, Herscovics A, et al. A novel ER alpha-mannosidase-like protein accelerates ER-associated degradation. EMBO Rep. 2001 May;2(5):415-22.

89. Hosokawa N, Wada I, Nagasawa K, Moriyama T, Okawa K, Nagata K. Human XTP3-B forms an endoplasmic reticulum quality control scaffold with the HRD1-SEL1L ubiquitin ligase complex and BiP. J Biol Chem. 2008 Jul 25;283(30):20914-2.

90. Scott DC, Schekman R. Role of Sec61p in the ER-associated degradation of short-lived transmembrane proteins. J Cell Biol. 2008 Jun 30;181(7):1095-10.

91. Lilley BN, Ploegh HL. Multiprotein complexes that link dislocation, ubiquitination, and extraction of misfolded proteins from the endoplasmic reticulum membrane. Proc Natl Acad Sci U S A. 2005 Oct 4;102(40):14296-301.

92. Lenk U, Yu H, Walter J, Gelman MS, Hartmann E, Kopito RR, et al. A role for mammalian Ubc6 homologues in ER-associated protein degradation. J Cell Sci. 2002 Jul 15;115(Pt 14):3007-14.

93. Mueller B, Lilley BN, Ploegh HL. SEL1L, the homologue of yeast Hrd3p, is involved in protein dislocation from the mammalian ER. J Cell Biol. 2006 Oct 23;175(2):261-70.

94. Bordallo J, Plemper RK, Finger A, Wolf DH. Der3p/Hrd1p is required for endoplasmic reticulum-associated degradation of misfolded lumenal and integral membrane proteins. Mol Biol Cell. 1998 Jan;9(1):209-22.

95. Ye Y, Shibata Y, Kikkert M, van Voorden S, Wiertz E, Rapoport TA. Inaugural article: Recruitment of the p97 ATPase and ubiquitin ligases to the site of retrotranslocation at the endoplasmic reticulum membrane. Proc Natl Acad Sci U S A. 2005 Oct 4;102(40):14132-8.

96. Elsasser S, Finley D. Delivery of ubiquitinated substrates to protein-unfolding machines. Nat Cell Biol. 2005 Aug;7(8):742-9.

97. Husnjak K, Elsasser S, Zhang N, Chen X, Randles L, Shi Y, et al. Proteasome subunit Rpn13 is a novel ubiquitin receptor. Nature. 2008 May 22;453(7194):481-8.

98. Kaneko M, Koike H, Saito R, Kitamura Y, Okuma Y, Nomura Y. Loss of HRD1-mediated protein degradation causes amyloid precursor protein accumulation and amyloid-beta generation. J Neurosci. 2010 Mar 17;30(11):3924-32.

99. Duennwald ML, Lindquist S. Impaired ERAD and ER stress are early and specific events in polyglutamine toxicity. Genes Dev. 2008 Dec 1;22(23):3308-19.

100. Germain D. Ubiquitin-dependent and -independent mitochondrial protein quality controls: Implications in ageing and neurodegenerative diseases. Mol Microbiol. 2008 Dec;70(6):1334-41.

101. Belcher CN, Vij N. Protein processing and inflammatory signaling in cystic fibrosis: Challenges and therapeutic strategies. Curr Mol Med. 2010 Feb;10(1):82-94.

102. Kroeger H, Miranda E, MacLeod I, Perez J, Crowther DC, Marciniak SJ, et al. Endoplasmic reticulum-associated degradation (ERAD) and autophagy cooperate to degrade polymerogenic mutant serpins. J Biol Chem. 2009 Aug 21;284(34):22793-802.

103. Dunn WA,Jr. Autophagy and related mechanisms of lysosome-mediated protein degradation. Trends Cell Biol. 1994 Apr;4(4):139-43.

104. Kang SW, Rane NS, Kim SJ, Garrison JL, Taunton J, Hegde RS. Substrate-specific translocational attenuation during ER stress defines a pre-emptive quality control pathway. Cell. 2006 Dec 1;127(5):999-1013.

105. Grant B, Greenwald I. The caenorhabditis elegans sel-1 gene, a negative regulator of lin-12 and glp-1, encodes a predicted extracellular protein. Genetics. 1996 May;143(1):237-4.

106. Biunno I, Cattaneo M, Orlandi R, Canton C, Biagiotti L, Ferrero S, et al. SEL1L a multifaceted protein playing a role in tumor progression. J Cell Physiol. 2006 Jul;208(1):23-38.

107. Ovcharenko I, Loots GG, Nobrega MA, Hardison RC, Miller W, Stubbs L. Evolution and functional classification of vertebrate gene deserts. Genome Res. 2005 Jan;15(1):137-45.

108. Biunno I, Castiglioni B, Rogozin IB, DeBellis G, Malferrari G, Cattaneo M. Cross-species conservation of SEL1L, a human pancreas-specific expressing gene. OMICS. 2002;6(2):187-98.

109. Seidah NG, Manjunath P, Rochemont J, Sairam MR, Chretien M. Complete amino acid sequence of BSP-A3 from bovine seminal plasma. homology to PDC-109 and to the collagen-binding domain of fibronectin. Biochem J. 1987 Apr 1;243(1):195-203.

110. Kornfeld S. Structure and function of the mannose 6-phosphate/insulinlike growth factor II receptors. Annu Rev Biochem. 1992;61:307-30.

111. Blatch GL, Lassle M. The tetratricopeptide repeat: A structural motif mediating protein-protein interactions. Bioessays. 1999 Nov;21(11):932-9.

112. Srinivasan M, Dunker AK. Proline rich motifs as drug targets in immune mediated disorders. Int J Pept. 2012;2012:634769.

113. Cattaneo M, Lotti LV, Martino S, Alessio M, Conti A, Bachi A, et al. Secretion of novel SEL1L endogenous variants is promoted by ER stress/UPR via

endosomes and shed vesicles in human cancer cells. PLoS One. 2011 Feb 17;6(2):e17206.

114. Cattaneo M, Lotti LV, Martino S, Cardano M, Orlandi R, Mariani-Costantini R, et al. Functional characterization of two secreted SEL1L isoforms capable of exporting unassembled substrate. J Biol Chem. 2009 Apr 24;284(17):11405-1.

115. Orlandi R, Cattaneo M, Troglio F, Campiglio M, Biunno I, Menard S. Production of a monoclonal antibody directed against the recombinant SEL1L protein. Int J Biol Markers. 2002 Apr-Jun;17(2):104-11.

116. Urano F, Calfon M, Yoneda T, Yun C, Kiraly M, Clark SG, et al. A survival pathway for caenorhabditis elegans with a blocked unfolded protein response. J Cell Biol. 2002 Aug 19;158(4):639-46.

117. Allen JR, Nguyen LX, Sargent KE, Lipson KL, Hackett A, Urano F. High ER stress in beta-cells stimulates intracellular degradation of misfolded insulin. Biochem Biophys Res Commun. 2004 Nov 5;324(1):166-70.

118. Christianson JC, Shaler TA, Tyler RE, Kopito RR. OS-9 and GRP94 deliver mutant alpha1-antitrypsin to the Hrd1-SEL1L ubiquitin ligase complex for ERAD. Nat Cell Biol. 2008 Mar;10(3):272-8.

119. Furue M, Zhang Y, Okamoto T, Hata RI, Asashima M. Activin A induces expression of rat sel-1l mRNA, a negative regulator of notch signaling, in rat salivary gland-derived epithelial cells. Biochem Biophys Res Commun. 2001 Apr 6;282(3):745-9.

120. Cattaneo M, Orlandini S, Beghelli S, Moore PS, Sorio C, Bonora A, et al. SEL1L expression in pancreatic adenocarcinoma parallels SMAD4 expression and delays tumor growth in vitro and in vivo. Oncogene. 2003 Sep 25;22(41):6359-68.

121. Orlandi R, Cattaneo M, Troglio F, Casalini P, Ronchini C, Menard S, et al. SEL1L expression decreases breast tumor cell aggressiveness in vivo and in vitro. Cancer Res. 2002 Jan 15;62(2):567-74.

122. Granelli P, Cattaneo M, Ferrero S, Bottiglieri L, Bosari S, Fichera G, et al. SEL1L and squamous cell carcinoma of the esophagus. Clin Cancer Res. 2004 Sep 1;10(17):5857-61.

123. Cattaneo M, Fontanella E, Canton C, Delia D, Biunno I. SEL1L affects human pancreatic cancer cell cycle and invasiveness through modulation of PTEN and genes related to cell-matrix interactions. Neoplasia. 2005 Nov;7(11):1030-8.

124. Barberis MC, Roz E, Biunno I. SEL1L expression in prostatic intraepithelial neoplasia and adenocarcinoma: An immunohistochemical study. Histopathology. 2006 Apr;48(5):614-6.

125. Ferrero S, Falleni M, Cattaneo M, Malferrari G, Canton C, Biagiotti L, et al. SEL1L expression in non-small cell lung cancer. Hum Pathol. 2006 May;37(5):505-12.

126. Ashktorab H, Green W, Finzi G, Sessa F, Nouraie M, Lee EL, et al. SEL1L, an UPR response protein, a potential marker of colonic cell transformation. Dig Dis Sci. 2012 Apr;57(4):905-12.

127. Saltini G, Dominici R, Lovati C, Cattaneo M, Michelini S, Malferrari G, et al. A novel polymorphism in SEL1L confers susceptibility to alzheimer's disease. Neurosci Lett. 2006 May 1;398(1-2):53-8.

128. Kyostila K, Cizinauskas S, Seppala EH, Suhonen E, Jeserevics J, Sukura A, et al. A SEL1L mutation links a canine progressive early-onset cerebellar ataxia to the endoplasmic reticulum-associated protein degradation (ERAD) machinery. PLoS Genet. 2012 Jun;8(6):e1002759.

129. Odom DT, Zizlsperger N, Gordon DB, Bell GW, Rinaldi NJ, Murray HL, et al. Control of pancreas and liver gene expression by HNF transcription factors. Science. 2004 Feb 27;303(5662):1378-81.

130. Sitia R, Braakman I. Quality control in the endoplasmic reticulum protein factory. Nature. 2003 Dec 18;426(6968):891-4.

131. Chakrabarti A, Chen AW, Varner JD. A review of the mammalian unfolded protein response. Biotechnol Bioeng. 2011 Dec;108(12):2777-93.

132. Schroder M, Kaufman RJ. ER stress and the unfolded protein response. Mutat Res. 2005 Jan 6;569(1-2):29-63.

133. Travers KJ, Patil CK, Wodicka L, Lockhart DJ, Weissman JS, Walter P. Functional and genomic analyses reveal an essential coordination between the unfolded protein response and ER-associated degradation. Cell. 2000 Apr 28;101(3):249-58.

134. McCracken AA, Brodsky JL. Evolving questions and paradigm shifts in endoplasmic-reticulum-associated degradation (ERAD). Bioessays. 2003 Sep;25(9):868-77.

135. Kaneko M, Yasui S, Niinuma Y, Arai K, Omura T, Okuma Y, et al. A different pathway in the endoplasmic reticulum stress-induced expression of human HRD1 and SEL1 genes. FEBS Lett. 2007 Nov 27;581(28):5355-60.

136. Urade R. Cellular response to unfolded proteins in the endoplasmic reticulum of plants. FEBS J. 2007 Mar;274(5):1152-71.

137. Francisco AB, Singh R, Li S, Vani AK, Yang L, Munroe RJ, et al. Deficiency of suppressor enhancer Lin12 1 like (SEL1L) in mice leads to systemic endoplasmic

reticulum stress and embryonic lethality. J Biol Chem. 2010 Apr 30;285(18):13694-703.

138. Yamamoto K, Sato T, Matsui T, Sato M, Okada T, Yoshida H, et al. Transcriptional induction of mammalian ER quality control proteins is mediated by single or combined action of ATF6alpha and XBP1. Dev Cell. 2007 Sep;13(3):365-76.

139. Gallagher SR. Protein blotting: Immunoblotting. Current Protocols Essential Laboratory Techniques. 2010;4(8.3):1.

140. Banas A, Yamamoto Y, Teratani T, Ochiya T. Stem cell plasticity: Learning from hepatogenic differentiation strategies. Dev Dyn. 2007 Dec;236(12):3228-41.

141. Deniaud A, Sharaf el dein O, Maillier E, Poncet D, Kroemer G, Lemaire C, et al. Endoplasmic reticulum stress induces calcium-dependent permeability transition, mitochondrial outer membrane permeabilization and apoptosis. Oncogene. 2008 Jan 10;27(3):285-99.

142. Liu Y, Choudhury P, Cabral CM, Sifers RN. Oligosaccharide modification in the early secretory pathway directs the selection of a misfolded glycoprotein for degradation by the proteasome. J Biol Chem. 1999 Feb 26;274(9):5861-7.

143. Hua JY, Smith SJ. Neural activity and the dynamics of central nervous system development. Nat Neurosci. 2004 Apr;7(4):327-32.

144. Yagishita N, Ohneda K, Amano T, Yamasaki S, Sugiura A, Tsuchimochi K, et al. Essential role of synoviolin in embryogenesis. J Biol Chem. 2005 Mar 4;280(9):7909-16.

145. Eura Y, Yanamoto H, Arai Y, Okuda T, Miyata T, Kokame K. Derlin-1 deficiency is embryonic lethal, derlin-3 deficiency appears normal, and herp deficiency is intolerant to glucose load and ischemia in mice. PLoS One. 2012;7(3):e34298.

146. Kahn SE. The relative contributions of insulin resistance and beta-cell dysfunction to the pathophysiology of type 2 diabetes. Diabetologia. 2003 Jan;46(1):3-19.

147. Guerriero CJ, Brodsky JL. The delicate balance between secreted protein folding and endoplasmic reticulum-associated degradation in human physiology. Physiol Rev. 2012 Apr;92(2):537-76.

148. Ron D, Walter P. Signal integration in the endoplasmic reticulum unfolded protein response. Nat Rev Mol Cell Biol. 2007 Jul;8(7):519-2.

149. Wu J, Kaufman RJ. From acute ER stress to physiological roles of the unfolded protein response. Cell Death Differ. 2006 Mar;13(3):374-8.

150. Schubert U, Anton LC, Gibbs J, Norbury CC, Yewdell JW, Bennink JR. Rapid degradation of a large fraction of newly synthesized proteins by proteasomes. Nature. 2000 Apr 13;404(6779):770-4.

151. Li S, Francisco AB, Munroe RJ, Schimenti JC, Long Q. SEL1L deficiency impairs growth and differentiation of pancreatic epithelial cells. BMC Dev Biol. 2010 Feb 19;10:19.

152. Szot GL, Koudria P, Bluestone JA. Murine pancreatic islet isolation. J Vis Exp. 2007;(7)(7):255.

153. Regard JB, Kataoka H, Cano DA, Camerer E, Yin L, Zheng YW, et al. Probing cell type-specific functions of gi in vivo identifies GPCR regulators of insulin secretion. J Clin Invest. 2007 Dec;117(12):4034-43.

154. Thorn K, Bergsten P. Fatty acid-induced oxidation and triglyceride formation is higher in insulin-producing MIN6 cells exposed to oleate compared to palmitate. J Cell Biochem. 2010 Oct 1;111(2):497-50.

155. Sachdeva MM, Claiborn KC, Khoo C, Yang J, Groff DN, Mirmira RG, et al. Pdx1 (MODY4) regulates pancreatic beta cell susceptibility to ER stress. Proc Natl Acad Sci U S A. 2009 Nov 10;106(45):19090-5.

156. Haimes J KM.
Demonstration of a ΔΔCq calculation method to compute relative gene expression from qPCR data
. Lafayette, CO: Thermo Fisher Scientific; 2010.

157. Francisco AB, Singh R, Sha H, Yan X, Qi L, Lei X, et al. Haploid insufficiency of suppressor enhancer Lin12 1-like (SEL1L) protein predisposes mice to high fat diet-induced hyperglycemia. J Biol Chem. 2011 Jun 24;286(25):22275-82.

158. Wicksteed B, Brissova M, Yan W, Opland DM, Plank JL, Reinert RB, et al. Conditional gene targeting in mouse pancreatic ss-cells: Analysis of ectopic cre transgene expression in the brain. Diabetes. 2010 Dec;59(12):3090-8.

159. Barr FA, Nakamura N, Warren G. Mapping the interaction between GRASP65 and GM130, components of a protein complex involved in the stacking of golgi cisternae. EMBO J. 1998 Jun 15;17(12):3258-6.

160. Ladiges WC, Knoblaugh SE, Morton JF, Korth MJ, Sopher BL, Baskin CR, et al. Pancreatic beta-cell failure and diabetes in mice with a deletion mutation of the endoplasmic reticulum molecular chaperone gene P58IPK. Diabetes. 2005 Apr;54(4):1074-81.

161. Ishihara H, Takeda S, Tamura A, Takahashi R, Yamaguchi S, Takei D, et al. Disruption of the WFS1 gene in mice causes progressive beta-cell loss and impaired stimulus-secretion coupling in insulin secretion. Hum Mol Genet. 2004 Jun 1;13(11):1159-70.

162. Janson J, Soeller WC, Roche PC, Nelson RT, Torchia AJ, Kreutter DK, et al. Spontaneous diabetes mellitus in transgenic mice expressing human islet amyloid polypeptide. Proc Natl Acad Sci U S A. 1996 Jul 9;93(14):7283-8.

163. Huang CJ, Haataja L, Gurlo T, Butler AE, Wu X, Soeller WC, et al. Induction of endoplasmic reticulum stress-induced beta-cell apoptosis and accumulation of polyubiquitinated proteins by human islet amyloid polypeptide. Am J Physiol Endocrinol Metab. 2007 Dec;293(6):E1656-62.

164. Costes S, Huang CJ, Gurlo T, Daval M, Matveyenko AV, Rizza RA, et al. Beta-cell dysfunctional ERAD/ubiquitin/proteasome system in type 2 diabetes mediated by islet amyloid polypeptide-induced UCH-L1 deficiency. Diabetes. 2011 Jan;60(1):227-38.

165. Jung HS, Chung KW, Won Kim J, Kim J, Komatsu M, Tanaka K, et al. Loss of autophagy diminishes pancreatic β cell mass and function with resultant hyperglycemia. Cell Metabolism. 2008 10/8;8(4):318-24.

166. Ebato C, Uchida T, Arakawa M, Komatsu M, Ueno T, Komiya K, et al. Autophagy is important in islet homeostasis and compensatory increase of beta cell mass in response to high-fat diet. Cell Metab. 2008 Oct;8(4):325-32.

167. Unger RH. Lipotoxicity in the pathogenesis of obesity-dependent NIDDM. genetic and clinical implications. Diabetes. 1995 Aug;44(8):863-70.

168. Cnop M. Fatty acids and glucolipotoxicity in the pathogenesis of type 2 diabetes. Biochem Soc Trans. 2008 Jun;36(Pt 3):348-52.

169. Karaskov E, Scott C, Zhang L, Teodoro T, Ravazzola M, Volchuk A. Chronic palmitate but not oleate exposure induces endoplasmic reticulum stress, which may contribute to INS-1 pancreatic beta-cell apoptosis. Endocrinology. 2006 Jul;147(7):3398-407.

170. Cunha DA, Hekerman P, Ladriere L, Bazarra-Castro A, Ortis F, Wakeham MC, et al. Initiation and execution of lipotoxic ER stress in pancreatic beta-cells. J Cell Sci. 2008 Jul 15;121(Pt 14):2308-1.

171. Li X, Zhu H, Huang H, Jiang R, Zhao W, Liu Y, et al. Study on the effect of IRE1a on cell growth and apoptosis via modulation PLK1 in ER stress response. Mol Cell Biochem. 2012 Jun;365(1-2):99-108.

172. Caldwell SR, Hill KJ, Cooper AA. Degradation of endoplasmic reticulum (ER) quality control substrates requires transport between the ER and golgi. J Biol Chem. 2001 Jun 29;276(26):23296-303.

173. Taxis C, Vogel F, Wolf DH. ER-golgi traffic is a prerequisite for efficient ER degradation. Mol Biol Cell. 2002 Jun;13(6):1806-18.

174. Ogden CL, Carroll MD, Kit BK, Flegal KM. Prevalence of obesity in the united states, 2009-2010. Hyattsville, MD: National Center for Health Statistics; 2012 January. Report No.: NCHS data brief, No. 82.

175. Enriori PJ, Evans AE, Sinnayah P, Cowley MA. Leptin resistance and obesity. Obesity (Silver Spring). 2006 Aug;14 Suppl 5:254S-8.

176. Banks WA, Farrell CL. Impaired transport of leptin across the blood-brain barrier in obesity is acquired and reversible. Am J Physiol Endocrinol Metab. 2003 Jul;285(1):E10-5.

177. Rutkowski DT, Hegde RS. Regulation of basal cellular physiology by the homeostatic unfolded protein response. J Cell Biol. 2010 May 31;189(5):783-94.

178. Stunkard AJ, Harris JR, Pedersen NL, McClearn GE. The body-mass index of twins who have been reared apart. N Engl J Med. 1990 May 24;322(21):1483-7.

179. Allison DB, Kaprio J, Korkeila M, Koskenvuo M, Neale MC, Hayakawa K. The heritability of body mass index among an international sample of monozygotic twins reared apart. Int J Obes Relat Metab Disord. 1996 Jun;20(6):501-6.

180. Wadden TA. Treatment of obesity by moderate and severe caloric restriction. results of clinical research trials. Ann Intern Med. 1993 Oct 1;119(7 Pt 2):688-93.

181. Wadden TA, Considine RV, Foster GD, Anderson DA, Sarwer DB, Caro JS. Short- and long-term changes in serum leptin dieting obese women: Effects of caloric restriction and weight loss. J Clin Endocrinol Metab. 1998 Jan;83(1):214-8.

182. Cao X, Peterson JR, Wang G, Anrather J, Young CN, Guruju MR, et al. Angiotensin II-dependent hypertension requires cyclooxygenase 1-derived prostaglandin E2 and EP1 receptor signaling in the subfornical organ of the brain. Hypertension. 2012 Apr;59(4):869-76.

183. Young CN, Cao X, Guruju MR, Pierce JP, Morgan DA, Wang G, et al. ER stress in the brain subfornical organ mediates angiotensin-dependent hypertension. J Clin Invest. 2012 Oct 15.

184. Luu YK, Lublinsky S, Ozcivici E, Capilla E, Pessin JE, Rubin CT, et al. In vivo quantification of subcutaneous and visceral adiposity by micro-computed tomography in a small animal model. Med Eng Phys. 2009 Jan;31(1):34-41.

185. Wiley JC, Pettan-Brewer C, Ladiges WC. Phenylbutyric acid reduces amyloid plaques and rescues cognitive behavior in AD transgenic mice. Aging Cell. 2011 Jun;10(3):418-2.

186. Fruehwald-Schultes B, Oltmanns KM, Kern W, Born J, Fehm HL, Peters A. The effect of experimentally induced insulin resistance on the leptin response to hyperinsulinaemia. Int J Obes Relat Metab Disord. 2002 Apr;26(4):510-6.

187. Wellhoener P, Fruehwald-Schultes B, Kern W, Dantz D, Kerner W, Born J, et al. Glucose metabolism rather than insulin is a main determinant of leptin secretion in humans. J Clin Endocrinol Metab. 2000 Mar;85(3):1267-71.

188. Kaushik S, Arias E, Kwon H, Lopez NM, Athonvarangkul D, Sahu S, et al. Loss of autophagy in hypothalamic POMC neurons impairs lipolysis. EMBO Rep. 2012 Mar 1;13(3):258-65.

189. Coupe B, Ishii Y, Dietrich MO, Komatsu M, Horvath TL, Bouret SG. Loss of autophagy in pro-opiomelanocortin neurons perturbs axon growth and causes metabolic dysregulation. Cell Metab. 2012 Feb 8;15(2):247-55.

190. Wilkinson CW. Roles of acetylation and other post-translational modifications in melanocortin function and interactions with endorphins. Peptides. 2006 Feb;27(2):453-71.

191. Cui Y, Huang L, Elefteriou F, Yang G, Shelton JM, Giles JE, et al. Essential role of STAT3 in body weight and glucose homeostasis. Mol Cell Biol. 2004 Jan;24(1):258-69.

192. Kubota N, Terauchi Y, Tobe K, Yano W, Suzuki R, Ueki K, et al. Insulin receptor substrate 2 plays a crucial role in beta cells and the hypothalamus. J Clin Invest. 2004 Oct;114(7):917-2.

193. Mori H, Inoki K, Munzberg H, Opland D, Faouzi M, Villanueva EC, et al. Critical role for hypothalamic mTOR activity in energy balance. Cell Metab. 2009 Apr;9(4):362-74.

194. Leibowitz SF, Hammer NJ, Chang K. Hypothalamic paraventricular nucleus lesions produce overeating and obesity in the rat. Physiol Behav. 1981 Dec;27(6):1031-40.

195. Dallman MF, Strack AM, Akana SF, Bradbury MJ, Hanson ES, Scribner KA, et al. Feast and famine: Critical role of glucocorticoids with insulin in daily energy flow. Front Neuroendocrinol. 1993 Oct;14(4):303-47.

196. Kow LM, Pfaff DW. The effects of the TRH metabolite cyclo(his-pro) and its analogs on feeding. Pharmacol Biochem Behav. 1991 Feb;38(2):359-64.

197. Verbalis JG, Blackburn RE, Hoffman GE, Stricker EM. Establishing behavioral and physiological functions of central oxytocin: Insights from studies of oxytocin and ingestive behaviors. Adv Exp Med Biol. 1995;395:209-25.

198. Xu B, Goulding EH, Zang K, Cepoi D, Cone RD, Jones KR, et al. Brain-derived neurotrophic factor regulates energy balance downstream of melanocortin-4 receptor. Nat Neurosci. 2003 Jul;6(7):736-42.

199. Michaud JL, Boucher F, Melnyk A, Gauthier F, Goshu E, Levy E, et al. Sim1 haploinsufficiency causes hyperphagia, obesity and reduction of the paraventricular nucleus of the hypothalamus. Hum Mol Genet. 2001 Jul 1;10(14):1465-73.

200. Balthasar N, Dalgaard LT, Lee CE, Yu J, Funahashi H, Williams T, et al. Divergence of melanocortin pathways in the control of food intake and energy expenditure. Cell. 2005 Nov 4;123(3):493-505.

201. Farooqi IS, O'Rahilly S. Monogenic human obesity syndromes. Recent Prog Horm Res. 2004;59:409-24.

202. Lubrano-Berthelier C, Durand E, Dubern B, Shapiro A, Dazin P, Weill J, et al. Intracellular retention is a common characteristic of childhood obesity-associated MC4R mutations. Hum Mol Genet. 2003 Jan 15;12(2):145-53.

203. Bille DS, Banasik K, Justesen JM, Sandholt CH, Sandbaek A, Lauritzen T, et al. Implications of central obesity-related variants in LYPLAL1, NRXN3, MSRA, and TFAP2B on quantitative metabolic traits in adult danes. PLoS One. 2011;6(6):e20640.

204. Heard-Costa NL, Zillikens MC, Monda KL, Johansson A, Harris TB, Fu M, et al. NRXN3 is a novel locus for waist circumference: A genome-wide association study from the CHARGE consortium. PLoS Genet. 2009 Jun;5(6):e1000539.

205. Hotta K, Nakamura M, Nakamura T, Matsuo T, Nakata Y, Kamohara S, et al. Polymorphisms in NRXN3, TFAP2B, MSRA, LYPLAL1, FTO and MC4R and their effect on visceral fat area in the japanese population. J Hum Genet. 2010 Nov;55(11):738-42.

206. Kieffer TJ, Habener JF. The adipoinsular axis: Effects of leptin on pancreatic beta-cells. Am J Physiol Endocrinol Metab. 2000 Jan;278(1):E1-E14.

207. Cusin I, Zakrzewska KE, Boss O, Muzzin P, Giacobino JP, Ricquier D, et al. Chronic central leptin infusion enhances insulin-stimulated glucose metabolism and favors the expression of uncoupling proteins. Diabetes. 1998 Jul;47(7):1014-9.

208. Obici S, Zhang BB, Karkanias G, Rossetti L. Hypothalamic insulin signaling is required for inhibition of glucose production. Nat Med. 2002 Dec;8(12):1376-82.

209. Menendez JA, Atrens DM. Insulin and the paraventricular hypothalamus: Modulation of energy balance. Brain Res. 1991 Aug 2;555(2):193-201.

210. Gloyn AL, Weedon MN, Owen KR, Turner MJ, Knight BA, Hitman G, et al. Large-scale association studies of variants in genes encoding the pancreatic beta-cell KATP channel subunits Kir6.2 (KCNJ11) and SUR1 (ABCC8) confirm that the KCNJ11 E23K variant is associated with type 2 diabetes. Diabetes. 2003 Feb;52(2):568-72.

211. Chistiakov DA. The peroxisomal proliferator-activated receptor gamma isoform 2 (PPARgamma2) is an established susceptibility marker for type 2 diabetes (T2D). Autoimmunity. 2008 Aug;41(5):338-9.

212. Frayling TM, Timpson NJ, Weedon MN, Zeggini E, Freathy RM, Lindgren CM, et al. A common variant in the FTO gene is associated with body mass index and predisposes to childhood and adult obesity. Science. 2007 May 11;316(5826):889-94.